Investigations of glacier terminus changes on weekly to decadal time scales

Taryn Elizabeth Black

A dissertation

submitted in partial fulfillment of the

requirements for the degree of

Doctor of Philosophy

University of Washington

2022

Reading Committee:

Ian Joughin, Chair

Benjamin Smith

Michelle Koutnik

Knut Christianson

Program Authorized to Offer Degree:

Earth and Space Sciences

© Copyright 2022

Taryn Elizabeth Black

University of Washington

Abstract

Investigations of glacier terminus changes on weekly to decadal time scales

Taryn Elizabeth Black

Chair of the Supervisory Committee:

Ian Joughin

Applied Physics Laboratory

Glacier retreat and mass loss are contributing to global sea-level rise and environmental change. One method to improve our understanding of how glaciers affect local and global environments is to measure historical and ongoing glacier retreat. In this dissertation, I use satellite images to measure glacier terminus change in Greenland and Alaska. In both regions, I quantify glacier retreat and advance on time scales ranging from seasons to decades.

In northwest and central-west Greenland, I investigate multi-decadal outlet glacier retreat and its potential driving mechanisms from 1972 through 2021. Over this time period, glaciers in this region of Greenland represented nearly half of Greenland's total contribution to sea-level rise. I show that regional glacier retreat accelerated from 1996, and that this retreat is most sensitive to runoff and ocean temperatures. Because runoff and ocean temperatures can influence terminus

positions through several mechanisms, it is likely that multiple mechanisms are contributing to the observed retreat in this region.

I also examine multi-decadal glacier retreat, as well as seasonal terminus variations, for maritime glaciers in Kenai Fjords National Park, Alaska, from 1984 through 2021. I show that most glaciers retreated substantially, and those that did not were predominantly tidewater. Seasonally, tidewater, lake-terminating, and land-terminating glaciers all tended to retreat during the summer; in the winter, tidewater glaciers tended to advance, while lake-terminating glaciers continued to retreat, and land-terminating glaciers were more variable. Glacier change in Kenai Fjords National Park is driving changes in landcover and viewscapes, which affects local ecosystems and ecotourism.

Finally, I characterize seasonal terminus variations around the full margin of Greenland at monthly and six-day temporal resolution. I show that nearly 75% of outlet glaciers exhibit terminus position seasonality, with seasonal retreat typically beginning in mid-May and continuing through early October. The onset and duration of the retreat period appears to be related to the timing of the onset of melt, while the magnitude of terminus position seasonality correlates with glacier velocity. Glacier dynamics are influenced by conditions at the terminus, and terminus position seasonality can affect projections of future ice-sheet mass balance.

Table of Contents

List of Figures

List of Tables

Acknowledgements

I must first thank my advisor, Ian Joughin, for his excellent supervision over the years. He has shown endless patience, provided constructive writing critiques and engaging scientific conversations, and always supported me in figuring out my career path. I also appreciate the time of the rest of my committee – Michelle Koutnik, Ben Smith, and Knut Christianson – who have always been willing to offer me guidance and advice when I asked.

Deb Kurtz has been like a second advisor for the past two years. She initially took me on for a summer internship and stuck around as that internship evolved into a dissertation chapter and capstone project. I will miss our video calls, and hope that we eventually get to meet in person.

My collaborators on projects outside of this dissertation have helped me to expand my research in new and interesting directions. Sophie Goliber and Ginny Catania introduced me to my first large collaboration, and to the curation and analysis of large data assemblages. Twila Moon and Ben Cohen have happily encouraged me in exploring new and unfamiliar data.

The University of Washington glaciology group has enhanced my education through lively discussions at g-lunch and at reading seminars. The g-women group, in particular, has been a source of support and knowledge for the past several years. T.J. Fudge has also been a friend and mentor throughout.

The Earth and Space Sciences department has formed the core of my community here. Courses and academic events have shaped my official PhD experience, but the friendships that grew from hallway chats and pub nights are the thread binding everything together. These are too numerous to count, but a few particular standouts include: Andrew Shumway; Addien Wray and Ayla Heinze Fry; and Zack McIntire and Virginia Littell.

I have had the long-standing support of many friends outside of the university as well. The geoladies (Kim Smith, Katie Higgins, Dana Hansen, Chelsea Mackaman-Lofland, and Sylvana Bendaña) have always cheered each other on. Kim Smith and Austin Keder have kept our meetups going since the days of undergraduate physics. Eric Schoettle has been a stalwart hiking companion and fellow geology enthusiast, often at the same time. Serginio Remmelzwaal and Cody Messick have engaged in long-distance PhD commiseration and celebration. Heather Chilton and Gabe Eggers saw me through the process of finding a PhD program that was the right fit.

My family has supported me on my long journey through higher education. My dad, especially, has always been curious about my research. Bret and Sheri Sutterley have also taken me in and encouraged and motivated me. Finally, and most importantly, I want to thank my partner, Tyler Sutterley, for his wholehearted love and support. He has been my constant companion, my sanity in a pandemic, and my source of strength and comfort for these past few years.

To Grandpa George,

who would have sent me newspaper clippings about glaciers.

Chapter 1. Introduction

1.1 Motivation

By the year 2100, global mean sea level is projected to rise by anywhere from 0.6 to 1.1 m relative to 1986–2005 levels if greenhouse gas emissions continue on their current trajectory (IPCC, 2019). Under the upper end of that scenario, some 630 million people in today's global population distribution would be subject to flooding events associated with rising sea levels; this estimate does not account for future population growth or migration (Kulp and Strauss, 2019). In order to mitigate the human and environmental impacts of global sea-level rise, it is important to be able to accurately constrain how quickly sea level will rise. Global mean sea-level rise is dominated by contributions from glaciers and ice sheets, and the future evolution of these ice masses represents one of the largest sources of uncertainty in projecting future sea-level rise (IPCC, 2019). Although Antarctica is the largest reservoir of ice, currently the Greenland Ice Sheet and global glaciers outside of ice sheets are outpacing Antarctica in contributions to global mean sea level (IPCC, 2019). Of glaciers outside of ice sheets, the largest contribution to global mean sea level comes from Alaskan glaciers (Hugonnet et al., 2021; Zemp et al., 2019).

In addition to contributing to global sea-level rise, glaciers and ice sheets affect local and regional environments. In glacierized fjords, subglacial meltwater discharge from marine-terminating glaciers drives upwelling of nutrient-rich waters, which supports phytoplankton productivity (Meire et al., 2017). High phytoplankton productivity in turn supports higher trophic levels; a variety of species, such as narwhals and harbor seals, are associated with glacierized marine environments (Laidre et al., 2016; Hoover-Miller and Armato, 2018). Glaciers also affect freshwater and terrestrial ecosystems through the timing, quantity, and chemistry of glacial melt

(O'Neel et al., 2015), and glacier retreat will have complex effects on these ecosystems, by both creating and destabilizing habitats (*e.g.*, Pitman et al., 2020, 2021).

Glacier retreat is a consequence of changes in mass balance and ice dynamics. Mass balance is composed of changes in surface mass balance (mainly snow accumulation and melting), and, if the glacier is water-terminating, changes in ice discharge (calving) and basal mass balance (melting or accretion of ice underneath a glacier or ice shelf). Changes in mass balance cause changes in ice surface elevation and areal coverage (glacier width and length). Since the late 1990s, many marine-terminating glaciers in Greenland have retreated, thinned, and accelerated (Joughin et al., 2010; Moon et al., 2012; Rignot and Kanagaratnam, 2006). Similarly, nearly all of Alaska's glaciers are thinning and retreating (Larsen et al., 2007, 2015; McNabb and Hock, 2014). While natural climate variability drives glacier changes to some extent (*e.g.*, Roe and O'Neal, 2009), anthropogenic climate change is increasingly implicated in the observed widespread retreat of glaciers and ice sheets (Roe et al., 2017; Christian et al., 2022).

Monitoring glacier advance and retreat is a critical component of our understanding of glacier change. Historically, methods such as field sketches and ground-based and aerial photography have helped scientists track glacier change, and these methods continue to be used today. However, these field-based methods are limited by the impracticalities of monitoring large numbers of glaciers, monitoring at frequent intervals, monitoring over extended periods of time, and accessing the often remote and inhospitable environments in which these glaciers exist. Publicly available satellite data have enabled the monitoring of glacier and ice sheet conditions over much broader spatial scales than are feasible in field studies, and on time scales ranging from days to decades. The Landsat mission, first launched in 1972, is the longest-running earth-observing satellite mission, and has provided half a century of earth observations. Over time, the quality and quantity

of earth-observing satellites has increased. Now, constellations of public and commercial satellites monitor the Earth and its ice masses at high spatiotemporal resolution at a variety of wavelengths. This dissertation capitalizes on the capabilities of earth-observing satellites to explore measurements of glacier terminus changes in Greenland and Alaska on a range of time scales.

1.2 Research methods

In this dissertation, I use observations of glacier extents to explore modern glacier changes in Greenland and Alaska. I manually digitized glacier extents from optical (Landsat 1–8) and synthetic aperture radar (Sentinel-1A/B) satellite imagery to produce time series of glacier length and area. These time series span spatial scales ranging from a peninsula to an ice sheet, and temporal scales ranging from days to decades.

1.3 Organization of the dissertation

This dissertation is organized into five chapters. It begins with this introduction and ends with a summary and suggestions for future work. The three middle chapters are scientific papers.

Chapter 2 is published in *The Cryosphere* as **Multi-decadal retreat of marine-terminating outlet glaciers in northwest and central-west Greenland** (Black and Joughin, 2022). This paper catalogues annual terminus positions for 87 marine-terminating outlet glaciers in northwest and central-west Greenland from 1972 to 2021 and explores climatic factors contributing to regional glacier retreat. The results show that regional terminus retreat accelerated around 1996, and that terminus retreat is most sensitive to increased runoff and ocean temperatures. The supplement for this paper can be found in Appendix A.

Chapter 3 is published in *Journal of Glaciology* as **Maritime glacier retreat and terminus area change in Kenai Fjords National Park, Alaska, between 1984 and 2021** (Black and Kurtz,

2022b). This project grew out of a research internship with the National Park Service in the summer of 2020. The paper catalogs spring and autumn terminus positions for 19 maritime glaciers in Kenai Fjords National Park between 1984 and 2021 and explores differences in glacier behavior based on whether the glaciers were tidewater, lake-terminating, or land-terminating. The results show that most glaciers retreated substantially, while those that did not were predominantly tidewater, and that regional ice area loss was nearly evenly distributed between the terminus and the lateral margins of the glaciers. The supplement for this paper can be found in Appendix B.

Chapter 4 will be submitted to *The Cryosphere* in September 2022 as **Weekly to monthly terminus variability of Greenland's marine-terminating outlet glaciers**. This paper characterizes the timing and magnitude of seasonal terminus position variability for 219 marine-terminating outlet glaciers in Greenland at weekly to monthly temporal resolution between 2015 and 2021. The results show that seasonal terminus position variability is common, that retreat typically occurs from mid-May through early October, and that the magnitude of terminus position seasonality for most glaciers is less than 250 m. The supplement for this paper can be found in Appendix C.

Chapter 2. Multi-decadal retreat of marine-terminating outlet glaciers in northwest and central-west Greenland

Abstract. The retreat and acceleration of marine-terminating outlet glaciers in Greenland over the past 2 decades have been widely attributed to climate change. Here we present a comprehensive annual record of glacier terminus positions in northwest and central-west Greenland and compare it against local and regional climatology to assess the regional sensitivity of glacier termini to different climatic factors. This record is derived from optical and radar satellite imagery and spans 87 marine-terminating outlet glaciers from 1972 through 2021. We find that in this region, most glaciers have retreated over the observation period and widespread regional retreat accelerated from around 1996. The acceleration of glacier retreat coincides with the timing of sharp shifts in ocean surface temperatures, the duration of the sea-ice season, ice-sheet surface mass balance, and meltwater and runoff production. Regression analysis indicates that terminus retreat is most sensitive to increases in runoff and ocean temperatures, while the effect of offshore sea ice is weak. Because runoff and ocean temperatures can influence terminus positions through several mechanisms, our findings suggest that a variety of processes – such as ocean-interface melting, mélange presence and rigidity, and hydrofracture-induced calving – may contribute to, but do not conclusively dominate, the observed regional retreat.

2.1 Introduction

The Greenland Ice Sheet has lost significant mass over the last few decades (Enderlin et al., 2014; Shepherd et al., 2020) as many of its glaciers have retreated (Hill et al., 2017; Howat and Eddy, 2011; King et al., 2020; Moon and Joughin, 2008; Murray et al., 2015), and ice flow has accelerated (Joughin et al., 2010; Moon et al., 2012; Rignot and Kanagaratnam, 2006). Recent

Greenland ice loss has contributed to rates at times approaching 1 mm a^{-1} of global sea-level rise (Shepherd et al., 2020), with the contribution from northwest and central-west Greenland combined representing nearly half of the cumulative contribution from Greenland to sea-level rise since 1972 (Mouginot et al., 2019). Although surface mass balance has dominated Greenland's mass loss in the past 2 decades, over half of the mass loss in northwest and central-west Greenland is currently due to ice discharge (Mouginot et al., 2019), which has accelerated since 2000 in this region (King et al., 2020).

Changes in ice discharge are often related to changes to glacier terminus positions, with terminus retreat into deeper water driving acceleration and upstream thinning (Howat et al., 2008; Joughin et al., 2008b). Because of the relationship between the terminus position and calving rate, initial perturbations that increase calving can trigger further glacier retreat. While glacier retreat and acceleration are generally linked to changes at the terminus, it remains unclear which processes are most responsible for controlling perturbations to calving rates and subsequent terminus retreat (Straneo et al., 2013).

The recent acceleration and retreat of Greenland outlet glaciers have been attributed to warmer ocean temperatures (Fahrner et al., 2021; Holland et al., 2008; Howat et al., 2008; Morlighem et al., 2016; Rignot et al., 2012; Slater et al., 2019; Wood et al., 2021), to changes in the characteristics of sea ice and mélange – icebergs bound by a sea-ice matrix (Amundson et al., 2010; Carr et al., 2013; Cassotto et al., 2015; Foga et al., 2014; Joughin et al., 2008a; Moon et al., 2015), and to increased melting and crevassing associated with warming air temperatures (Benn et al., 2007; Nick et al., 2013; van der Veen, 1998). In turn, responses to these forcings are modulated by geometric factors associated with individual glaciers such as bed topography and fjord width (Carr et al., 2015; Catania et al., 2018; Felikson et al., 2021; Schild and Hamilton,

2013); for many glaciers, these modulating factors necessitate detailed records of terminus position changes in order to identify the importance of different forcing mechanisms on decadal-scale outlet glacier changes across a large area.

Most previous studies of Greenland outlet glacier terminus positions have been temporally or spatially limited. Some studies cover the entire ice sheet for over a decade but map termini only decadally or in non-consecutive years (Howat and Eddy, 2011; Moon and Joughin, 2008). Other studies map termini more frequently but only for a small sector of the ice sheet (Bjørk et al., 2012; McFadden et al., 2011; Moon et al., 2015) or for a few specific glaciers (Holland et al., 2016; Joughin et al., 2008b; Larsen et al., 2016; Motyka et al., 2017; Schild and Hamilton, 2013). Murray et al. (2015) mapped terminus positions at high spatial and temporal resolutions but only for a single decade. More recent studies have attempted to fill these observational gaps with ice-sheet-wide analyses of annual terminus positions spanning multiple decades (Fahrner et al., 2021; King et al., 2020; Wood et al., 2021), although they come to differing conclusions about the drivers of observed terminus retreat.

In this paper, we analyze glacier change at a high spatiotemporal resolution by constructing a multi-decadal (49 years) record of annual terminus positions for 87 marine-terminating outlet glaciers in northwest and central-west Greenland. This record allows us to identify the behavior of individual glaciers as well as regional trends in the magnitude and timing of glacier retreat. We compare this regional behavior with climate data – sea-surface and subsurface temperatures; sea-ice concentration; and ice-sheet surface mass balance, precipitation, melt, and runoff – to assess the relative influence of different forcing mechanisms on multi-decadal and annual terminus retreat in this sector of Greenland. It is important to note that we do not account for the effect of geometric

factors such as bed topography on modulating the retreat of individual glaciers, as we instead focus on terminus retreat in connection with regional climate trends.

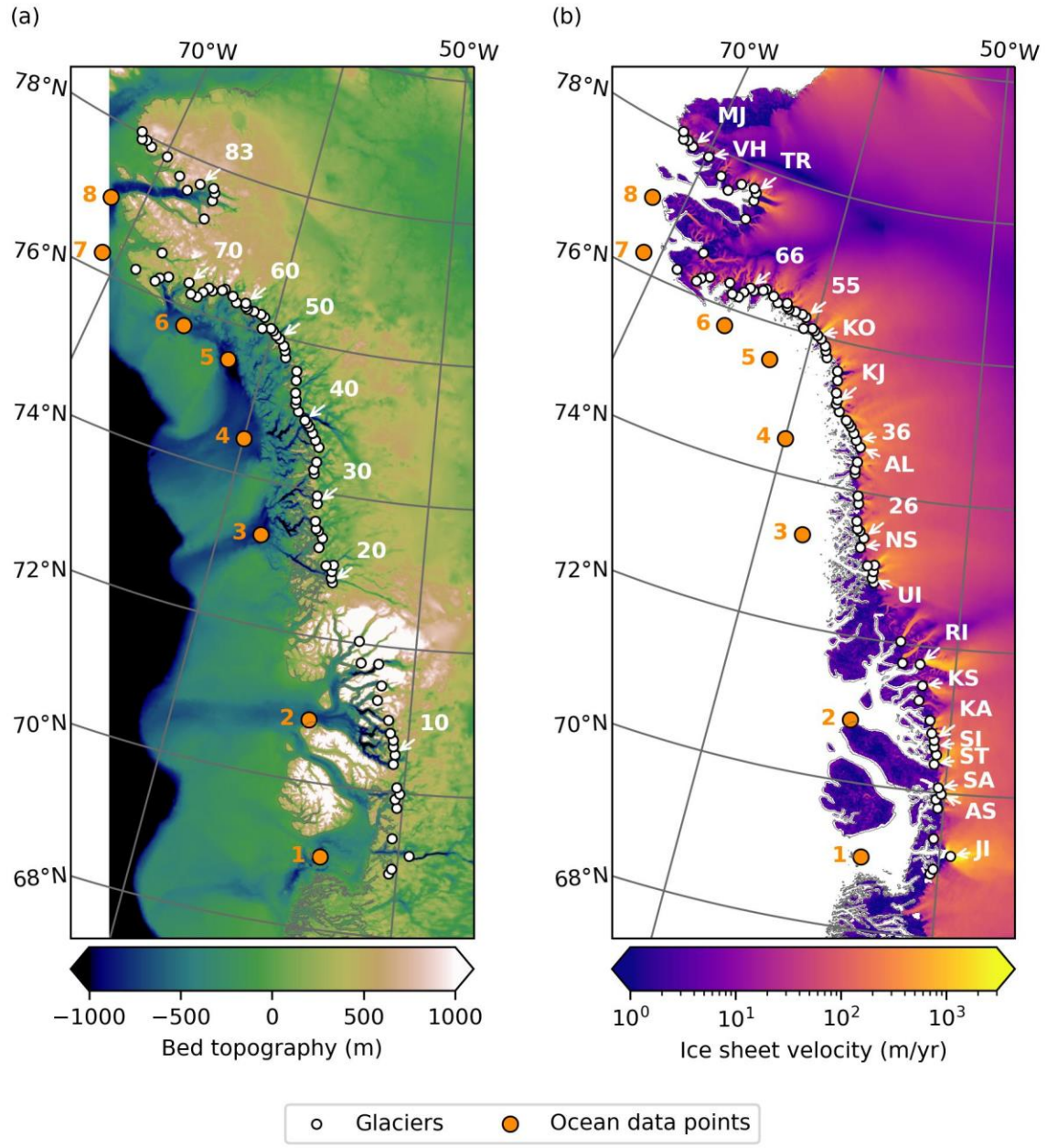

Figure 2.1: Map of study area in northwest and central-west Greenland.
Map of study area, showing individual glacier locations (white) and points where ocean data were acquired (orange, numbered). Glacier labels are (a) every 10th glacier, numbered, and (b) specific glaciers named in the paper, abbreviated as follows: Jakobshavn Isbræ (JI), Alianaatsup Sermia (AS), Sermeq Avannarleq (SA), Store Gletsjer (ST), Sermilik Isbræ (SI), Kangilleq (KA),

Kangerlussuup Sermia (KS), Rink Isbræ (RI), Upernavik Isstrøm (UI), Naajarsuit Sermiat (NS), unnamed glacier no. 26 (26), Alison Glacier (AL), unnamed glacier no. 36 (36), Kjer Gletsjer (KJ), Kong Oscar Gletsjer (KO), unnamed glacier no. 55 (55), unnamed glacier no. 66 (66), Tracy Gletsjer (TR), Verhoeff Gletsjer (VH), and Morris Jesup Gletsjer (MJ). Basemaps are (a) bed topography from BedMachine Greenland V3 (Morlighem et al., 2017a, b) and (b) ice-sheet velocity from MEaSUREs GIMP (Joughin et al., 2016b, 2018a).

2.2 Data and methods

We used 455 synthetic aperture radar (SAR) mosaics and optical satellite images to trace annual terminus positions for 87 marine-terminating outlet glaciers in northwest and central-west Greenland (68.9° N to 78.2° N) (Figure 2.1) from 1972 through 2021.

2.2.1 Satellite images

We digitized terminus positions from SAR images acquired by the European Copernicus Programme's Sentinel-1A and Sentinel-1B and the Canadian Space Agency's Radarsat-1 satellites for 13 of the 49 years in our record. These radar satellites are able to image the surface regardless of clouds or darkness. For the most recent 7 years (2014/15 through 2020/21), we traced terminus positions in mosaics of Copernicus Sentinel-1A and Sentinel-1B images (Joughin et al., 2016a). These mosaics are typically created from images acquired in the early February of their respective years and have a 25 or 50-m product-dependent resolution. Radarsat-1 mosaics were used to trace terminus positions for six winters (2000/01, 2005/06–2008/09, 2012/13) (Joughin et al., 2015; Moon and Joughin, 2008). These mosaics are formed from images collected from October through March and have nominal resolutions of 20 m.

For the remaining 36 years in our record, we used imagery from all Landsat missions to map terminus positions. We also used Landsat imagery to map individual glacier termini where they were missing from or indiscernible in the SAR imagery. We prescreened images in the USGS

Global Visualization Viewer (GloVis) to confirm that glaciers of interest were not obscured by clouds and that the images were georeferenced well. We continued to use Landsat 7 images after the instrument's scan-line corrector failure in 2003 as Landsat 5 images were typically unavailable over our study area during this period, although we kept only images which retained a sufficient number of data to map the terminus. In those images, we digitized across the scan-line corrector gaps when they crossed a glacier terminus (Figure A. 1); comparison of temporally close images with different data gaps indicates that this method only marginally increases errors. In all, the scan-line corrector gaps affected 348 terminus traces (9.7% of the dataset). Due to winter darkness, we could not select images from the same time of year as the SAR mosaics; instead, we chose images as close to winter as possible, with a preference for spring over autumn to capture a more winter-like state to reduce the effects of seasonal variation (Figure 2.2). As a result, the majority of the Landsat images we used were collected in spring (March–May). Because of the difficulty in finding sunlit, cloud-free imagery, however, we had to use data from other periods, so all months except January and December are represented. For some glaciers there are several years with missing data. The image resolution ranges from 15 m (Landsat 8 panchromatic band) to 60 m (Landsat 1-5 Multispectral Scanner). We digitized termini using the panchromatic band for Landsat 7 and Landsat 8, and using a single band that provided high image contrast (typically band 2) for Landsat 1–Landsat 5.

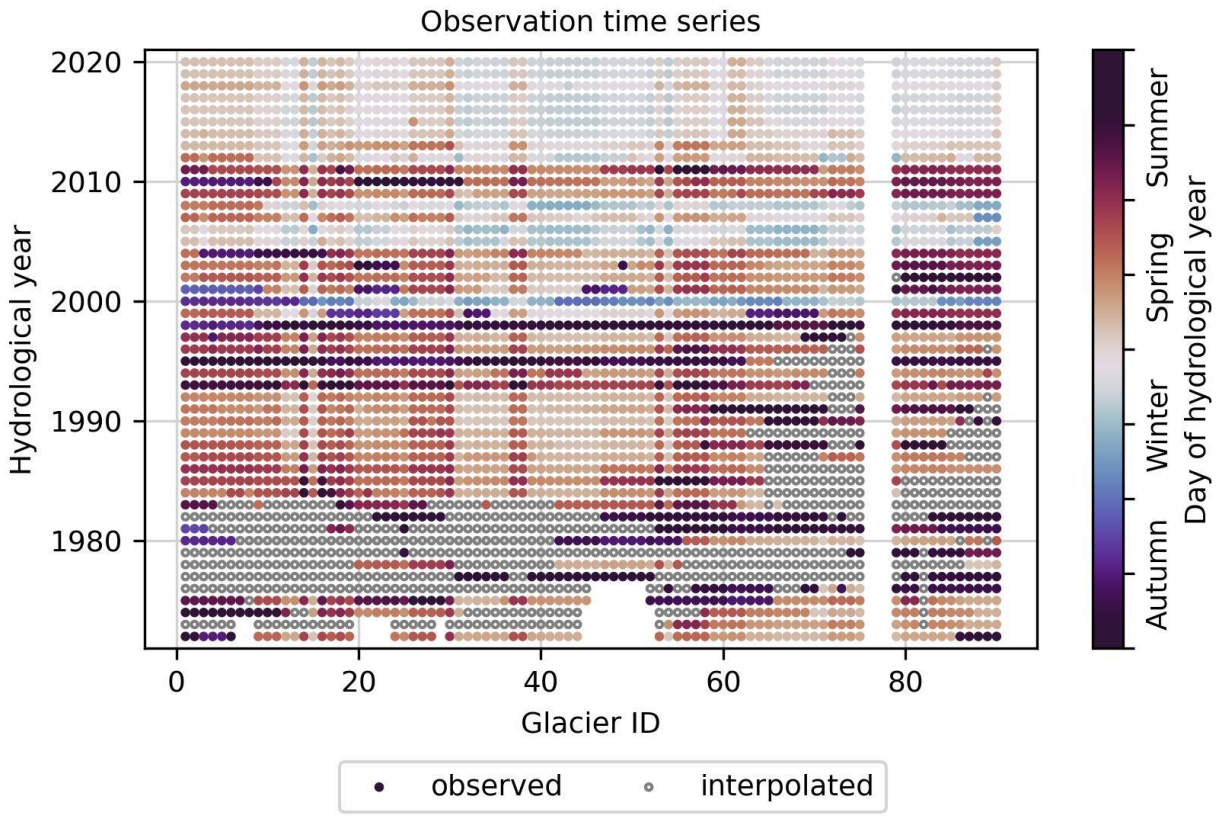

Figure 2.2: Glacier observation time series.
Years in which a terminus position was observed (filled circles) for each glacier, colored by the season of the observation. If a terminus position was not observed, an estimated position was interpolated (open circles) from prior and subsequent observations to use in annual analyses. Glacier nos. 76-78 are not shown because they are not ice-sheet outlet glaciers and therefore are not included in this study.

2.2.2 Terminus positions

Using ArcGIS, we manually traced annual terminus positions from the radar and Landsat imagery. This dataset builds on a preexisting dataset covering six winters between 2000 and 2013 (Joughin et al., 2015; Moon and Joughin, 2008). The study area ranges from Saqqarliup Sermia (68.9° N, 50.3° W; ~35 km southwest of Jakobshavn Isbræ) to Bamse Gletsjer (78.2° N, 72.7° W) (Figure 2.1). Individual glacier names and coordinates are detailed in Table A. 1. To focus our analysis on glaciers that produce substantial ice discharge, we limited our analysis to marine-terminating outlet

glaciers that are at least ~1.5 km wide at the terminus and are flowing at a rate of at least ~1000 m a^{-1}. We traced each glacier's terminus position once per hydrological year (September 1 through August 31; Ettema et al., 2009) in every year for which suitable imagery was available. We used winter or near-winter imagery whenever possible as indicated by Figure 2.2.

Errors in terminus position may arise from both the imagery used and the digitization process. The primary sources of errors introduced by the image data are the uncertainties in position after orthorectification and georeferencing. To reduce such errors, candidate images were compared with control images and discarded if they were noticeably offset or distorted. Manual digitization also introduces errors, which are exacerbated by poor image resolution and image artifacts (such as shadows or an indistinct transition from glacier to mélange) (Joughin et al., 2015). If a terminus position was ambiguous in one image, it was flagged during tracing and compared with close-in-time images from the same satellite platform or other satellite platforms when possible. Digitization errors are typically comparable to the image resolution; for example, a 25 m error for a Landsat 7 image with a 30 m resolution (Moon et al., 2015).

In addition to the errors associated with digitization of the images, there is additional uncertainty introduced by sampling seasonal variability at different times of year. For the terminus positions mapped from Landsat imagery, it was not possible to obtain sunlit and cloud-free images over each glacier at the same time every year (Figure 2.2). This timing variation complicates the year-to-year comparison at a glacier, which might include seasonal variability in the terminus position. Such seasonal variability could produce some short-term deviations in our data; for example, Moon et al. (2015) found a mean annual terminus range of 610 m for a subset of our study glaciers. However, the data collection season is largely consistent across each of our glaciers (Figure 2.2), and because these seasonal errors are not independent, they tend to cancel out over longer periods.

Since we mostly focus on decadal-scale trends, issues of seasonal sampling should not greatly affect our results.

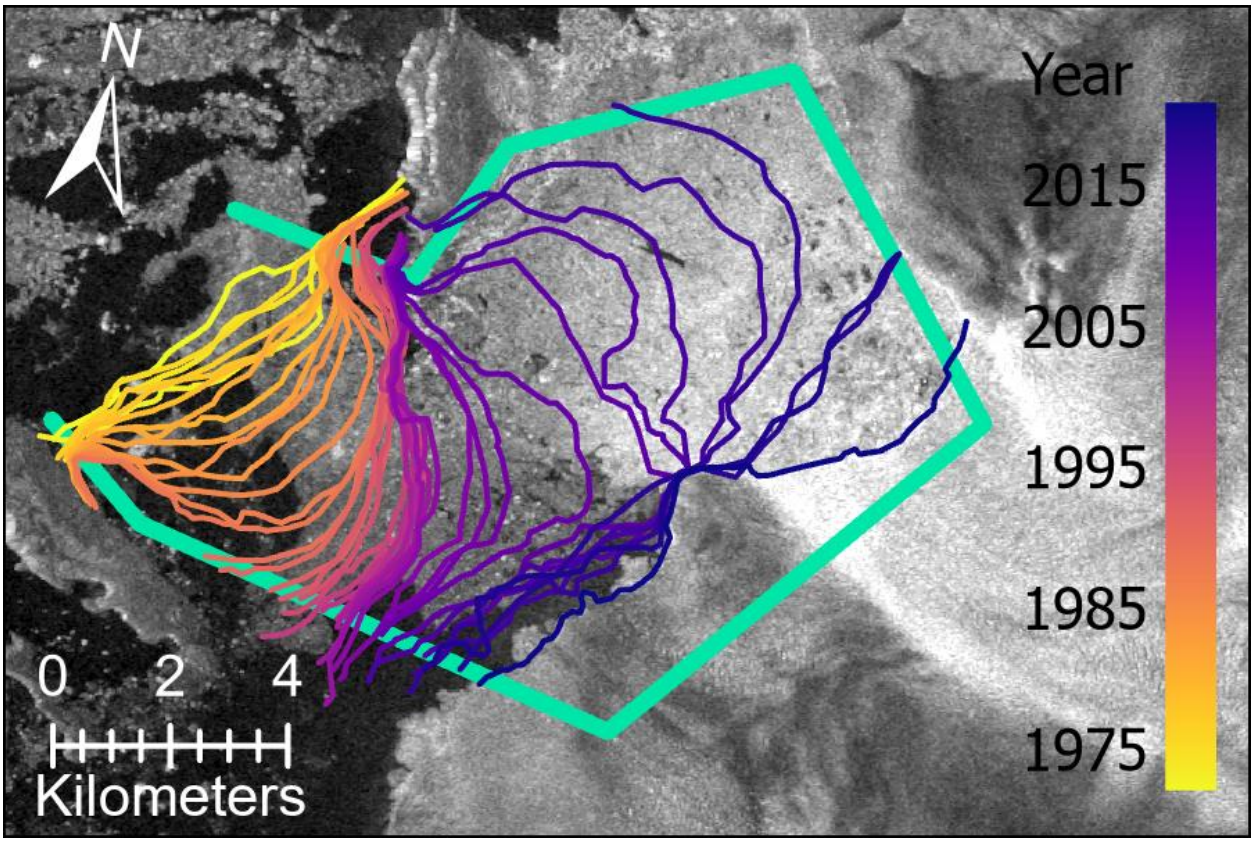

Figure 2.3: Illustration of terminus traces and box method.
Illustration of terminus traces and box method for Kjer Gletsjer (no. 42). Each trace intersects the glacier's box (green) to form a closed polygon. The areas of sequential polygons are differenced to create a time series of glacier area change. The basemap is a Sentinel-1 SAR mosaic from February 4–9, 2020.

2.2.3 Glacier change measurements

We calculated glacier area change over time using the box method (Moon and Joughin, 2008). Each glacier has a static, open-ended reference box (polygon) that approximately delineates the main region of ice flow. The box sides are roughly parallel to ice flow, and the 'back' of the box is perpendicular to ice flow at an arbitrary location up-glacier of the extent of maximum observed

terminus retreat (see example in Figure 2.3). Where a terminus trace intersects the open end of the box, the polygon is closed, and the area of that polygon represents the glacier's reference area at that point in time. Repeating this process for each terminus trace for a glacier forms a time series of reference areas, from which we determine the annual area change. While the areas are arbitrarily determined by the box size, the area differences between successive terminus traces represent the annual gain or loss of area. By focusing on the area change between measurements rather than the absolute area of each measurement, we can ignore the arbitrariness of how the boxes are drawn, as well as any small regions of stagnant ice that may be included within the box boundaries. There is a small error associated with these area-change measurements because the boxes do not completely conform to the glacier sides.

As length change can provide a more intuitive measure of retreat than area change, we determine the nominal length change by scaling the area change by the average width of the box to obtain an approximate length change. This measurement should be interpreted as a proxy for length change rather than an exact measurement. Compared to the centerline method of measuring length change, this method is less sensitive to uncertainties in the centerline position at the terminus.

In years when no observations were made, we linearly interpolated between the prior and subsequent observations to estimate glacier length and area during the missing years (Figure 2.2). For glaciers with missing observations at the beginning of the record, we did not interpolate prior to the first observation in the record. The largest temporal gap interpolated is 9 years (1975/76 through 1983/84), at Sermeq Avannarleq (no. 8). Most temporal gaps are in the 1970s and early 1980s, with additional gaps into the 1990s for some high-latitude glaciers, and there are no temporal gaps after 2002.

Because it is difficult to compare changes in area between glaciers of different sizes, we also determined the percent area change over time for each glacier. For each individual glacier area time series, we normalized the minimum observed glacier area to 0 and the maximum observed glacier area to 1, and linearly scaled the other measured areas between those set points. This method normalizes every glacier's area change to the same 0–1 scale, allowing straightforward comparison of size changes between different glaciers. Because the equivalent length is simply a scaled area, the results are identical for area and length.

To pinpoint the timing of changes in glacier area and length, we performed a break-point analysis on the time series for each glacier. We fit each time series with a piecewise linear function with two segments (Jekel and Venter, 2019); the break point between the two segments corresponds to a year in the time series that is the best fit for approximating the time series as a two-segment piecewise linear function. We performed an *F* test to determine whether the piecewise linear function was statistically a better fit than a single linear regression and discarded any break points that were not statistically significant ($p<0.05$).

2.2.4 Climate data

Earlier work has shown that climate-related processes including terminus ablation and undercutting (driven by ocean warming) (Holland et al., 2008; Motyka et al., 2011; Slater et al., 2019; Rignot et al., 2012; Wood et al., 2021), mélange rigidity (driven by changes in ocean temperature, sea-ice concentration, and/or runoff) (Carr et al., 2017; Joughin et al., 2020; Moon et al., 2015; Sohn et al., 1998; Todd and Christoffersen, 2014), and enhanced hydrofracture (driven by changes in runoff and surface mass balance) (Benn et al., 2007; Nick et al., 2010) may affect terminus position. Hence, we acquired several ice-sheet and oceanographic datasets in order to compare our glacier terminus position changes with climatic factors. For each variable and dataset,

we considered the annual and decadal mean values. For the ice-sheet variables, we considered the annual mean at a fixed location near the front of each glacier, as well as the population annual and decadal means. For the oceanographic data, due to lack of reliable long-term data in narrow fjords, we used offshore observations as a proxy for fjord conditions. We used eight points offshore (Figure 2.1), selected to be representative of clusters of glaciers: Disko Bay, Uummannaq Fjord, Upernavik Icefjord and north, south Melville Bay–Wilcox Head, central Melville Bay, north Melville Bay/Cape York, Wolstenholme Bay/Thule, and Inglefield Fjord (coordinates for each point are detailed in Table A. 2).

Ice-sheet surface mass balance, snowfall, rainfall, meltwater production, and runoff were extracted from the Modèle Atmosphérique Régional (MAR), Version 3.11, on a 6km x 6km grid over the period 1979–2020 (Fettweis et al., 2017).

Sea-surface temperatures came from the NASA JPL Estimating the Circulation and Climate of the Ocean (ECCO) consortium ocean circulation model, Version 5 (Forget et al., 2015; Zhang et al., 2018), on a 1/3° x 1/3° grid over the period 1992–2017, and the merged Hadley-OI sea-surface temperature and sea-ice concentration dataset (Hurrell et al., 2008; Shea et al., 2020), on a 1° x 1° grid over the period 1972–2020.

We also obtained subsurface temperatures from ECCO for most of our study area. In the Disko Bay area we used field observations from the ICES Dataset on Ocean Hydrography (ICES, 2014), collected over the period 1977–2016 by the Greenland Institute of Natural Resources. For both datasets, subsurface temperatures were averaged over the lower 60% of the water column in order to capture warm water at depth while excluding the near-surface mixed layer. For the ECCO data, we applied a temperature correction to bring the data in line with Wood et al. (2021) (see Appendix A).

Sea-ice concentration came from the merged Hadley-OI dataset, as well as the NOAA/NSIDC Climate Data Record of Passive Microwave Sea Ice Concentration, Version 3 (Meier et al., 2017; Peng et al., 2013), on a 25km x 25km grid over the period 1978–2019. For the sea-ice concentration, we calculated the annual duration of the period when sea-ice concentration exceeds 15%, as well as the seasonal mean sea-ice concentration.

2.3 Results

We produced a comprehensive multi-decadal dataset of terminus positions for glaciers in our study area, and collected climate data both near the termini of these glaciers and in the ocean offshore of clusters of these glaciers.

2.3.1 Terminus positions

We created a dataset of 3606 annual terminus positions for our 87 selected glaciers from 1972–1973 through 2020–2021 (see example in Figure 2.3). The median number of annual observations per glacier is 41, and nearly all glaciers were observed in 38 to 46 of the 49 years examined. Only three glaciers have fewer (33–34) observations; these glaciers are located just south of Thule Air Base and have limited imagery available in the 1980s and early 1990s. After interpolating area changes between glacier observations, the first year with either an observation or an interpolation available for each glacier is 1977–1978. Therefore, our glacier analyses start in this year except where noted.

2.3.1.1 Terminus behavior

The majority of the glaciers in our study area retreated between 1977 and 2021. The cumulative area loss of all of these glaciers is 1067 km^2, equivalent to a cumulative retreat of 287 km. The individual area and length changes are plotted in Figure 2.4 with glaciers with the greatest change

broken out separately. We identify these dominant glaciers as those with a net change falling more than 2 standard deviations beyond the population mean, which yields four glaciers that dominate the area change: Jakobshavn Isbræ (no. 3; -130.9 km^2), Alison Glacier (no. 35; -59.4 km^2), Kjer Gletsjer (no. 42; -81.5 km^2), and Tracy Gletsjer (no. 81; -58.7 km^2). These glaciers together are responsible for 31.0% of the total area loss. Five glaciers dominate the length change: Jakobshavn Isbræ (-16.9 km), Alison Glacier (-14.7 km), Kjer Gletsjer (-14.7 km), Tracy Gletsjer (-14.0 km), and one unnamed glacier (no. 36; -11.1 km). These glaciers are cumulatively responsible for 24.9% of the total retreat. For the remaining glaciers, the mean area change is -8.9 km^2 and the mean length change is -2.6 km. Net area and length changes for individual glaciers are detailed in Table A. 3.

A total of 15 glaciers were stable in that the net changes in area were within 2 standard deviations of their respective observed interannual variability, and no glaciers advanced significantly over the observation period. The 15 stable glaciers are as follows: Alianaatsup Sermia (no. 7); Sermeq Avannarleq (no. 8); Store Gletsjer (no. 9); Sermilik (no. 11); Kangilleq (no. 12); Kangerlussuup Sermia (no. 16); Rink Isbræ (no. 17); Upernavik Isstrøm (no. 21); Naajarsuit Sermiat (no. 25); Kong Oscar Gletsjer (no. 51); Verhoeff Gletsjer (no. 86); Morris Jesup Gletsjer (no. 87); and unnamed glacier nos. 26, 55, and 66.

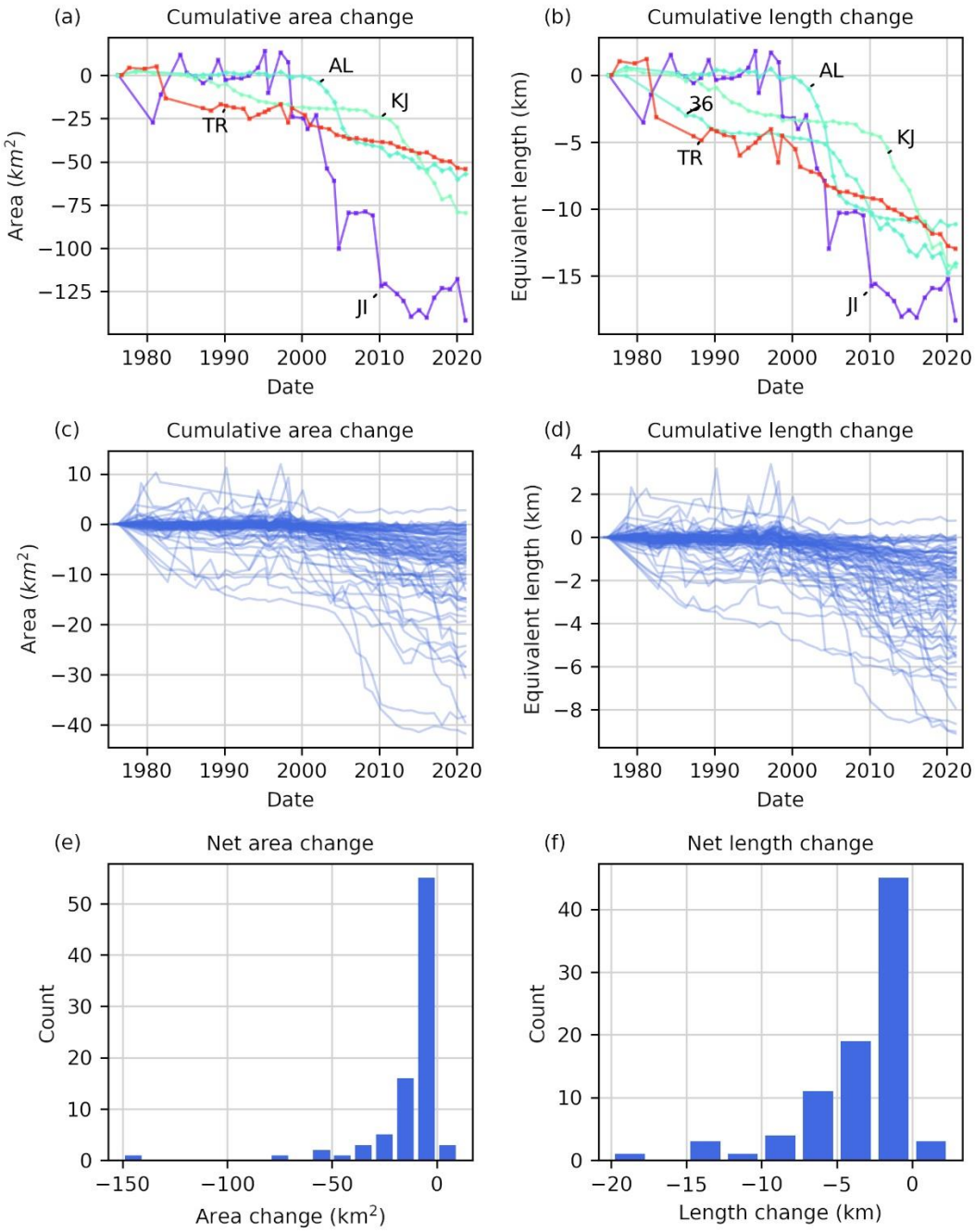

Figure 2.4: Cumulative and net area and length change for glaciers in this study.
Cumulative (a) area change and (b) length change for large glaciers that dominate the total observed change. Glacier changes in each plot are labeled using the abbreviation scheme in Figure 2.1. The color map follows the order of the glaciers (from south to north), so glaciers with similar colors are spatially closer together. For all other glaciers, cumulative (c) area change and (d) length change are provided but not distinguished by glacier. The final net (e) area change and (f) length change are reported as histograms.

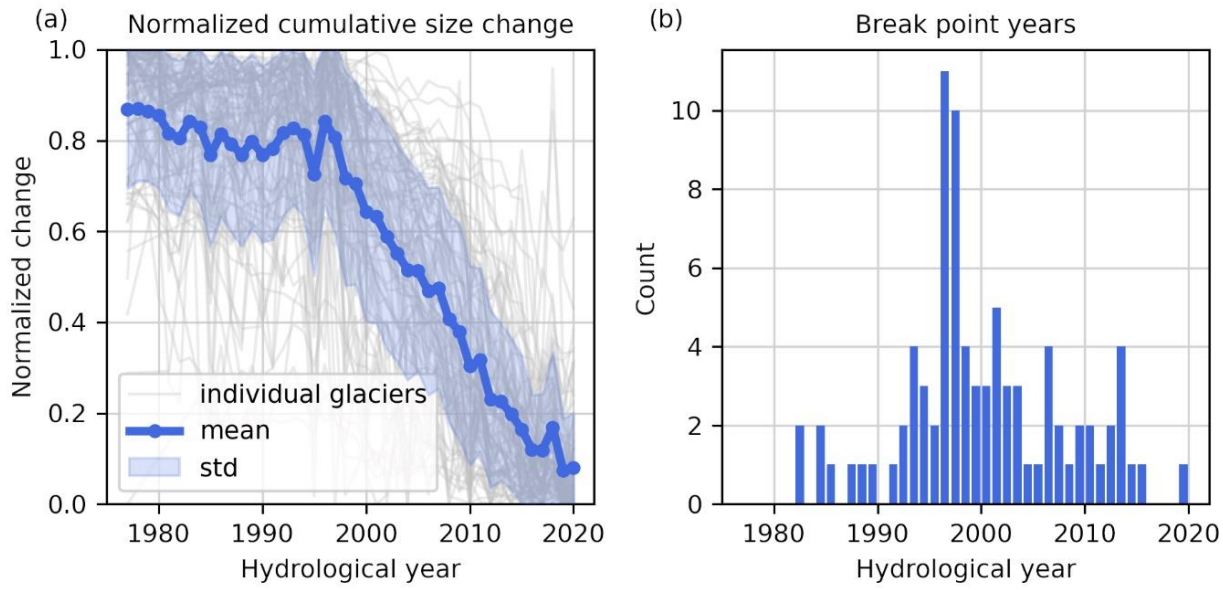

Figure 2.5: Break-point analysis of timing of glacier change.
Break-point analysis to identify the onset of increased terminus retreat rates. (a) Glacier cumulative area change is normalized such that for each glacier the greatest observed extent is 1 and the smallest observed extent is 0 so that glaciers of all sizes are placed on a common scale. Each glacier's cumulative change is then approximated as a two-segment piecewise linear function, and for cases where the piecewise linear function is statistically better than a linear regression, we compute (b) a histogram of the break-point year between the two segments.

2.3.1.2 Timing of change

Because a small number of glaciers tend to dominate the overall trends in glacier changes, we scaled each glacier's length and area to a 0–1 scale as described above in order to consistently compare the relative timing of each glacier's behavior (Figure 2.5a). The resulting data are noisy, so to better identify overall trends we computed the mean and standard deviation of the scaled glacier changes (blue overlay in Figure 2.5a). Of the observed mean size change (area or equivalent length), ~4% occurs each decade before 1996, and ~31% occurs each decade after 1996. The population of glaciers notably readvanced in 2017 and 2018, but began to retreat again in 2019.

We performed a break-point analysis (see Sect. 2.2.3) for each glacier's area time series (Figure 2.5b). The step change in retreat rates in around 1996 for the normalized time series is consistent with the time series break points for individual glaciers. The most common break-point years were 1996–1997 and 1997–1998, with additional smaller peaks in break points in the mid-1990s and mid-2000s. The break-point years for each glacier are detailed in Table A. 3.

2.3.2 Climate data

All of the climate variables that we surveyed showed long-term trends consistent with regional climate warming. Most of these variables, in most of the locations that we sampled, also showed a sharp change in their long-term trends between the 1990s and 2000s.

Figure 2.6 summarizes the data from the MAR climate model. While there is considerable interannual variability, the data indicate a net decrease in surface mass balance (Figure 2.6a) and a net increase in both meltwater production (Figure 2.6b) and runoff (Figure 2.6c), with corresponding increases in the annual number of meltwater production days (Figure 2.6d) and runoff days (Figure 2.6e), that have occurred since the late 1970s. The mean surface mass balance was steady in the 1980s and 1990s but dropped by 0.48 m a^{-1} between the 1990s and the 2000s, primarily due to substantial increases in meltwater production (+0.42 m a^{-1}) and runoff (+0.48 m a^{-1}). By contrast, there were only small changes to the mean snowfall (-0.01 m a^{-1}; Figure 2.6f) and the mean rainfall (+0.02 m a^{-1}; Figure 2.6g) from the 1980s to the 2010s. For the 2010s, while the annual surface mass balance anomaly was positive in 2013, 2017, and 2018, it reached its lowest values for the full record in 2019 and 2020. These extremes are reflected in coincident meltwater production and runoff anomalies. For this decade as a whole, the decadal mean surface mass balance anomaly is slightly more negative than that of the 2000s, and the decadal mean meltwater production and runoff continued to increase.

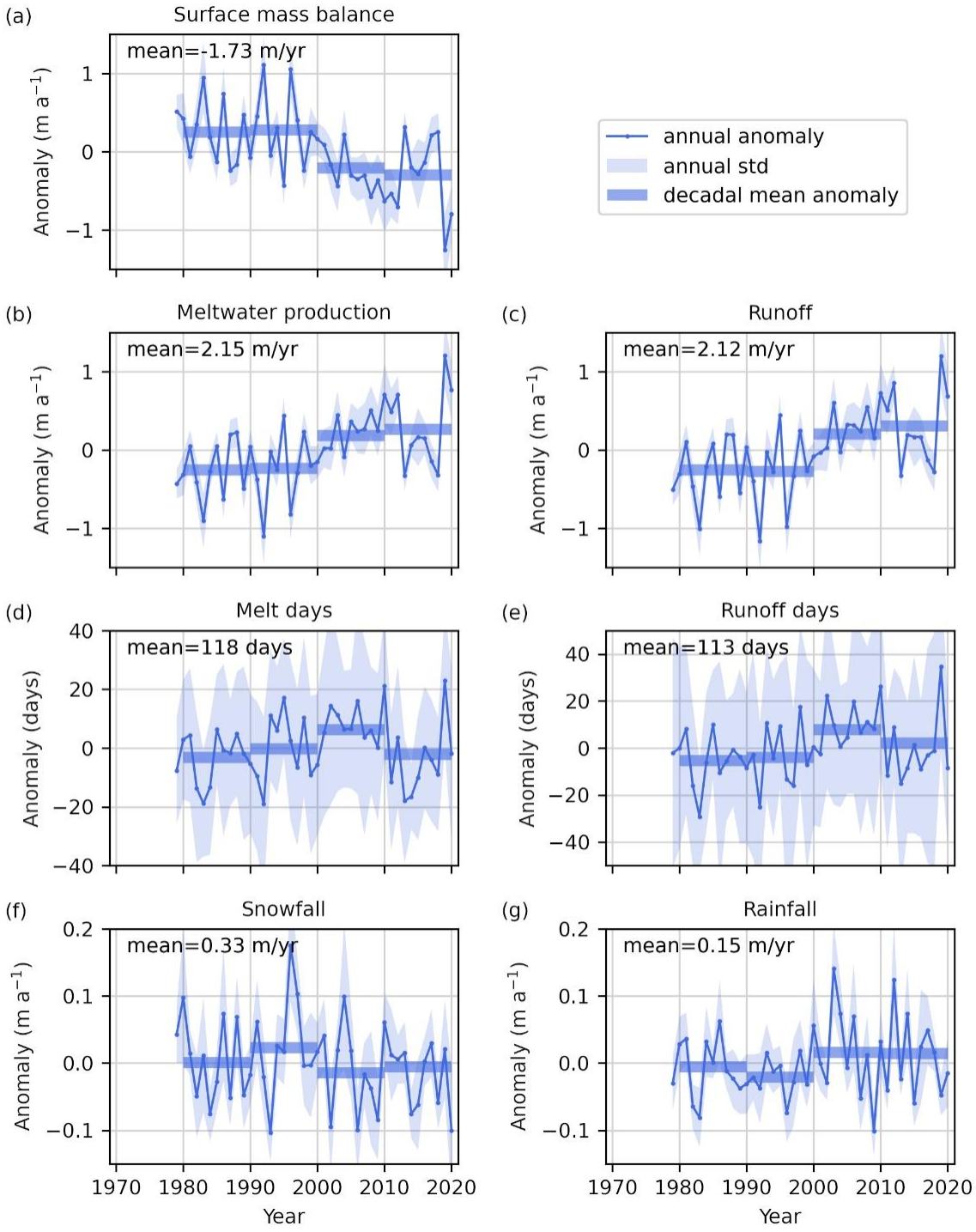

Figure 2.6: Annual and decadal mean MAR data.

Annual and decadal mean anomaly of (a) surface mass balance, (b) meltwater production, (c) number of melt days, (d) runoff, (e) number of runoff days, (f) snowfall, and (g) rainfall, from the MAR climate model, averaged over all glacier fronts in the study area. The mean for each anomaly is reported in each panel.

Like the mean meltwater production and runoff, the mean number of melt days (Figure 2.6d) and runoff days (Figure 2.6e) increased between the 1990s and the 2000s by 7 days and 12 days, respectively. However, instead of continuing to increase in the 2010s, the number of melt and runoff days decreased, suggesting that the net increase in meltwater production and runoff was due to more intense melt events rather than a greater number of melt events.

Figure 2.7a shows that Disko Bay warmed by between 0.21 °C (ICES) and 0.69 °C (ECCO) between the 1990s and 2000s and cooled in 2016–2017 (the final years of the two subsurface temperature datasets). North of Disko Bay (Figure 2.7b-h), the decadal subsurface ocean temperatures followed a continuously increasing trend at every location we sampled. The temperature warmed substantially (0.79–1.07 °C) between the 1990s and 2000s at each of these locations, with a lesser magnitude of warming (0.01–0.45 °C) between the 2000s and the 2010s. The temperature trends, especially between the 1990s and the 2000s, are largely imposed by the corrections from Wood et al. (2021) (see Appendix A).

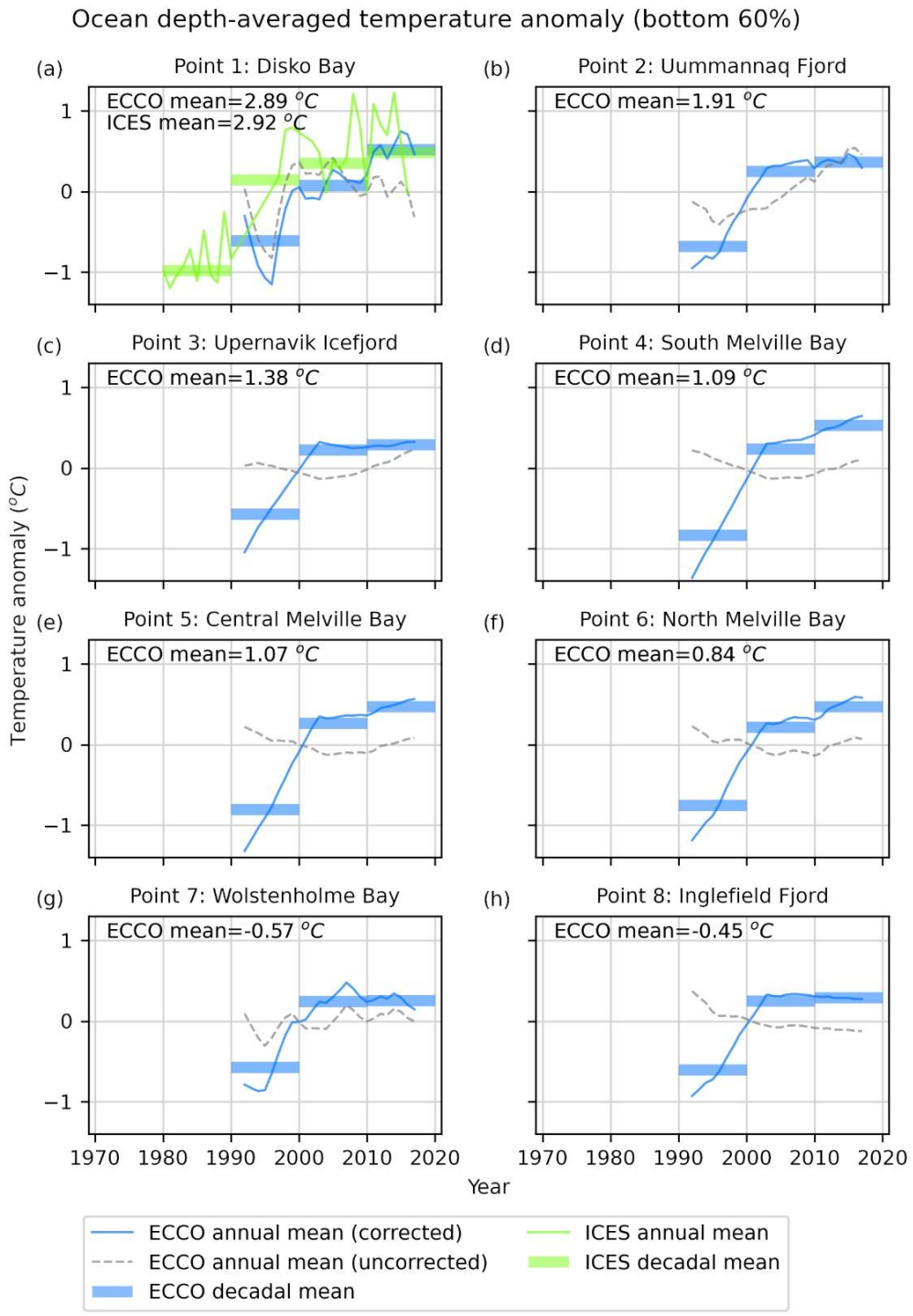

Figure 2.7: Annual and decadal mean deepwater ocean temperature anomaly.
Annual and decadal mean deepwater (bottom 60%) ocean temperature anomaly from ECCO (blue) and ICES (green). Each panel corresponds with an ocean point in Figure 2.1. The mean for each anomaly is reported in each panel. The "decadal" means are not taken over the entire decade in the 1990s (for ECCO) and 2010s due to lack of data.

Figure 2.8 shows that sea-surface temperatures (SST) were relatively steady in the 1970s and 1980s. At some locations the SSTs dipped slightly in the 1990s, followed by a sharp rise (0.57–0.78 °C from ECCO; 0.33–0.81 °C from Hadley-OI) in SSTs in the 2000s at all sites. SSTs in the 2010s were slightly warmer or cooler than in the 2000s, depending on the location and data source, but remained consistently above the pre-2000s temperatures.

Figure 2.9 shows that the annual duration of the sea-ice season (defined as when sea-ice concentration exceeds 15%) has shortened since the 1970s. In particular, from Upernavik Icefjord north to Wolstenholme Bay (Figure 2.9c-g), while the decadal mean sea-ice season length was relatively steady from the 1970s through the 1990s, it decreased by 1 to 2 months between the 1990s and the 2000s and remained relatively steady at the new shorter duration in the 2000s and 2010s. This pattern is borne out in the seasonal sea-ice concentration as well at many locations (Figure A. 2–5).

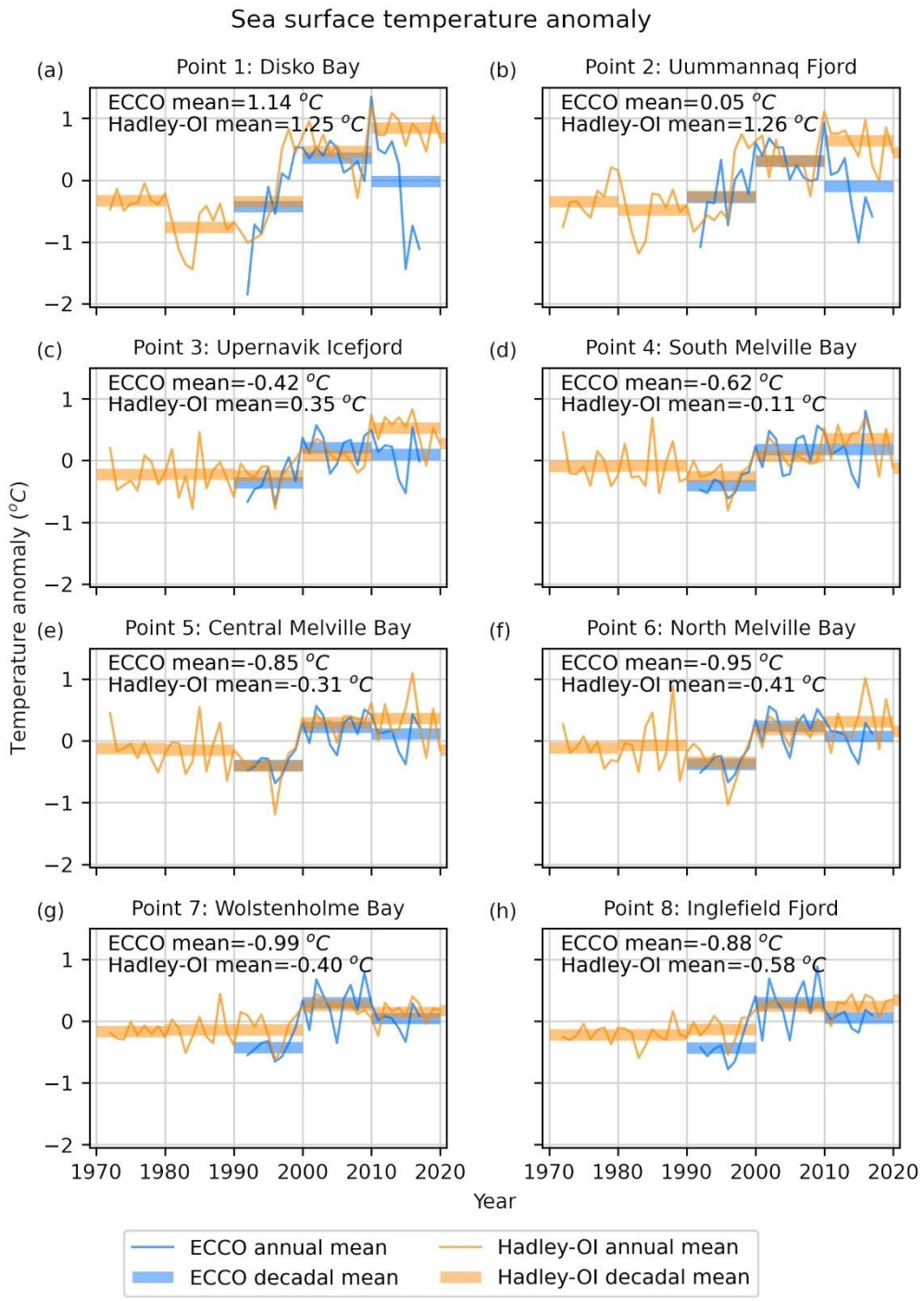

Figure 2.8: Annual and decadal mean sea-surface temperature anomaly.
Annual and decadal mean sea-surface temperature anomaly from ECCO (blue) and Hadley-OI (orange). Each panel corresponds with an ocean point in Figure 2.1. The mean for each anomaly is reported in each panel.

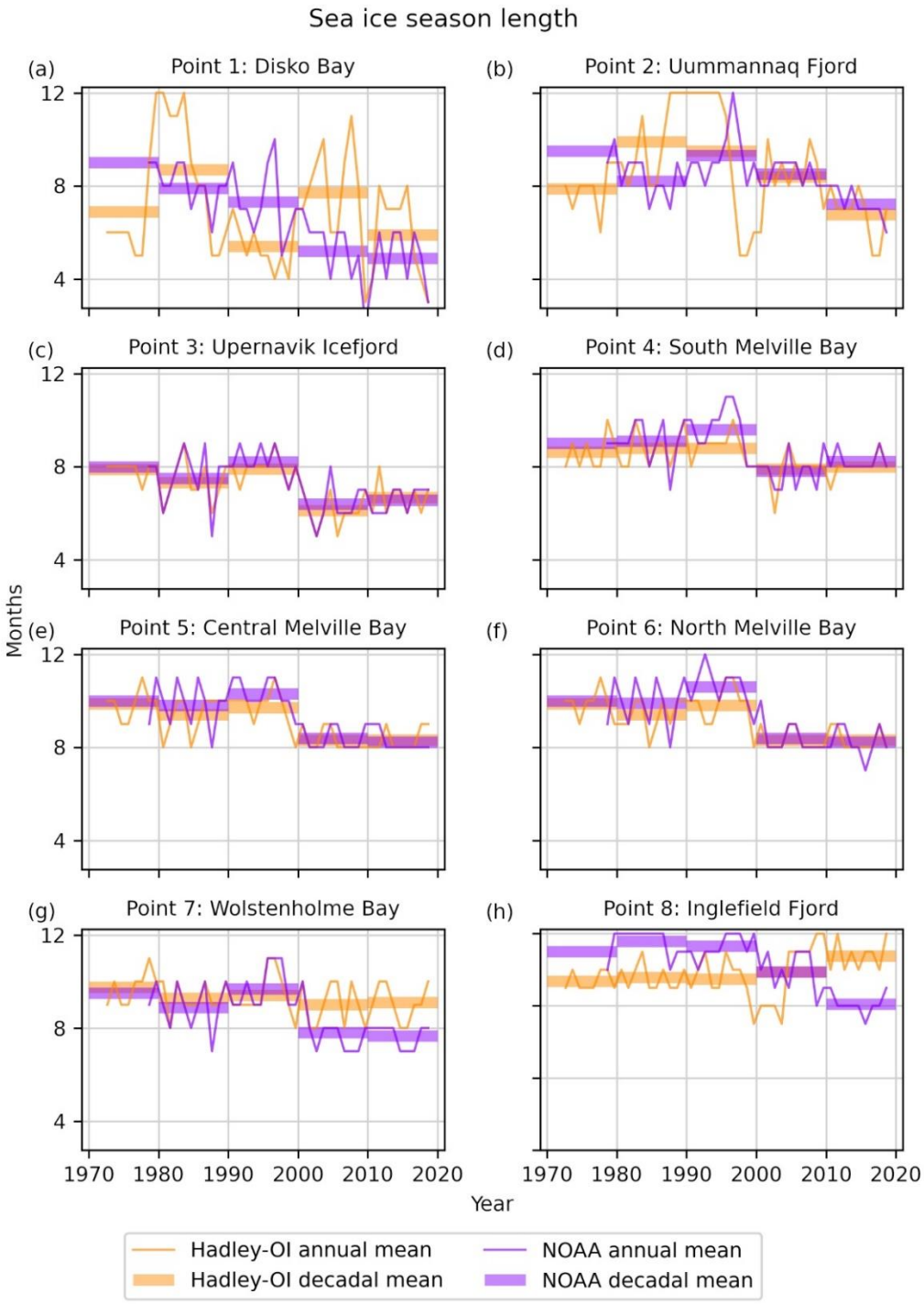

Figure 2.9: Annual and decadal mean duration of sea-ice season.
Annual duration of sea-ice season (when sea-ice concentration is greater than 15%) from Hadley-OI (orange) and NOAA (purple). Each panel corresponds with an ocean point in Figure 2.1.

2.3.3 Regression analysis

We conducted a suite of multiple linear regressions of key climate variables against terminus retreat (Table 2.1), using data from 1992–2017, where we have data available for all variables. We ran two cases with all variables included: one with the corrected ECCO deepwater temperatures, and one with the original uncorrected ECCO deepwater temperatures. The remaining cases systematically drop one of the variables at a time and then include only one type of variable (ocean temperatures, sea ice, runoff). For each case, we report the sensitivity of terminus retreat to each climate variable with 1σ errors, as well as the R^2 value of the regression.

While it is difficult to interpret the results because of multiple correlations between the different parameters, it is clear that runoff has the dominant effect. Overall, terminus retreat appears to be most sensitive to runoff, moderately sensitive to ocean temperatures, and least sensitive to sea ice. For each case, the R^2 value is small, likely due to large interannual variability in the climate variables. When we drop runoff from the regression, the R^2 value drops by 0.098, suggesting that runoff accounts for ~10% of the variance in terminus sensitivity. Aside from runoff, dropping any individual variable seems to have little effect. Although dropping ocean temperatures (surface and deepwater) from the regressions has a small effect, keeping only ocean temperatures accounts for about half as much variance (0.094) as keeping only runoff (0.186). The sea-ice parameter sensitivities are not significantly different from zero, and the effect of dropping them is weak.

Table 2.1: Multiple linear regression of terminus sensitivity to climate variables.

Sensitivities of terminus retreat to different climate variables for a suite of multiple linear regressions, with 1σ error.

Case	Sensitivity to deep water	Sensitivity to SST (km °C^{-1})	Sensitivity to mean annual sea-ice conc.	Sensitivity to sea ice season (km	Sensitivity to snowfall (km	Sensitivity to runoff (km m^{-1})	R^2
All variables	-0.0406 ± 0.029	-0.0515 ± 0.034	-0.0015 ± 0.002	-0.0097 ± 0.012	0.0861 ± 0.162	-0.1458 ± 0.029	0.205
All variables	0.0279 ± 0.022	-0.0931 ± 0.052	-0.0026 ± 0.002	-0.0011 ± 0.012	0.0891 ± 0.162	-0.1526 ± 0.028	0.203
Drop deep water temp		-0.0441 ± 0.033	-0.0010 ± 0.002	-0.0065 ± 0.011	0.0814 ± 0.162	-0.1610 ± 0.027	0.197
Drop SST	-0.0339 ± 0.028		0.0010 ± 0.001	-0.0072 ± 0.012	0.0442 ± 0.160	-0.1447 ± 0.029	0.196
Drop annual sea	-0.0367 ± 0.028	-0.0314 ± 0.020		-0.0121 ± 0.011	0.0631 ± 0.158	-0.1432 ± 0.029	0.203
Drop sea ice season	-0.0360 ± 0.028	-0.0474 ± 0.033	-0.0020 ± 0.002		0.0911 ± 0.161	-0.1464 ± 0.029	0.202
Drop snowfall	-0.0403 ± 0.029	-0.0484 ± 0.033	-0.0013 ± 0.002	-0.0100 ± 0.012		-0.1486 ± 0.029	0.204
Drop runoff	-0.0931 ± 0.028	-0.0474 ± 0.036	-0.0003 ± 0.002	-0.0112 ± 0.012	0.2332 ± 0.168		0.107
Only ocean temps	-0.0887 ± 0.026	-0.0301 ± 0.016					0.094
Only sea ice			0.0030 ± 0.001	-0.0030 ± 0.012			0.047
Only runoff						-0.1683 ± 0.025	0.186

2.4 Discussion

Our measurements (Figure 2.5) show a multi-decadal trend of regional glacier retreat with a step change in the terminus retreat rate from around 1996. Several mechanisms have been proposed as drivers of outlet glacier retreat, including ocean-warming-induced terminus ablation and undercutting, mélange rigidity, and enhanced hydrofracture, all of which can affect calving (Straneo et al., 2013). All of these mechanisms are tied to climatic warming in some sense, whether due to rising air or ocean temperatures, and associated changes in meltwater production, runoff, and sea-ice concentration. Our observed step change in terminus retreat rate was approximately coincident with sharp increases in meltwater production (22%; Figure 2.6b), runoff (26%; Figure 2.6c), deepwater temperature (0.21–1.07 °C; Figure 2.7), and sea-surface temperature (0.33–0.81 °C; Figure 2.8) and a sharp decrease in the duration of the sea-ice season (1–2 months; Figure 2.9). Thus, any or all processes related to these anomalies could have contributed to the terminus retreat rates. Multiple linear regressions suggest that runoff is the dominant contributor to terminus retreat, with ocean temperatures accounting for much of the remaining variance. Offshore sea ice has a small and likely negligible effect.

2.4.1 Observations of regional retreat

The timing of our observed step change in the terminus retreat rate is consistent with previous studies of northwest and/or central-west Greenland that identified accelerated glacier retreat (Carr et al., 2017; Catania et al., 2018; Fahrner et al., 2021; Howat and Eddy, 2011; Wood et al., 2021) and ice speedup and discharge (Joughin et al., 2018b; King et al., 2020) beginning in the middle to late 1990s. Nearly all glaciers in our study region retreated between the onset of this step change and the end of our observations in 2021, in line with other observations of sustained retreat in the 21st century (Bunce et al., 2018; Fahrner et al., 2021; Howat and Eddy, 2011; Murray et al., 2015).

Howat and Eddy (2011) found that between 2000 and 2010, nearly 100% of glaciers in northwest Greenland retreated; although we considered a larger set of glaciers, we found that 85% of our glaciers retreated and 15% were stable over the same time period. Between 2010 and 2020, 74% of glaciers retreated and 22% were stable. In both decades, 69% of glaciers retreated and 9% were stable. Overall, between 2000 and 2020, 86% of glaciers retreated and 14% maintained stable terminus positions.

We observed a brief period of regional advance in 2017 and 2018, which was negated by regional retreat in 2019 (Figure 2.5). This broad pattern of readvance coincides with the readvance of Jakobshavn Isbræ in 2017 and 2018 (Khazendar et al., 2019); however, while Jakobshavn Isbræ remained in a relatively advanced position in 2019 and 2020 and retreated in 2021 (Figure 2.4a,b), the region as a whole began to retreat again in 2019. The regional behavior is coincident with a sustained negative runoff and meltwater production anomaly (and positive surface mass balance anomaly) in 2017 and 2018 with values near the 20th-century mean anomaly. This negative anomaly was followed by the strong positive anomalies in the record in 2019 and 2020 (Figure 2.5a). Although we lack sufficient ocean temperature or sea-ice data during this period to assess a relationship between those factors and regional glacier behavior, our regression analysis indicates that runoff anomalies have the strongest effect on terminus position.

2.4.2 Terminus melting

Ocean subsurface warming and surface warming in Baffin Bay and adjacent fjords have been cited as contributors to regional glacier retreat (Rignot et al., 2012; Slater et al., 2019; Wood et al., 2021) as well as to retreat for individual glaciers (Holland et al., 2008; Khazendar et al., 2019; Motyka et al., 2011; Rignot et al., 2010). Warmer ocean water increases melt at the calving face, and, in conjunction with subglacial discharge plumes, subsurface warming undercuts the terminus

(Motyka et al., 2013; Slater et al., 2015, 2017), which could enhance calving (How et al., 2019; Luckman et al., 2015; Morlighem et al., 2019; Rignot et al., 2015).

Wood et al. (2021) found that ocean thermal forcing switched from a stable period to one of rapid warming between 1997 and 1998, consistent with the timing of the sharp step change in glacier retreat rate we observed. Based on the same ocean dataset, we found that ocean subsurface temperatures increased an average of 0.90 °C coincident with our observed step change in glacier retreat rate (Figure 2.7) and together with sea-surface temperatures were moderately associated with terminus retreat. Wood et al. (2021) identified deep glaciers sitting in warmer water as those that are retreating the most. Terminus response, however, tends to scale non-linearly with depth and deeper termini should be more responsive to any change that induces retreat (Schoof, 2007). As evidence of this effect, we note the strong response to seasonal perturbations on three of Greenland's deepest outlet glaciers (Jakobshavn, Kangerlussuaq, and Helheim), which is large compared to the degree of melting at the terminus (Joughin et al., 2020; Kehrl et al., 2017). Thus, irrespective of the forcing that caused the initial perturbation, a greater response would be expected for the deeper glaciers (>100 m depth), whether the forcing is due to ocean melting or some other process.

Similarly to ocean subsurface temperatures, sea-surface temperatures averaged over all of our subregions also increased (0.58 °C) in concert with accelerated glacier retreat (Figure 2.8). Fahrner et al. (2021) found a significant relationship between sea-surface temperatures and terminus change in northwest Greenland, whereas Murray et al. (2015) found no relationship between retreat and sea-surface temperature in this region. Elsewhere in Greenland, warming sea-surface temperatures have been linked with rapid terminus retreat (Howat et al., 2008).

2.4.3 Mélange rigidity

Models indicate that the absence of a rigid mélange may be more important than ocean-driven melting of the terminus in enhancing glacier retreat (Todd and Christoffersen, 2014). Observations show a correlation between terminus change and sea-ice and mélange conditions (Carr et al., 2017; Moon et al., 2015; Sohn et al., 1998) and that reduced sea ice and mélange formation could have triggered retreat at several Greenland glaciers (Amundson et al., 2010; Howat et al., 2010; Joughin et al., 2008a; Sohn et al., 1998). The presence of a rigid mélange can exert sufficient force to inhibit calving, facilitating seasonal glacier advance (Amundson et al., 2010; Cassotto et al., 2015; Cook et al., 2021; Reeh et al., 2001; Robel, 2017). We observed a sharp reduction in both the duration of the sea-ice season (Fig. 9) and sea-ice concentrations (Figure A. 2–5), coincident with a step change in the regional glacier retreat rate in 1996; however, our regression analysis indicated that offshore sea-ice conditions have only a weak connection with terminus retreat. This suggests that the effect of offshore sea ice on terminus retreat is weak, although we note that the data we sampled are an imperfect proxy for near-terminus sea-ice conditions.

Runoff increases and ocean warming are both coincident with terminus retreat. While these factors also contribute to terminus melt, the majority of the ocean heat in the fjords goes into melting icebergs (thus weakening mélange) rather than the terminus face (Moon et al., 2018; Mortensen et al., 2020). Moreover, the runoff-enhanced iceberg melting lags discharge, causing iceberg melt to peak in late summer and early autumn (Moon et al., 2018). At least for Jakobshavn Isbræ, reductions in mélange rigidity appear to correspond to periods of warmer temperatures at depth in the fjord (Joughin et al., 2020). Warmer sea-surface temperatures, although unlikely to contribute to submarine undercutting of the terminus, may also inhibit sea-ice formation and reduce mélange rigidity. Additionally, the observed increase of 26% in runoff and 11% in the number of runoff

days (Figure 2.6c,e), coincident with the observed step change in terminus retreat rates, may have seasonally contributed to more mobile mélange near the terminus. Thus, the combination of increased runoff, sea-surface temperature, and subsurface temperature together suggests a reduction in mélange presence and rigidity that might have increased calving and retreat.

2.4.4 Enhanced hydrofracture

In addition to reducing mélange rigidity, increased meltwater production and runoff could also increase hydrofracture-induced calving. Crevasses filled with surface melt penetrate deeper than dry crevasses (van der Veen, 1998; Weertman, 1973), and if a crevasse near the terminus penetrates the full thickness of the ice, it can cause calving (Nick et al., 2010; Sohn et al., 1998). We observed a sustained 26% increase in runoff (Figure 2.6c) coincident with accelerated glacier retreat in 1996, which could contribute to increased filling of surface crevasses and subsequent hydrofracture, which would facilitate greater calving and retreat. Although runoff remained high in the 2010s, the duration of the runoff season decreased by 6 days (Figure 2.6e) while sustained glacier retreat continued. These results suggest that to the extent that hydrofracture may have contributed to retreat, it is through increased runoff volume rather than seasonal duration.

2.5 Conclusions

We have built a comprehensive record of annual terminus positions for 87 marine-terminating outlet glaciers in northwest and central-west Greenland from 1972 through 2021. The majority of these glaciers retreated and lost area over the observation period, with retreat accelerating after 1996. We observed a brief regional readvance in 2017 and 2018, which was offset by losses in 2019. Ice-sheet climate data indicate that surface mass balance, meltwater production, and runoff increased substantially between the 1990s and 2000s, coincident with accelerated glacier retreat.

Similarly, in most regions sea-surface and deepwater temperatures increased and sea-ice season duration decreased between the 1990s and 2000s.

Our results indicate that increased runoff and ocean temperatures correspond with periods of increased terminus retreat. Runoff and ocean warming are expected to increase terminus retreat through a combination of terminus undercutting and reducing mélange rigidity; runoff could also increase calving rates through enhanced hydrofracture. Thus, some combination of these processes is likely responsible for the widespread observed retreat across northwest and central-west Greenland. In order to more conclusively reveal the primary drivers of retreat, future studies would benefit from additional information such as more spatiotemporally dense oceanographic measurements and estimates in fjords (*e.g.*, Wood et al., 2021) and more widespread analysis of fjord mélange conditions (*e.g.*, Joughin et al., 2020). Further research is needed to improve our understanding of the dominant processes contributing to terminus retreat and the resulting increases in ice discharge.

Acknowledgements

T.B. and I.J. were supported by the NASA MEaSUREs program (80NSSC18M0078). T.B. was also supported by an NSF Graduate Research Fellowship early in the project. Twila Moon digitized the original six-year dataset of terminus positions. The authors thank the Greenland Institute of Natural Resources, Nuuk, Greenland, for collection of hydrographic data in Disko Bay as part of its Standard Hydrographic Coastal Monitoring Program. Comments by Michael Wood and the anonymous reviewer also improved the manuscript.

Chapter 3. Maritime glacier retreat and terminus area change in Kenai Fjords National Park, Alaska, between 1984 and 2021

Abstract. Glacier change in Kenai Fjords National Park in southcentral Alaska affects local terrestrial, freshwater, and marine ecosystems and will likely impact ecotourism. We used Landsat 4–8 imagery from 1984 through 2021 to manually map lower glacier ice margins for 19 maritime glaciers in Kenai Fjords National Park. Of these glaciers, six are tidewater, three are lake-terminating, six are land-terminating, and four terminated in more than one environment throughout the study period. We used the mapped ice margins to quantify seasonal terminus position and areal change, including distinguishing between ice loss at glacier termini and along glacier margins. Overall, 13 glaciers substantially retreated (more than 2σ), 14 lost substantial area, and only two underwent both net advance and area gain. The glaciers that had insubstantial length and area changes were predominantly tidewater. Cumulatively, these 19 glaciers lost 42 km^2 of ice, which was nearly evenly distributed between the terminus and the lateral margins. The rapid rate of glacier change and subsequent landcover changes are highly visible to visitors and locals at Kenai Fjords National Park, and this study quantifies those changes in terms of glacier length and area.

3.1 Introduction

Alaska contains 12% of the world's glacier area outside of the ice sheets (Pfeffer et al., 2014). Nearly all of Alaska's glaciers are thinning and retreating (Larsen et al., 2007, 2015; McNabb and Hock, 2014; Radić and Hock, 2014; Yang et al., 2020) at increasing rates of melt (Arendt et al., 2009; Zemp et al., 2019). Hugonnet et al. (2021) determined that, between 2000 and 2019, Alaska's glaciers lost 66.7 Gt a^{-1} or 25% of global glacier mass loss outside of ice sheets,

constituting the greatest regional glacier mass loss in the world. Most of Alaska's glaciers are located along the state's southcentral and southeastern coastline between latitudes 56 to 62°N in the Pacific coastal temperate rainforest. This coastline frames the northern shores of the biologically productive Gulf of Alaska and is experiencing some of the highest rates of glacier mass loss on Earth (Gardner et al., 2013; O'Neel et al., 2015). Although all mountain glaciers make up a small percentage of global glacier area when compared to Antarctica and Greenland, their melt rate contributes approximately half of all glacier meltwater to sea-level rise (Gardner et al., 2013; Wouters et al., 2019; Zemp et al., 2019).

Glacier mass loss results in a reduction of glacier ice which appears on the landscape as a decrease in surface elevation (thinning) or a decrease in a glacier's area and length (retreating). The change in glacier area results in a reconfiguration of landcover; areas previously covered by ice are replaced with a different surface type. Tidewater glacier retreat allows marine waters to flood in their wake, creating or elongating a fjord. With continuous retreat they may eventually exit the water and become land-terminating glaciers. When land-terminating glaciers retreat, they leave behind lakes, rivers, or freshly disturbed terrain that will be colonized and eventually vegetated. The retreat of lake-terminating glaciers results in the expansion of the lake and, once they retreat onto land, terrestrial disturbance. In each case, the landcover mosaic and each associated habitat changes from ice to marine water, freshwater, or terrestrial vegetation. It is imperative for land management agencies such as the National Park Service to know the landcover within and around their boundaries for effective management. National parks with glaciers and glacier-affected areas preserve the aesthetic (scenic), cultural, ecological, educational, recreational, and touristic values embodied by glaciers (Capps, 2017).

Most of Alaska's temperate rainforest coastline is dominated by mountains and fjords (Nowacki et al., 2003; Bidlack et al., 2021). Perennial snow and ice cover 17% of the coastal landscape rimming the northern Gulf of Alaska (Beamer et al., 2016) including land-terminating, lake-terminating, and tidewater glaciers. Active tidewater glacier fjords are unique ecosystems that occur in high-latitude coastal environments in Alaska, Antarctica, the Canadian Arctic, Russian Arctic, Greenland, Chile, Iceland, and Svalbard (Bianchi et al., 2020). The Kenai Fjords, located on the Kenai Peninsula in Southcentral Alaska (Figure 3.1), were carved by glaciers flowing east from the Harding Icefield, a 2,080 km^2 icefield (Loso et al., 2014). Today only three of the fjords have active tidewater glaciers. Land-terminating and lake-terminating glaciers are also present along the coast; some continue to flow outward from the Harding Icefield while others are now disconnected from the icefield. Alaska's maritime glaciers are strongly influenced by their proximity to the northeast Pacific Ocean and its relatively warm, wet climate (Josberger et al., 2007). As the climate changes, it will affect glacier mass balance as increasing temperatures increase surface ablation (Larsen et al., 2015; O'Neel et al., 2019) and the changing quantity and phase of precipitation affect winter snow accumulation (O'Neel et al., 2019; Hugonnet et al., 2021). All glacier types are sensitive to climate change, but tidewater glaciers tend to be more dynamic as they respond to both climate forcing and fjord geometry (Post et al., 2011), resulting in a pattern of advance and retreat known as the tidewater glacier cycle (Trabant et al., 1991). While several Alaskan tidewater glaciers have recently advanced (Ritchie et al., 2008; Truffer et al., 2009; McNabb and Hock, 2014), climate change is overriding the tidewater cycle and most tidewater glaciers in Alaska and around the world are retreating (Arendt et al., 2002; Larsen et al., 2007; McNabb and Hock, 2014; Wouters et al., 2019; Zemp et al., 2019; King et al., 2020). These tidewater glaciers are predicted to continue retreating (Hock et al., 2019; Slater et al., 2019), with

consequent contributions to sea level rise (Arendt et al., 2002; Gardner et al., 2013; Huss and Hock, 2015) and marine ecosystems (Lydersen et al., 2014; O'Neel et al., 2015; Arimitsu et al., 2016; Hoover-Miller and Armato, 2018).

The Harding Icefield has been the focus of numerous glacier change studies, including quantification of changes to areal extent (Wiles and Calkin, 1994; Wiles et al., 1995; Giffen et al., 2014; Loso et al., 2014), Holocene and modern terminus retreat (Barclay et al., 2009; Kurtz and Baker, 2016), surface elevation (Adalgeirsdóttir et al., 1998; Sapiano et al., 1998; Echelmeyer et al., 2002; Arendt et al., 2002; VanLooy et al., 2006; Loso et al., 2014; Larsen et al., 2015), mass balance (Kurtz, report in preparation), and estimates of the magnitude and timing of seasonal terminus variations of tidewater glaciers (McNabb and Hock, 2014). Results of these studies conclude that the icefield is shrinking and the rate of areal loss is increasing.

Here we map lower glacier ice margins for 19 maritime glaciers in the Kenai Fjords to quantify nearly four decades of seasonal areal and terminus position change. The selected glaciers include tidewater, lake-terminating, and land-terminating glaciers. We chose these 19 glaciers due to their various stages of retreat from the marine environment, their role in proglacial lake and river development, and/or their status as a tourist attraction for visitors to Kenai Fjords National Park. Mapping glacier outlines from satellite imagery provides historical context for glacier area and length change and gives information about changes to land cover and habitat. Although the processes that influence glacier area and length also drive changes to glacier mass, we do not intend to use our measurements as a proxy for mass balance, as glacier area and length changes are influenced by, but do not necessarily correspond to glacier mass change (Roe, 2011; O'Neel et al., 2019). However, changes to a glacier's geometry due to surface melt and areal change

contribute to mass balance changes, while long-term negative mass balance measurements result in changes in glacier length and area.

3.2 Study area

The Harding Icefield is situated in the Kenai Mountains between latitudes 59.5° and 60.3° N on the southern portion of the Kenai Peninsula in southcentral Alaska (Figure 3.1). The glaciers that make up the Harding Icefield flow outward in all directions from the central plateau, terminating on land, in lakes, or, on the southeastern part of the icefield, into the marine environment of the Kenai Fjords. The fjords are located along the northwestern coast of the Gulf of Alaska in the Northern Pacific Ocean, an area known for its marine wildlife and dramatic scenery. Management of the Harding Icefield falls under the jurisdiction of the Kenai National Wildlife Refuge to the west and Kenai Fjords National Park to the east. The area currently managed by Kenai Fjords National Park is within the ancestral lands of the Alutiiq or Sugpiaq people, many of whom now reside in the Alaska Native villages of Port Graham and Nanwalek on the southwest corner of the Kenai Peninsula. Glaciers, specifically the tidewater glaciers, are one of the main features that draw visitors to the Kenai Fjords. In 2018, tour boat companies reported that nearly 123,000 people travelled into the fjords on tour boats and viewed the park's maritime glaciers.

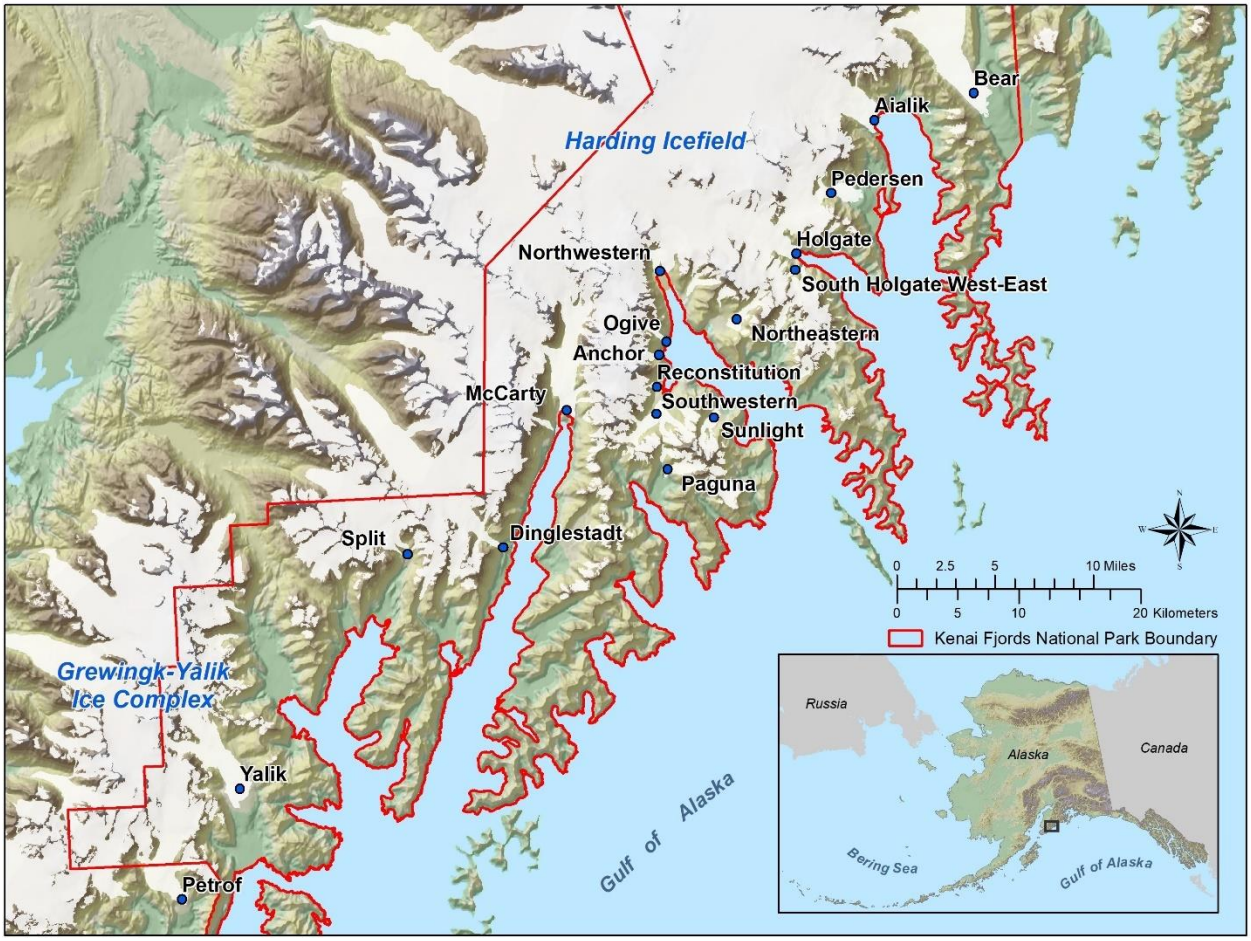

Figure 3.1: Overview map of Kenai Fjords National Park maritime glaciers.
Overview map of all glaciers in study area (blue points) with each glacier's name, the Kenai Fjords National Park boundary in red, and an inset indicating the location of the study area.

Table 3.1: Reference information about individual Kenai Fjords maritime glaciers.
Reference information including official or unofficial name, termination type, GLIMS ID number, centroid coordinates, and length and area from the Randolph Glacier Inventory (RGI) v6.0 for each glacier in the study area.

Name	Termination	GLIMS ID	Centroid	RGI Area	RGI Length
Bear Glacier *	Lake	G210235E60050N	60.04°N, 149.72°W	198.091	36.600
Aialik Glacier *	Tidewater	G210091E59984N	59.97°N, 149.84°W	141.533	19.206
Pedersen Glacier *	Lake	G210146E59907N	59.91°N, 149.85°W	31.634	11.409
Holgate Glacier *	Tidewater	G210021E59901N	59.89°N, 149.98°W	97.125	24.303
South Holgate Glacier – West †	Land	G210103E59831N	59.83°N, 149.90°W	2.626	3.494
South Holgate Glacier – East †	Tidewater/Land	G210135E59826N	59.83°N, 149.86°W	5.463	3.878
Northeastern Glacier	Land	G210061E59818N	59.82°N, 149.94°W	5.396	6.030
Northwestern Glacier *	Tidewater	G209902E59882N	59.88°N, 150.07°W	50.299	15.184
Ogive Glacier	Tidewater	G209874E59806N	59.80°N, 150.09°W	7.501	6.706
Anchor Glacier	Tidewater	G209874E59787N	59.80°N, 150.13°W	6.867	5.326
Reconstitution Glacier	Tidewater/Land	G209876E59766N	59.76°N, 150.09°W	4.905	4.981
Southwestern Glacier	Land/Lake	G209894E59736N	59.74°N, 150.10°W	14.597	7.008
Sunlight Glacier	Land	G209989E59718N	59.73°N, 150.02°W	3.687	4.806
Paguna Glacier	Land	G209947E59704N	59.70°N, 150.05°W	3.239	3.909
McCarty Glacier *	Tidewater	G209749E59808N	59.80°N, 150.25°W	110.053	19.124
Dinglestadt Glacier *	Land	G209617E59675N	59.67°N, 150.38°W	24.315	9.681
Split Glacier *	Land	G209508E59678N	59.68°N, 150.50°W	12.422	7.077
Yalik Glacier *	Lake	G209214E59535N	59.53°N, 150.78°W	41.538	15.254
Petrof Glacier *	Lake/Land	G209166E59462N	59.46°N, 150.83°W	43.424	15.126

** indicates official name designated by U.S. Board on Geographic Names*
† South Holgate Glacier – West/East are also known together as Surprise Glacier or Little Holgate Glacier

3.3 Data and methods

We manually digitized lower glacier outlines for 19 maritime glaciers in Kenai Fjords National Park (Figure 3.1) using available spring and autumn Landsat 4–8 images between 1984 and 2021. Geographic details about each glacier are provided in Table 3.1. We used the manually digitized glacier outlines and additional reference features for each glacier to measure their area and length and determine changes in size over the observational period. We also visited most of the study glaciers in the spring and summer of 2021 and made additional observations about current conditions that were difficult to discern in satellite images. Except for Petrof Glacier, all of the glaciers in this study are documented by the park's repeat photo collection, which is updated annually. The collection is archived at the park and as a special photo collection at the National Snow and Ice Data Center's Glacier Photo Collection (National Snow and Ice Data Center, 2021).

3.3.1 Data acquisition

For each glacier, we created the following static features: 1) a point marking the glacier centroid location; 2) a centerline from the Randolph Glacier Inventory (RGI Consortium, 2014), modified as needed to extend to the maximum observed length of the glacier (Figure 3.2a); 3) a reference box, with one side drawn perpendicular to glacier flow and down-glacier of any tributary glaciers connecting to the main trunk, two additional lines extending laterally along the glacier edges past the terminus, and open-ended in the down-flow direction (Figure 3.2b); and 4) a reference line (or "gate") with which to intersect each digitized glacier outline, equivalent to the back end of the reference box but extended beyond the full width of the glacier (Figure 3.2c). Each of these features was stored within a corresponding feature class in an ESRI File Geodatabase.

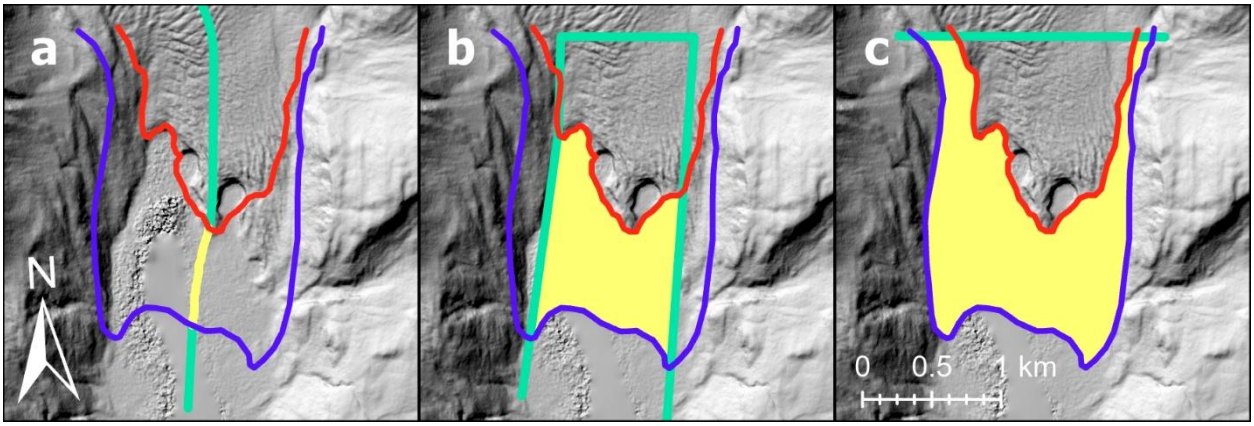

Figure 3.2: Illustration of methods for measuring glacier retreat and area change.
Illustration of the (a) centerline method, (b) box method, and (c) outline method for measuring glacier change, using McCarty Glacier as an example. Glacier outlines are shown in purple (1984-06-18) and red (2020-09-09). The centerline (a), reference box (b), and reference line (c) are shown in green. Change measurements (a) along the centerline, (b) within the reference box, and (c) beyond the reference line are shown in yellow. The base image is a hillshade of a DEM derived from a U.S. Fish and Wildlife Service-led structure-from-motion data acquisition in 2016.

We used spring and autumn Landsat images to study long-term glacier change in Kenai Fjords National Park. We limited our image search to spring (May and June) and autumn (mid-August through mid-October) to approximately capture the seasonal maximum and minimum extents of the glaciers. Additionally, because repeat mapping of glacier features requires high geometric precision, we included only images with Landsat's Tier 1 (T1) and Level-1 Precision and Terrain (L1TP) classifications, which meet Landsat's highest geometric precision standards. While this selection ensures high geometric precision within a given Landsat scene coordinate, we observed that the geometric precision between overlapping scene coordinates was inconsistent. Therefore, we limited our image search to scene coordinate 069/018 (under the Worldwide Reference System-2 (WRS-2) path/row notation), which fully covers the glaciers of interest in this study. The WRS-2 was first used with Landsat-4, launched in 1982. Prior to Landsat-4, the Landsat series used the WRS-1 system. The WRS-1 scene coordinate 074/018 covers our glaciers of interest; however,

we found no images at this coordinate that satisfied the T1 and L1TP criteria. Therefore, the earliest potential year from which we could acquire images was 1982.

With these constraints in mind, we searched the Landsat Public Data on Google Cloud Platform for all Landsat product identification numbers that met these requirements and downloaded all resulting images. All images were re-projected into the NAD83(2011) / Alaska Albers coordinate reference system (EPSG:6393), the standard system used by the NPS Alaska region, including Kenai Fjords National Park. The red, green, and blue bands were combined to create a true-color composite for each image. Finally, for Landsat-7 and Landsat-8, the color composite image was pan-sharpened using the panchromatic band. This process yielded over 200 true-color image candidates at 15m to 30m resolution.

3.3.2 Glacier outline digitization

For each glacier, we reviewed the candidate images and manually digitized the glacier outline down-glacier of its reference line, once during each season in which the outline was clearly visible. Our digitization approach differs from that of most ice margin data submitted to the Randolph Glacier Inventory (RGI Consortium, 2014) in that we digitized manually rather than through an automated process, we included some ground-truthing of glacier positions, and we did not digitize the entire ice margin. We discarded all images in which the Landsat-7 scan-line corrector failure "stripes" were present and passed over images in which the glacier was obscured by clouds. For spring outlines, we prioritized May images, and used June images when none from May were available. For autumn outlines, we prioritized September images, and used images from August 17–31 or October 1–16 when none from September were available. In the few cases where there were two viable images over a glacier in one season, we used the image in which the glacier outline

was clearest (*e.g.*, higher contrast, or fewer clouds). In cases where there were no viable images available within our defined seasons, we did not record any data.

We included metadata with the glacier outlines to assist data analysis and to ensure reproducibility. After digitizing a glacier outline, we noted the current termination type (land, lake, or tidewater), the Landsat Product ID of the image used for digitization, and a quality flag for the outline. The quality flag indicates whether the analyst was certain or uncertain about the accuracy of the outline, and was subjectively assigned. Uncertainty flags were typically due to image saturation or features that hindered interpretation, such as shadows, snow or debris cover, or scattered clouds. Additional attributes, such as the image date and associated season, were automatically generated based on the Landsat Product ID.

3.3.3 Glacier change measurements

We measured the length and lower glacier area change of each glacier between each observation using, respectively, the centerline method, and the box method (Moon and Joughin, 2008) and a variant which we term the outline method, which allows us to distinguish terminus retreat from total area loss. To determine glacier length, we measured from the up-glacier end of the centerline to where it intersects with the glacier outline (Figure 3.2a). The change in centerline length between observations approximates the length of glacier retreat and advance over time. To determine glacier area with the box method, we intersect a glacier's reference box, which contains the main body of the glacier, with a glacier outline to create a polygon (Figure 3.2b); we refer to this as the "terminus area". While the area of this polygon is arbitrary, depending on how the reference box is drawn, the change in area between observations represents the change in ice area at the glacier terminus. The outline method is conceptually similar to the box method, but we instead intersect the glacier outline with a straight reference line, which we chose to be coincident

with the up-glacier edge of the glacier reference box to allow direct comparison between the two methods (Figure 3.2c); we refer to this as the "lower glacier area". The change in area of this polygon between observations represents the total change in ice area – both laterally and at the terminus – down-glacier of the reference line. Therefore, the difference between the area changes as measured by the box and outline methods is approximately equivalent to the area change along the glacier sides, *i.e.*, narrowing or widening as glacier width changes. We use both the box method and the outline method because glacier area change does not necessarily occur solely at the terminus, and similarly, changes at the terminus do not necessarily correspond to area changes elsewhere on the glacier. After creating time series of glacier length and area changes, we calculated whether the net change exceeds two standard deviations (2σ) of the data, and used this threshold to define "substantial" glacier change over our observation period.

3.3.4 Seasonal variability

Although we attempted to measure each glacier in both spring and autumn annually, cloud cover, particularly for the spring images, and lack of imagery prevented us from creating a complete continuous time series at this temporal resolution. To assess seasonal changes in length, we filtered each glacier's time series down to only continuous spring-to-autumn (summer) and autumn-to-spring (winter) measurements. We differenced these measurements (*i.e.*, measured the advance or retreat from one season to the next) and found the median values of the difference for spring and autumn measurements. For example, if a glacier typically advanced from autumn to spring, its median difference value for spring would be positive. We did not assess seasonal changes in area because the timing of end-of-winter seasonal snow cover and/or avalanche debris along the margins varies annually, and so the ability to accurately delineate ice margins (and thus calculate

lower glacier area) was often hindered. This potential uncertainty in our spring area measurements could bias the seasonal area difference results.

3.3.5 Measurement uncertainty

Several factors may introduce uncertainty into our measurements. The lateral margins of glaciers were often more difficult to accurately digitize than termini due to marginal avalanche and landslide deposits, more extensive spring snow cover at higher elevations, and difficulty distinguishing supraglacial debris cover from lateral moraines. While calving glacier termini can also be difficult to digitize due to difficulty distinguishing glacier ice from mélange, sea ice, or lake ice, we did not encounter these complications with the images that we used. Therefore, the measurements derived from the outline method may have a greater uncertainty than those from the box method (*i.e.*, the terminus area change measurements). A single analyst traced all glacier outlines to minimize potential uncertainty introduced by differing interpretations of features such as snow cover and moraines. We do not expect that any error introduced by these potential sources of image misinterpretation are significant enough to obscure the overall trends in area change. We retained both the box and outline methods to provide multiple metrics for understanding trends in glacier change. The centerline method for measuring glacier length ideally represents the maximum extent of the glacier at the time of that observation. However, it may underestimate the maximum length if the terminus shape is concave, lopsided, or variable. All these methods measure changes in the surface extent of glaciers, and we do not extend these measurements to estimate volumetric changes.

3.4 Results

We digitized seasonal glacier outlines (spring and autumn) for 40 seasons between spring of 1984 and autumn of 2021, using 50 different Landsat images (Figure 3.3). Most observations were after the year 2000 due to limitations of available and viable imagery; there was a dearth of observations in the 1990s and scattered observations in the 1980s. Overall, we digitized an average of 32 outlines per glacier between 1984 and 2021 (Figure 3.4).

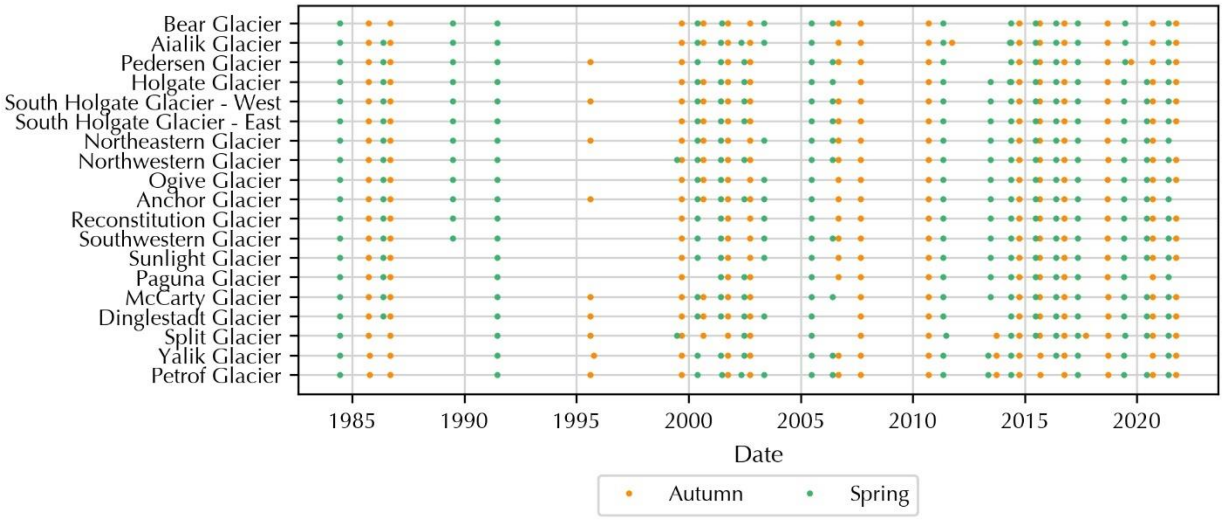

Figure 3.3: Timing of individual glacier observations.
Time series of individual seasonal observations for each glacier.

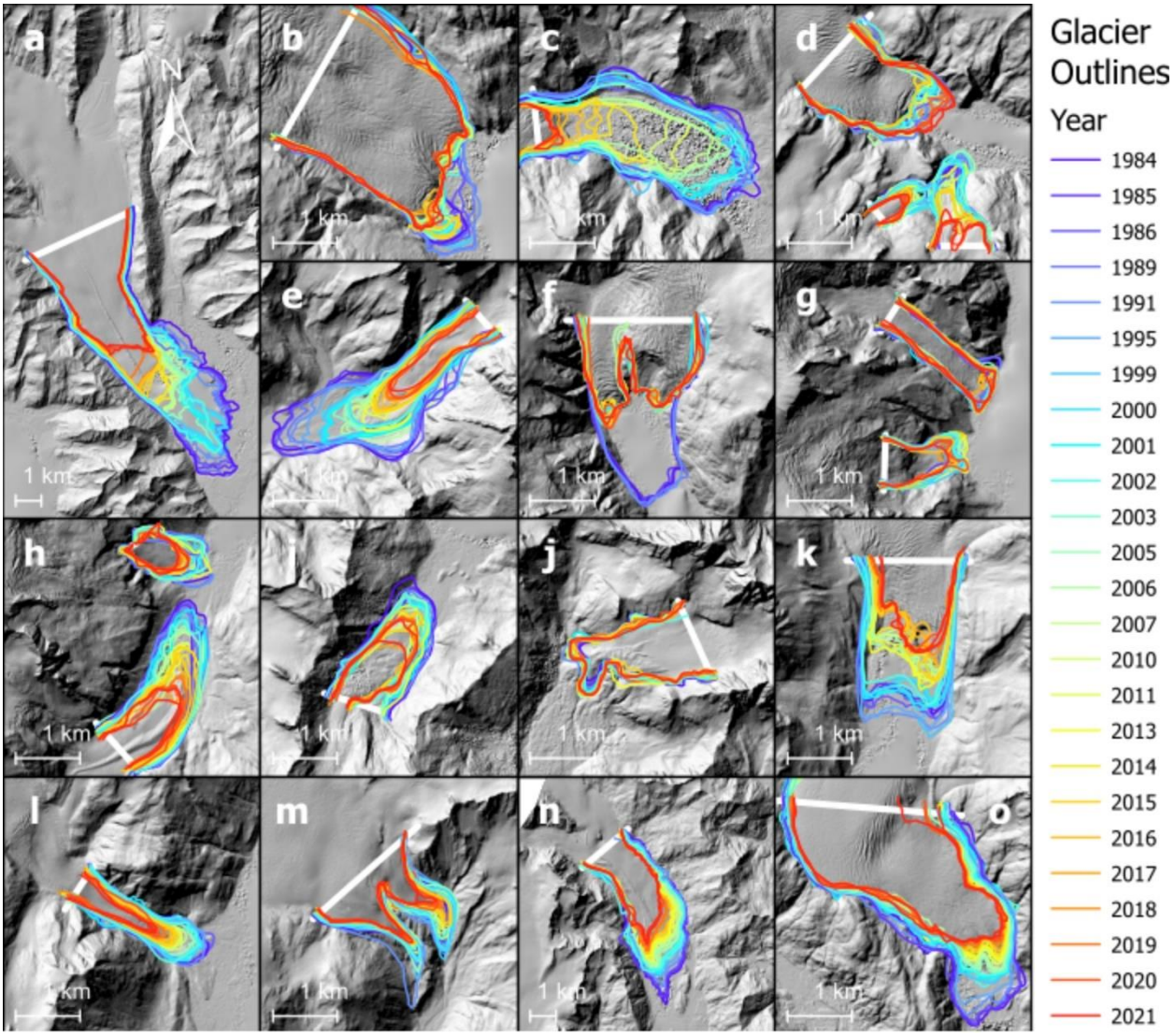

Figure 3.4: Maps of glacier outlines.

Maps of all seasonal outlines traced for (a) Bear Glacier; (b) Aialik Glacier; (c) Pedersen Glacier; (d) Holgate Glacier (top), South Holgate Glacier – West (bottom left), and South Holgate Glacier – East (bottom right); (e) Northeastern Glacier; (f) Northwestern Glacier; (g) Ogive Glacier (top) and Anchor Glacier (bottom); (h) Reconstitution Glacier (top) and Southwestern Glacier (bottom); (i) Sunlight Glacier; (j) Paguna Glacier; (k) McCarty Glacier; (l) Dinglestadt Glacier; (m) Split Glacier; (n) Yalik Glacier; and (o) Petrof Glacier. The color scale ranges from purple as the oldest (1984) to red as the youngest (2021). Glacier reference lines are shown in white. Maps (a) and (n) are shown at 1:250,000 scale, and all others are at 1:100,000 scale. The base image is a hillshade of a DEM from a U.S. Fish and Wildlife Service-led structure-from-motion data acquisition in 2016.

Between 1984 and 2021, the glaciers in our study cumulatively lost ~42 km^2 of lower glacier ice area (using the outline method), which was partitioned as ~24 km^2 at their termini (using the box method) and ~18 km^2 along their lateral margins (from differencing the outline and box methods). Of the 19 glaciers we examined, only two (Holgate and Paguna) underwent both net centerline advance and net area gain over the course of the study period. We also detected insubstantial centerline advance at Ogive Glacier. The net changes in centerline length, lower glacier area, and terminus area for individual glaciers are detailed in Table 3.2 and illustrated in the supplementary figures. The decadal rates of areal change and centerline length change are detailed in Table B. 1 and Table B. 2, respectively. When seasonal measurements were continuous, we found that most glaciers tended to retreat through the summer (between spring and autumn observations), while winter behavior (between autumn and spring observations) was more variable (Table 3.3). Below we group the glaciers into different termination types primarily to isolate the tidewater glaciers, which are influenced by processes occurring at the ice-marine interface in addition to climate change (Trabant et al., 1991). The termination types are also indicative of the proglacial habitats that are vulnerable to change as the glacier retreats. Specifically, tidewater glaciers influence marine ecosystems, lake-terminating glaciers influence freshwater lakes and associated stream outlets, and land-terminating glaciers affect freshwater riverine and terrestrial habitats.

Table 3.2: Net area and length changes.

Net centerline length change (ΔL), net lower glacier area change (ΔA), and net terminus area change (excluding lateral changes; ΔA_{term}) for each glacier from 1984 to 2021. Substantial (>2σ) values are indicated by bold type, and the 2σ values are given in parentheses.

Glacier	**Net ΔL (km)**	**Net ΔA (km^2)**	**Net ΔA_{term} (km^2)**
Bear Glacier	**-5.17** (3.08)	**-17.28** (9.55)	**-10.83** (6.56)
Aialik Glacier	-0.01 (0.33)	-0.60 (0.77)	-0.29 (0.36)
Pedersen Glacier	**-3.19** (2.65)	**-4.25** (3.14)	**-1.71** (1.34)
Holgate Glacier	**+0.47** (0.30)	+0.22 (0.30)	**+0.24** (0.17)
South Holgate Glacier – West	**-0.39** (0.22)	**-0.21** (0.15)	**-0.08** (0.06)
South Holgate Glacier – East	**-1.26** (0.92)	**-0.47** (0.40)	**-0.28** (0.23)
Northeastern Glacier	**-2.07** (1.26)	**-2.43** (1.58)	**-1.05** (0.64)
Northwestern Glacier	**-1.59** (1.20)	**-1.63** (1.28)	**-1.40** (1.09)
Ogive Glacier	+0.49 (0.08)	-0.07 (0.09)	+0.01 (0.05)
Anchor Glacier	-0.12 (0.27)	-0.12 (0.17)	-0.05 (0.09)
Reconstitution Glacier	**-0.31** (0.29)	**-0.42** (0.28)	**-0.42** (0.28)
Southwestern Glacier	**-1.55** (0.88)	**-1.38** (0.89)	**-0.55** (0.39)
Sunlight Glacier	**-0.61** (0.50)	**-0.91** (0.60)	**-0.27** (0.17)
Paguna Glacier	**+0.21** (0.13)	-0.03 (0.12)	**+0.12** (0.08)
McCarty Glacier	-0.75 (0.75)	**-1.84** (1.54)	**-0.96** (0.91)
Dinglestadt Glacier	**-0.90** (0.55)	**-0.75** (0.52)	**-0.37** (0.23)
Split Glacier	**-0.55** (0.49)	**-0.68** (0.53)	**-0.46** (0.40)
Yalik Glacier	**-2.27** (1.24)	**-6.92** (3.97)	**-5.07** (2.87)
Petrof Glacier	**-1.03** (0.57)	**-2.33** (1.33)	**-1.06** (0.69)

Table 3.3: Seasonal length changes.
Median difference between consecutive spring-to-autumn (*i.e.*, summer) and autumn-to-spring (*i.e.*, winter) centerline length measurements for each glacier. Values greater than the typical image resolution (~15m) are indicated by bold type.

Glacier	Median summer length change (m)	Median winter length change (m)
Bear Glacier	**-16** (n=7)	-10 (n=9)
Aialik Glacier	-4 (n=9)	**24** (n=11)
Pedersen Glacier	-11 (n=9)	**-34** (n=9)
Holgate Glacier	-11 (n=9)	**21** (n=10)
South Holgate Glacier – West	**-19** (n=10)	10 (n=10)
South Holgate Glacier – East	**-24** (n=10)	6 (n=10)
Northeastern Glacier	**-22** (n=8)	**-21** (n=10)
Northwestern Glacier	-1 (n=11)	4 (n=10)
Ogive Glacier	-11 (n=8)	12 (n=10)
Anchor Glacier	-1 (n=8)	9 (n=11)
Reconstitution Glacier	**24** (n=7)	**-28** (n=9)
Southwestern Glacier	**-76** (n=8)	**18** (n=9)
Sunlight Glacier	**-23** (n=7)	**23** (n=9)
Paguna Glacier	6 (n=6)	-3 (n=8)
McCarty Glacier	**-68** (n=9)	**56** (n=10)
Dinglestadt Glacier	**-32** (n=9)	-3 (n=11)
Split Glacier	**-27** (n=8)	**15** (n=8)
Yalik Glacier	**-81** (n=7)	-5 (n=8)
Petrof Glacier	-13 (n=7)	-11 (n=8)

3.4.1 Tidewater glaciers

Six glaciers were tidewater for the duration of the study period: Aialik Glacier, Holgate Glacier, Northwestern Glacier, Ogive Glacier, Anchor Glacier, and McCarty Glacier. Each of these glaciers experienced net growth and centerline advance between 1986 and 1990, and net loss and centerline retreat between 1990 and 1999 (note that we only have 2-3 observations in the 1990s for most of these glaciers, so we cannot define this retreat period more precisely), after which their individual behaviors became more variable (Figure 3.5a,b). The majority of the measured area change in the lower glacier was at the terminus for all tidewater glaciers except Aialik and Anchor Glaciers, which experienced the majority of their area change in the lower glacier along their margins. When

seasonal measurements were continuous, they indicated that all of these tidewater glaciers tended to retreat in the summer and advance in the winter. However, in most cases the median seasonal advance or retreat was less than the typical image resolution (15 m for most of the continuous measurements), and so could be difficult to detect in satellite images. The exceptions to this resolution limit were Aialik and Holgate Glaciers (in winter), and McCarty Glacier (in both summer and winter).

Aialik Glacier (net centerline length change -0.01 km, net lower glacier area change -0.60 km^2) was stable at the terminus centerline from 2000 through 2021, after advancing and then retreating ~600 m in the late 1980s and 1990s, respectively. The glacier continued losing ice area laterally for nearly two decades while the terminus was stable. The lateral loss is almost entirely restricted to the northeastern margin of the glacier. Despite the concentrated area loss along part of the terminus, neither the length change, lower glacier area change, nor terminus area change at Aialik Glacier qualified as substantial (>2σ).

Holgate Glacier (+0.47 km, +0.22 km^2) had cycles of advance and retreat between 1984 and 2021 and was the only tidewater glacier that substantially gained both terminus area and length since the beginning of the observation period in 1984 (lower glacier area change was insubstantial). Nearly all area gained was at the terminus, suggesting that the glacier did not widen as it advanced.

Northwestern Glacier (-1.59 km, -1.63 km^2) retreated in the 1990s and was relatively stable between ~1999 and 2021. The centerline length, lower glacier area, and terminus area changes were all substantial.

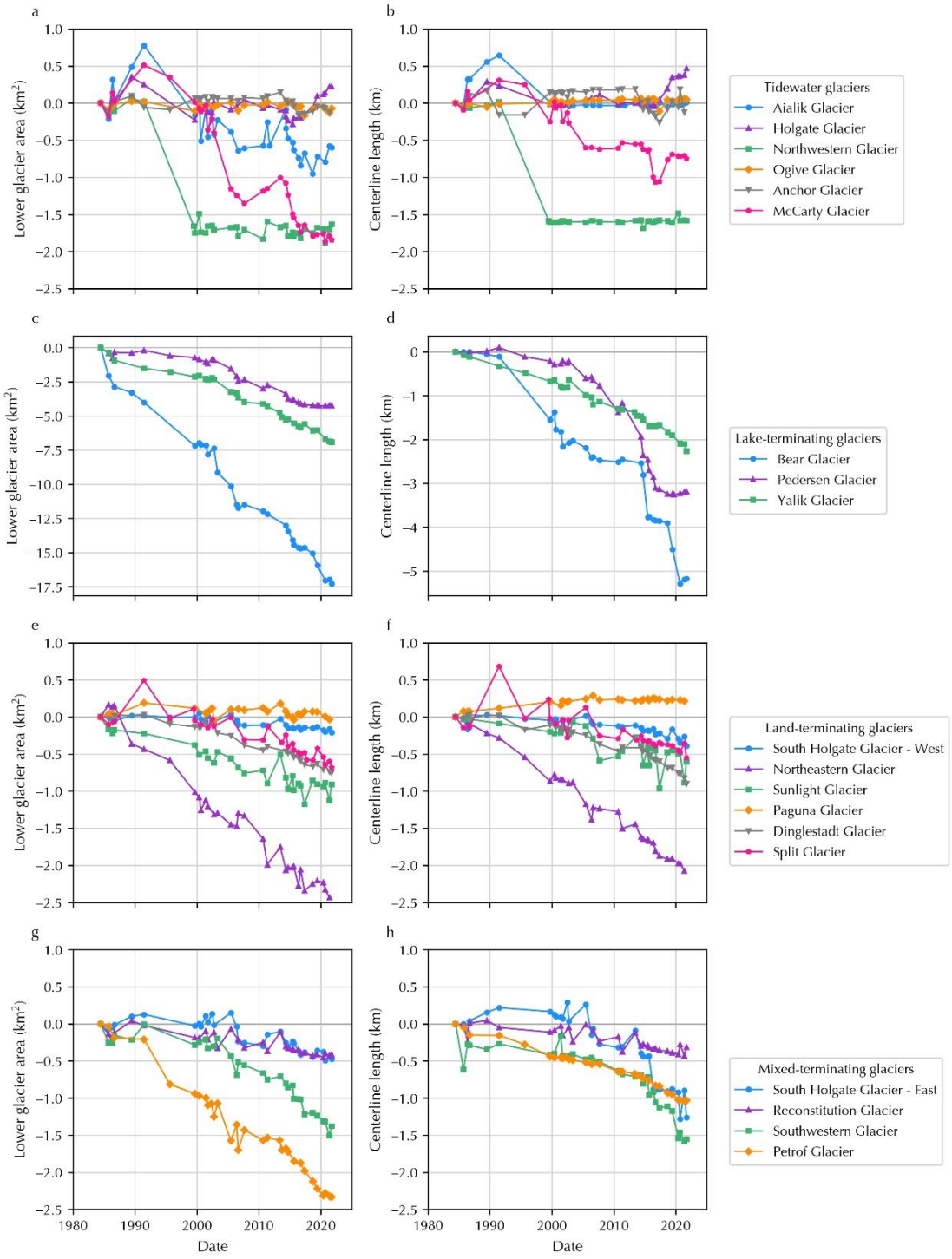

Figure 3.5: Individual glacier area and length change grouped by glacier type.
Summary of observed (left column) lower glacier area and (right column) centerline length changes for (a, b) tidewater glaciers, (c, d) lake-terminating glaciers, (e, f) land-terminating glaciers, and (g, h) mixed-terminating glaciers. Note that the vertical scale is the same for all plots except the lake-terminating glaciers (c, d).

Ogive Glacier (+0.49 km, -0.07 km^2) may have had multiple periods of small-magnitude advance and retreat at the centerline between 1984 and 2021. It experienced insubstantial lower glacier area loss, as well as insubstantial advance and terminus area gain. However, the glacier front is small and debris-covered, making it difficult to distinguish the sediment-laden ice from the adjacent unconsolidated material in satellite images. Therefore, Ogive Glacier's area and length measurements may be subject to more error than the measurements for other glaciers. Due to the small absolute magnitudes of measured advance and retreat, we cannot confidently disentangle this imprecision from the glacier's true behavior. In 2021, Ogive Glacier terminated in the tidal zone, where it lost contact with marine waters during low tides.

Anchor Glacier (-0.12 km, -0.12 km^2) experienced cycles of advance and retreat at the centerline including an advance from 2017 through 2020. Overall, it experienced a net lower glacier area loss between 1984 and 2021, including a small decrease in area at the terminus. This indicated that the glacier is continuing to lose ice along the margins despite its recent advance, although neither the net area changes nor the centerline length change were substantial. Recent areal gains at the terminus were likely the result of icefall and avalanche debris reconstituting the lower glacier area.

McCarty Glacier (-0.75 km, -1.84 km^2) has undergone periods of advance, stability, and retreat, resulting in a net loss of centerline length and area between 1984 and 2021. Although the length change was insubstantial, the lower glacier and terminus area changes were substantial.

3.4.2 Lake-terminating glaciers

Three glaciers were lake-terminating for the duration of the study period: Bear Glacier, Pedersen Glacier, and Yalik Glacier. These glaciers experienced the greatest magnitudes of centerline retreat and lower glacier and terminus area losses of all glaciers in the study area (Figure 3.5c,d). These

glaciers also retreated continually throughout the duration of the study period, with no notable observed advances. At Bear and Yalik Glaciers, the majority of area loss in the lower glacier was at the terminus, while at Pedersen Glacier the majority of area loss in the lower glacier was along the margins. Retreat of these glaciers corresponded with growth of their proglacial lakes. Continuous seasonal measurements indicated that all three of these glaciers tended to retreat during both the summer and the winter. These seasonal changes were greater than the typical image resolution in the summer at Bear and Yalik Glaciers, and in the winter at Pedersen Glacier.

Bear Glacier (-5.17 km, -17.28 km^2) lost substantial centerline length and lower glacier and terminus area between 1984 and 2021, with periods of accelerated retreat between 2014 and 2016 and between 2018 and 2021.

Pedersen Glacier (-3.19 km, -4.25 km^2) lost substantial centerline length and lower glacier and terminus area between 1984 and 2021. The glacier advanced ~100 m along its centerline between 1984 and 1991, but then retreated at an increased decadal rate until 2016 when the retreat rate rapidly decelerated, and the terminus has remained nearly stable through 2021.

Yalik Glacier (-2.27 km, -6.92 km^2) lost substantial centerline length and lower glacier and terminus area between 1984 and 2021. Over half of the terminus rested on a terminal moraine from approximately 2005 through 2017.

3.4.3 Land-terminating glaciers

Six glaciers were land-terminating for the duration of the study period: South Holgate Glacier – West, Northeastern Glacier, Sunlight Glacier, Paguna Glacier, Dinglestadt Glacier, and Split Glacier. During the Little Ice Age, South Holgate – West, Northeastern, Sunlight, and Dinglestadt Glaciers were tidewater glaciers, or tributaries thereof, and retreated onto land sometime before

our study period (Grant and Higgins, 1913; Wiles et al., 1995; Calkin et al., 2001). We did not find any references indicating whether Paguna Glacier and Split Glacier were tidewater or tidewater glacier tributaries during the Little Ice Age. Most of these glaciers experienced net centerline retreat at rates following an overall decreasing trend, except for Paguna Glacier, which continuously advanced from at least 1984 until ~2007 when its terminus position became stationary (Figure 3.5e,f). Both Paguna Glacier and Sunlight Glacier are partially covered with debris from landslides related to the M9.2 Alaska Earthquake that occurred in 1964 (Post, 1967). All of these glaciers had persistent proglacial stream systems visible in satellite imagery throughout the study period. In particular, Dinglestadt and Split Glaciers' stream systems appeared to have active deltas that produced large sediment plumes in their respective fjords. Dinglestadt and Split Glaciers, as well as South Holgate Glacier – West, also experienced the majority of their measured lower glacier area loss at the terminus, while the other three glaciers experienced the majority of their area loss in the lower glacier along their margins. Continuous seasonal measurements indicated that these land-terminating glaciers tended to retreat during the summer and that this retreat was greater than the typical image resolution, except at Paguna Glacier, which tended to have advance below the typical image resolution. Winter behavior was more variable, with Northeastern, Paguna, and Dinglestadt Glaciers tending to retreat, and South Holgate – West, Sunlight and Split Glaciers tending to advance. In the winter, only the retreat at Northeastern Glacier and the advance at Sunlight Glacier were greater than the typical image resolution.

South Holgate Glacier – West (-0.39 km, -0.21 km^2) substantially retreated along its centerline and lost lower glacier and terminus area from the late 1980s through 2021. Small, ephemeral lakes visible in Landsat imagery may have been present at or near the terminus in 2014, 2015, and 2020. South Holgate Glacier – West and mixed-terminating South Holgate Glacier – East shared a joint

terminus through 2005 and separated into two distinct termini by spring of 2006. While the glaciers shared a terminus, they were mapped as two distinct features with a shared edge located approximately where the two glaciers merged.

Northeastern Glacier (-2.07 km, -2.43 km^2) experienced periods of both advance and retreat along its centerline between 1984 and 2021, particularly due to observed seasonal variations in size. However, its overall trend has been of retreat and lower glacier and terminus area loss, and the net length and area losses were substantial.

Sunlight Glacier (-0.61 km, -0.91 km^2) lost both substantial centerline length and lower glacier and terminus area between 1984 and 2021, at variable rates. In the early 2010s the glacier underwent a readvance of ~300 m. Young alder growth on the debris-covered surface of the glacier also suggests a recent slowdown of glacier flow.

Paguna Glacier (+0.21 km, -0.03 km^2) was the only land-terminating glacier that substantially advanced along its centerline between 1984 and 2021. However, the rate of advance slowed each decade, and the terminus position was stationary from ~2007 to 2021. The glacier's area fluctuated between growth and loss; the lower glacier area experienced insubstantial loss, while the terminus area experienced substantial gain. Lateral ice loss exceeded the area gained by terminus advance.

Dinglestadt Glacier (-0.90 km, -0.75 km^2) gained centerline length and lower glacier area between 1984 and 1991, but retreated and decreased in area from 1991 to 2021, resulting in an overall substantial net loss of both length and lower glacier and terminus areas.

Both arms of Split Glacier (-0.55 km, -0.68 km^2) experienced periods of both retreat and advance along its centerline, resulting in an overall substantial net loss of both length and lower glacier and

terminus areas. While the majority of area lost was at the terminus, the north arm experienced more lateral ice loss than the south arm.

3.4.4 Mixed-terminating glaciers

Mixed-terminating glaciers were observed to be some combination of land-terminating, lake-terminating, and/or tidewater over the course of our study period. There were four glaciers with mixed termination types: South Holgate Glacier – East, Reconstitution Glacier, Southwestern Glacier, and Petrof Glacier. Most of these glaciers transitioned between termination types in the 2010s and experienced accelerated retreat from 2015 or 2016 through 2021. Petrof Glacier was the exception as it transitioned and accelerated earlier than the others. All of these were either relatively static in area and centerline length or advanced between 1984 and 1992, after which all followed a variable but overall decline in both lower glacier area and centerline length (Figure 3.5g,h). The majority of measured area loss in the lower glacier was at the terminus at South Holgate Glacier – East and Reconstitution Glacier, while at Southwestern and Petrof Glaciers the majority of area loss in the lower glacier was along the margins. Continuous seasonal measurements indicated that these mixed-terminating glaciers tended to retreat during the summer, with the exception of Reconstitution Glacier, which tended to advance. Summer length change tended to be greater than the typical image resolution, except at Petrof Glacier. Winter behavior was more variable, with South Holgate Glacier – East and Southwestern Glacier tending to advance, and Reconstitution and Petrof Glaciers tending to retreat. In the winter, only the retreat at Reconstitution Glacier and the advance at Southwestern Glacier were greater than the typical image resolution.

South Holgate Glacier – East (-1.26 km, -0.47 km^2) terminated in the tidal zone until 2014, after which observations indicated it has only terminated on land. Shortly after this, between 2015 and

2016, the glacier appeared to retreat rapidly along its centerline, then slowed and began to split into two fingers to retreat around a bedrock knob. This rapid retreat was the result of significant steepening of the underlying bedrock near the terminus. In 2016, the glacier thinned dramatically along this nearly vertical slope, eventually separating into an upper and lower terminus along the bedrock wall; we mapped the upper terminus that remained connected to the rest of the glacier. All centerline length and lower glacier and terminus area changes were substantial.

Reconstitution Glacier (-0.31 km, -0.42 km^2) was purely tidewater from the beginning of our study period until 1999, terminated in the tidal zone from 1999 through 2014, then became purely land-terminating through 2021. Like Ogive Glacier, Reconstitution Glacier's small size and debris cover made it difficult to map from satellite images. However, despite this uncertainty, Reconstitution Glacier experienced a strong trend of retreat and area loss; all centerline length and lower glacier and terminus area changes were substantial. Reconstitution Glacier's name comes from the fact that the glacier is separated from its accumulation zone and receives snow and ice primarily from ice fall and avalanches.

Southwestern Glacier (-1.55 km, -1.38 km^2) was a predominantly land-terminating glacier until it began developing a proglacial lake in 2013, and it terminated in the lake from 2014 through 2016. After 2016, the terminus retreated beyond the lake, while the lake persisted and grew slightly larger. All centerline length and lower glacier and terminus area changes were substantial.

Petrof Glacier (-1.03 km, -2.33 km^2) was a lake-terminating glacier that retreated onto a bedrock knob and became land-terminating in 2006. The proglacial lake expanded slightly between 1984 and 2006 as the terminus retreated, although part of the area revealed by terminus retreat during that time was bedrock. All centerline length and lower glacier and terminus area changes were substantial.

3.5 Discussion

Of the 19 glaciers in this study, 13 substantially retreated along their centerlines, 14 substantially lost lower glacier area, and 14 substantially lost terminus area between 1984 and 2021. Two glaciers both substantially advanced and gained terminus area, and none of the glaciers substantially gained lower glacier area. All four glaciers that did not experience a substantial centerline length change were tidewater glaciers; similarly, four of the five glaciers that did not experience a substantial lower glacier area change, and all three of the glaciers that did not experience a substantial terminus area change, were tidewater. This relative lack of ice loss at the tidewater glaciers is consistent with the findings of Larsen et al. (2015) that Alaskan tidewater glaciers are losing mass at a much slower rate than other Alaskan glaciers. Although our dataset is limited in the availability of continuous seasonal measurements, our seasonal data indicate that most glaciers tended to retreat in the summer, while winter behavior was more variable (Table 3.3). For most glaciers, the median seasonal variability was less than the image resolution for at least one season. Overall, all tidewater glaciers tended to advance during winter and retreat during summer, all lake-terminating glaciers tended to retreat during both winter and summer, and land-terminating and mixed-terminating glaciers tended to retreat during the summer and showed a wider variety of winter behaviors (Table 3.3). There were no glaciers with a tendency to advance during both winter and summer.

Mass balance studies at other Alaskan maritime glaciers (*e.g.*, Wolverine Glacier on the Kenai Peninsula and Lemon Creek, Taku, and Mendenhall Glaciers on the Juneau Icefield in southeast Alaska) indicate that summer temperatures are driving negative mass balances through ablation processes, such as the areal retreat that we report on here (Motyka et al., 2003b; Criscitiello et al., 2010; O'Neel et al., 2019; McNeil et al., 2020). More specifically, studies at nearby Wolverine

Glacier, roughly 60 km northeast of Bear Glacier (the most northern glacier in our study), indicate that sensitivity to summer conditions is a recent change and that previously, winter precipitation drove mass balance (Bitz and Battisti, 1999; Josberger et al., 2007; O'Neel et al., 2019). Wolverine and Lemon Creek Glaciers are US Geological Survey Benchmark Glaciers, with long-term records of mass balance change. Both Wolverine and Lemon Creek Glaciers experienced cumulative mass loss over the period of record and saw an increase in the rate of mass loss since 1990, which is broadly consistent with our observations of ice area loss at many glaciers in Kenai Fjords National Park. If temperatures warm in either winter or summer or, worse, in both seasons, there will be an increase in the rate of mass loss at the park's maritime glaciers. Further, we speculate that the exposure of rock around these glaciers enhances the microclimate and summer melt, leading to increased ablation and greater mass loss. Given this study's glaciers' lower elevations and proximity to the ocean, we speculate that the mass loss of these glaciers may be higher than that observed at Wolverine and Lemon Creek Glaciers.

The glaciers in this study (except Bear Glacier) tend to be smaller with lower elevation ranges than Wolverine, Lemon Creek, Taku, and Mendenhall Glaciers, and they terminate nearer to the ocean than all but Taku Glacier. McGrath et al. (2017) determined that smaller glaciers and glaciers outflowing from icefields have a higher mass balance sensitivity to projected climate change. Most of our study glaciers are located with their termini at low elevation (at or slightly above sea level). Although we have not measured mass balance, looked at temperature or precipitation within the fjords, or conducted studies to look at annual equilibrium line of altitude variations, the average accumulation season (October–April) temperature in nearby Seward, Alaska hovers around freezing (32.11 °F based on the 1991-2020 normal) (NOAA National Centers for Environmental Information, 2021). A slight increase in winter temperatures over the nearby glaciers would result

in precipitation changing from snow to rain, impacting seasonal snow accumulation, and would increase the likelihood and amount of melt over the winter.

3.5.1 Tidewater glaciers

All six tidewater glaciers in our study experienced periods of both advance and retreat along their centerlines between 1984 and 2021. These tidewater glaciers also tended to advance in the winter and retreat in the summer; in particular, Aialik Glacier and Holgate Glacier (in winter) and McCarty Glacier (in summer and winter) had median seasonal variations greater than the typical image resolution. Several of these glaciers did not experience substantial centerline length, lower glacier area, and/or terminus area changes over the study period; only Northwestern Glacier experienced substantial changes in all three of these categories. Formerly-tidewater South Holgate Glacier – East and Reconstitution Glacier also experienced substantial centerline retreat and area loss, enough so that they both retreated onto land in 2014.

McNabb and Hock (2014) found that between 1991 and 2000, 60% of Alaskan tidewater glaciers retreated, and between 2001 and 2010, 46% of those glaciers retreated; for our subset of glaciers, these percentages are higher, with 100% of the tidewater glaciers retreating between 1991 and 2000 and 66% retreating between 2001 and 2010. McNabb et al. (2015) studied four of our six fully tidewater glaciers (Aialik, Holgate, McCarty, and Northwestern Glaciers) from 1985 through 2013, and found length changes ranging from -0.84 km (McCarty Glacier) to +0.23 km (Northwestern Glacier). Splitting our study period into 1985–2013 and 2013–2021 for comparison (Table 3.4), we found that McCarty and Northwestern glaciers retreated, while Aialik and Holgate glaciers marginally advanced. Between 2013 and 2021, we found that McCarty Glacier continued to retreat and Holgate Glacier further advanced, while the lengths of Aialik and Northwestern glaciers did not experience net change. We attribute the differences between our data and those of

McNabb et al. (2015) to differences in methodology: McNabb et al. (2015) used the box method to measure area and divided by width to estimate average length change, and averaged multiple seasonal observations to estimate annual lengths; we used the centerline method to directly measure length, and directly compared individual observations of length. We have also observed that at most of these glaciers, length change was not consistent across the width of the terminus, so the centerline length measurement will yield different results than length measurements made at other parts of the terminus. We cannot reconcile the large discrepancy between the measurements at Northwestern Glacier; however, based on retreat visible in satellite imagery we are confident in our observations.

Table 3.4: Comparison of tidewater length changes with McNabb et al. (2015).
Comparison of tidewater glacier length changes observed by McNabb et al. (2015) from 1985–2013 with our observations from 1985–2021, split into measurements from 1985–2013 and 2013–2021.

Name	1985–2013 ΔL (km)*	1985–2013 ΔL (km)	2013–2021 ΔL (km)
Aialik Glacier	0.17	0.03	0.00
Holgate Glacier	-0.46	0.05	0.47
McCarty Glacier	-0.84	-0.47	-0.19
Northwestern Glacier	0.23	-1.51	0.00

** data from McNabb et al. (2015)*

Tidewater glaciers make up 14% of Alaska's total glacierized area, but between 1994 and 2013 they were only responsible for 6% of regional mass loss (Larsen et al., 2015). Tidewater glaciers are unique from other glacier types in that local geographic factors such as sedimentation (Brinkerhoff et al., 2017), fjord geometry (Mercer, 1961; Catania et al., 2018), water depth (Meier et al., 1980; Post, 1980a, b), glacier geometry (Pfeffer, 2007) and ice speed and calving rates (Meier and Post, 1987; O'Neel et al., 2003; Ritchie et al., 2008; Post et al., 2011) can override the influence of climate change and can cause advance despite a negative mass balance (Larsen et al.,

2015). These additional factors cause the advance and retreat of tidewater glaciers to be less dependent on climate change compared to the behavior of lake- and land-terminating glaciers (Trabant et al., 1991). This can result in asynchronous behavior relative to other local glaciers, even other nearby tidewater glaciers (Mann, 1986; Larsen et al., 2016). Larsen et al. (2007) looked at volume changes in glaciers in southeast Alaska and Canada from 1948–1987 and found that several tidewater glaciers that had historically been retreating were in the advancing stage of the tidewater glacier cycle, as indicated by their expansion. In our study this asynchronicity is apparent at Holgate Glacier, which is the only tidewater glacier in Kenai Fjords National Park that was advancing as recently as 2021, and has oscillated between advancing and retreating during our period of record. Holgate Glacier's variable behavior is indicative of the classic tidewater glacier cycle (Meier and Post, 1987; Trabant et al., 1991), although Holgate Glacier's cyclical behavior occurs on a much faster time scale than classically described. Holgate Glacier's advance is likely due to the development of a shoal that was first observed and recognized as such in the field in 2020. High sedimentation rates allow tidewater glaciers to develop a submarine terminal moraine shoal that extends across the width of the fjord (Trabant et al., 1991). Although current elevation data is unavailable for this study, we speculate that Holgate Glacier's advance is associated with vertical thinning (Larsen et al., 2015) and there has not been an increase in ice volume, just terminal expansion due to shoal development. This shoal acts as a barrier to relatively warm marine waters that influence glacier melt and calving, thus allowing the glacier to advance while moving the moraine shoal forward. Because the development of a shoal can temporarily override the effects of climate change and allow a glacier to advance, once a glacier retreats back from the shoal it often experiences a rapid retreat such as that observed at McCarty and Northwestern Glaciers (Post, 1980a, b), as well as at Columbia Glacier (Post, 1975).

Changes to tidewater glaciers will influence nearshore oceanography and marine ecosystems (Lydersen et al., 2014; O'Neel et al., 2015; Arimitsu et al., 2016). The local fjord marine environments are changing as changes in glacier melt result in changes to the volume of freshwater input (Neal et al., 2010), which affects local physical oceanographic properties such as temperature, salinity, and turbidity (Etherington et al., 2007; Hood and Berner, 2009; Hood et al., 2009; Arimitsu et al., 2012, 2016; Jenckes et al., 2022), nutrients (Hood and Scott, 2008; Whitney et al., 2018), and currents (Royer, 1981). Meltwater and sediment discharge from tidewater glaciers drive fjord temperature and turbidity (Arimitsu et al., 2016). In cases where a tidewater glacier retreats onto land, for instance, water traveling from that glacier to the fjord will have a higher temperature and lower turbidity as it warms and drops sediment while traveling over land. These temperature and turbidity changes in turn affect nutrient concentrations and predator and prey abundances (Arimitsu et al., 2016); healthy predator-prey dynamics are important to ecotourism in the Kenai Fjords. Meltwater upwelling and iceberg calving from tidewater glaciers also help drive circulation patterns and the distribution of nutrients and planktonic food sources in fjords (Lydersen et al., 2014; O'Neel et al., 2015; Arimitsu et al., 2016; Urbanski et al., 2017), and tidewater glacier retreat from the marine environment could reduce or shut off the glacial contribution to fjord circulation. The ice-ocean interface also provides habitat for higher trophic level species such as harbor seals who haul out on icebergs (Hoover-Miller and Armato, 2018; Womble et al., 2021) near Aialik, Northwestern, and McCarty Glaciers and Kittlitz's murrelets that spend the summer breeding season near tidewater glaciers (Arimitsu et al., 2012).

3.5.2 Lake-terminating glaciers

All three lake-terminating glaciers in our study underwent substantial centerline retreat and lower glacier and terminus area losses between 1984 and 2021, as did Petrof Glacier, which was lake-

terminating through 2006. These four glaciers experienced accelerated centerline retreat in the 2010s. In particular, during those years Bear Glacier and Pedersen Glacier experienced greater net retreats than tidewater Northwestern Glacier's retreat in the 1990s, which was both the longest and fastest tidewater glacier retreat that we observed. These large retreats are consistent with observations of lake-terminating Ellsworth and Excelsior glaciers in nearby Sargent Icefield, which have also retreated rapidly after exposing over-deepened beds (Molnia, 2007; Maraldo, 2020). These rapid retreats could result in increased ice loss from higher elevations as occurred at Yakutat Glacier. Located on the outer coast of southern Alaska between southcentral and southeastern Alaska, Yakutat Glacier experienced lake calving and subsequent terminus retreat that led to a drawdown of glacier ice and rapid thinning (Trüssel et al., 2013, 2015). In southeast Alaska, lake-terminating glaciers have similarly been observed to have greater volume losses than tidewater glaciers (Larsen et al., 2007). The lake-terminating glaciers in our study also tended to retreat during both the summer and winter; Bear Glacier and Yalik Glacier had median retreats greater than image resolution in the summer, while Pedersen Glacier did so in the winter.

The rapid retreat of Bear Glacier that began in 2018 was initiated by a glacier lake outburst flood that occurred in August 2018 (Kurtz and Wolken, 2019). This outburst flood was unusual in that it breached the moraine separating the lake from the ocean, resulting in a sudden decrease in water levels, allowing marine water to temporarily enter the lake at high tides. The temporary 2018 breach demonstrated the protection that the moraine shoal provides to Bear Glacier and the vulnerability of terminus stability to infiltration of marine water into the proglacial lake (Motyka et al., 2003a). Ice thickness measurements on Bear Glacier identified areas of grounding below sea level at a minimum of 6.5 km above the current terminus position (Truffer, 2014), indicating the potential for an unstable and rapid retreat (Larsen et al., 2015) and a two-fold expansion of the

proglacial lake. This highlights the vulnerability of other shoal-protected glaciers in Alaska, such as Taku Glacier in southeast Alaska (McNeil et al., 2020).

The retreat of lake-terminating glaciers in Kenai Fjords National Park has resulted in the expansion of their proglacial lakes. As with tidewater glaciers, lake-terminating glaciers can decrease proglacial lake temperatures, increase turbidity, and alter biogeochemistry, which can limit nutrients and decrease biological productivity (Slemmons et al., 2013). As glaciers retreat and their proglacial lakes expand, new freshwater habitat is created for species such as sockeye salmon, which favor aquatic systems with lakes connected directly to the ocean via rivers for spawning and rearing (Milner and Bailey, 1989; Pitman et al., 2020). Numerous studies have been conducted in the maritime southeast Alaska environment of Glacier Bay to understand freshwater ecology and glacier retreat (Milner, 1987; Milner and Bailey, 1989; Milner et al., 2007), but little has been done in Kenai Fjords National Park. Past fish surveys were conducted in the park following the Exxon Valdez oil spill (Milner, 1990; Milner and Oswood, 1990). Recreationally, the proglacial lake at Bear Glacier is one of the most popular sites in the coastal areas of the park. Visitors travel to the lake via boats and helicopters to kayak, paddleboard, and camp on the shores of the iceberg-laden lake. Lake expansion provides more area to explore in personal watercraft.

3.5.3 Land-terminating glaciers

Nearly all of the six land-terminating glaciers in our study, as well as mixed- but predominantly land-terminating Southwestern Glacier, experienced substantial centerline retreat and lower glacier and terminus area losses between 1984 and 2021. The exception was Paguna Glacier, which substantially advanced and gained area at the terminus, but did not experience substantial lower glacier area change. Seasonally, land-terminating glaciers tended to retreat in the summer and have more variable behavior in the winter; however, median seasonal advance or retreat often fell below

the typical image resolution. The glaciers with seasonal behavior greater than typical image resolution include Northeastern Glacier (summer and winter retreat), Sunlight Glacier and Split Glacier (summer retreat, winter advance), and Dinglestadt Glacier (summer retreat).

Paguna Glacier has several attributes that make it unique from the other glaciers in this study. It is smaller, terminates higher above sea level (~70 m a.s.l.), is not known to have been tidewater or a tidewater tributary during the Little Ice Age, and has a higher percentage of debris cover than most glaciers in this study. This debris was deposited in 1964 when a magnitude 9.2 earthquake generated landslides in the Kenai Mountains and deposited debris on 50% of Paguna Glacier (Post, 1967). It is likely that this thick debris cover insulated the ice surface (Östrem, 1959), overriding effects of climate change on the glacier's surface melt, which allowed the glacier to advance for several decades. Although we have not analyzed surface elevation change in this study, we speculate that the contribution of mass in the form of rock debris resulted in a glacier response not unlike that observed following continued positive mass balance in which the glacier ice redistributes to a point of equilibrium. In this case, the debris not only insulated the glacier's surface, but the increase in mass resulted in an expansion of the glacier length. Through time, ice flow transported the debris to the ablation zone, further reducing climate-induced melt as the area most likely to melt was insulated. Based on field observations, the glacier now appears to be melting in place, and farther upglacier the rates of mass loss are likely higher than near the debris-covered terminus (Rounce et al., 2021).

Nearby Sunlight Glacier, which also received debris from the earthquake, did not advance. We suspect that this is because the landslide debris covered a smaller percentage of the entire glacier than on Paguna Glacier and because a higher percentage of the glacier is at a lower elevation than on Paguna (*i.e.*, the Accumulation Area Ratio was lower than Paguna Glacier's at the time of the

earthquake). Therefore, the percent of area of debris insulation and the input of mass were smaller than on Paguna Glacier.

The retreat of land-terminating glaciers in Kenai Fjords National Park has been accompanied by other terrestrial changes, including the development of forests and river systems resulting in expanded habitat for coastal wildlife. For instance, as river systems and lakes develop in the wake of glacier retreat, this increases the availability of habitat suitable for salmon (Milner and Bailey, 1989; Pitman et al., 2020) and the wildlife that thrive on it such as black and brown bears and bald eagles. These terrestrial changes contribute to changes in the nearshore marine environment as nutrient and sediment availability and transport evolve with the development of the terrestrial landscape (O'Neel et al., 2015). The deltas observed at the Dinglestadt and Split stream outlets are examples of post-glacier retreat coastal habitat. Recreationalists can also be found on the lands that have been recently deglaciated by land-terminating glaciers. These forelands offer the flattest terrain in the park for exploring on foot and the rivers that lead from glaciers such as Southwestern, Sunlight, and Northeastern Glacier provide a path to follow through the alder thickets. As Kenai Fjords' glaciers retreat, new recreational opportunities open up.

3.6 Conclusions

We have produced a multidecadal record of biannual observations of lower glacier outlines for 19 glaciers in Kenai Fjords National Park. Between 1984 and 2021, these glaciers cumulatively lost ~42 km^2 of ice area in their lower reaches (24 km^2 at their termini and 18 km^2 at their margins). Most glaciers lost substantial length and area, while only two gained substantial length and area. Most of the glaciers that did not experience substantial length, lower glacier area, or terminus area changes were tidewater glaciers. In contrast, all lake-terminating glaciers and nearly all land-terminating glaciers experienced substantial centerline retreat and ice area loss. Seasonally, all

tidewater glaciers tended to retreat in the summer and advance in the winter, while all lake-terminating glaciers tended to retreat in both the summer and winter; land-terminating glaciers tended to retreat in summer but showed more variable winter behavior.

Local effects resulting from the loss of ice in our study area impact both terrestrial and marine environments and change the distribution of landcover types. The loss of ice area will equal the gain or expansion of water bodies and/or coastal vegetation types and will change the viewscape and recreational opportunities for visitors. The freshwater rivers and lakes originating from glacier meltwater will form new aquatic and terrestrial vegetation habitats with impacts to the nearshore marine environment. The direct loss of glaciers and the indirect changes to the local fauna will likely impact tourism, as many people come to the Kenai Fjords to see calving tidewater glaciers and the abundant marine wildlife that thrive in the current conditions (Lambert et al., 2010; Kutzner, 2019; Salim et al., 2021).

Glacier changes have made untold impacts to the Alutiiq/Sugpiaq people who have inhabited coastal environments of southcentral Alaska for millennia. Today, Chugach Alaska Corporation and the Alaska Native Claims Settlement Act village corporations of English Bay and Port Graham are the largest nonfederal stakeholders in the park. Traditional hunting and gathering activities have been minimal in the park during the forty-year period of our study. However, ecotourism activities are common, including on an inholding where Port Graham leases land to a wilderness lodge located in Aialik Bay near Pedersen Glacier. The retreat of this glacier may impact the visitor experience at this site.

Climate change predictions indicate that glaciers in southcentral Alaska will continue to lose mass at current or increased rates. Given this rapid rate of change, our final 2021 measurement may no longer represent the current condition of every glacier in the database by the time of this

publication. In order for resource managers to make informed decisions, they must understand current conditions, including glacier dynamics and subsequent land cover and habitat changes. These changes can help identify the potential for new geohazards related to glaciers such as ice falls, landslide potential resulting from rapid retreat and slope debuttressing, or the development of new ice-dammed lakes that could cause glacier lake outburst floods. Our observations of ice margins revealed the development of new landcover types and habitats where, four decades ago, there was ice. Most obviously, the Kenai Fjords viewscape is changing dramatically as tidewater glaciers retreat onto land and land-terminating glaciers retreat into the alpine or out of sight around a bend. Therefore, we recommend that this database, and similar measurements elsewhere, be updated on a timescale that is manageable by resource managers and meaningful for decision-makers. Given the dynamic nature of the Kenai Fjords, this could arguably be annually. Our measurements indicate that most of the glaciers in Kenai Fjords National Park are shrinking rapidly, leading to measurable annual landscape change.

Acknowledgements

T.B. thanks Kenai Fjords National Park and the Future Park Leaders of Emerging Change program (now Scientists in Parks Fellows), through the Ecological Society of America and the U.S. National Park Service, for sponsoring this research internship project. We thank Andy Bliss, Joanna Young, an anonymous reviewer, the Scientific Editor Shad O'Neel, and the Chief Editor Hester Jiskoot for providing valuable comments that improved the manuscript. Any use of trade, firm, or product names is for descriptive purposes only, and does not imply endorsement by the US Government.

Chapter 4. Weekly to monthly terminus variability of Greenland's marine-terminating outlet glaciers

Abstract. Seasonal terminus-position variability is superimposed on multi-decadal trends of glacier retreat. To characterize this seasonal variability, we manually digitized terminus positions for 219 marine-terminating glaciers in Greenland from January 2015 through December 2021 using Sentinel-1 SAR mosaics. We digitized at a monthly frequency for 199 glaciers and at a six-day frequency for 20 glaciers. We found that nearly 75% of glacier termini in Greenland vary significantly on a seasonal basis. For these seasonally-varying glaciers, seasonal retreat typically begins in mid-May, and seasonal advance generally commences in early October. The duration of the retreat period appears to be related to the timing of the onset of ice-sheet surface melt. The rate of retreat events peaks in late summer and reaches a minimum in late winter and early spring. The median magnitude of terminus position seasonality, the difference between glacier length at the dates of peak advance and retreat, is about 220 m. We find a stronger correlation between this magnitude and glacier velocity than between magnitude and glacier width. Terminus position seasonality can influence longer-term glacier dynamics and, consequently, ice-sheet mass balance. This study contributes to our understanding of terminus position seasonality for individual glaciers and collectively for glaciers around the entire Greenland Ice Sheet.

4.1 Introduction

The majority of marine-terminating outlet glaciers in Greenland have retreated over the past several decades, and regionally this retreat accelerated in the 1990s and 2000s (Black and Joughin, 2022; Fahrner et al., 2021; Carr et al., 2017; Howat and Eddy, 2011; King et al., 2020). This terminus position retreat is linked to increasing ice discharge (King et al., 2020, 2018; Mouginot

et al., 2019). Between 2012 and 2017, ice discharge contributed to ~43% of the net mass loss from the Greenland Ice Sheet (Shepherd et al., 2020), and projections of future ice-sheet mass loss estimate that discharge will contribute as much as 50 ± 20% by 2100 (Choi et al., 2021).

The multidecadal behavior of marine-terminating outlet glaciers in Greenland is well-characterized (Goliber et al., 2022). Superimposed on these multidecadal trends, many glaciers exhibit seasonal terminus-position variability. This seasonal variability is typically expressed as wintertime advance and summertime retreat (Carr et al., 2013; Cassotto et al., 2015; Fried et al., 2018; Howat et al., 2010; Joughin et al., 2008b; Kehrl et al., 2017; Kneib-Walter et al., 2021; Moon et al., 2015; Murray et al., 2015; Sakakibara and Sugiyama, 2019; Schild and Hamilton, 2013; Seale et al., 2011). Seasonal terminus-position variability spatially varies in amplitude (Fried et al., 2018; Howat et al., 2010; Kehrl et al., 2017; Moon et al., 2015; Seale et al., 2011), and it has been suggested that the amplitude may depend on glacier width (Schild and Hamilton, 2013; Seale et al., 2011) or calving style (Fried et al., 2018). Most studies of seasonal terminus-position variability have examined either Greenland's largest outlet glaciers (Cassotto et al., 2015; Joughin et al., 2008b; Kehrl et al., 2017; Schild and Hamilton, 2013), a regional subset of glaciers (Carr et al., 2013; Fried et al., 2018; Howat et al., 2010; Moon et al., 2015; Sakakibara and Sugiyama, 2019; Seale et al., 2011), or a small number of glaciers around the ice sheet (Bevan et al., 2012).

Previous studies have suggested that seasonal terminus-position variability is driven by proglacial mélange, or by meltwater runoff. In front of some glaciers, a rigid mélange tends to form in the winter as sea ice freezes and binds icebergs together. At several glaciers in Greenland, the presence of a rigid mélange in front of a glacier terminus has been shown to inhibit calving and promote glacier advance, and similarly the clearing out or weakening of mélange is associated with glacier retreat (Carr et al., 2013; Cassotto et al., 2015; Fried et al., 2018; Howat et al., 2010; Joughin et

al., 2008a; Kehrl et al., 2017; Kneib-Walter et al., 2021; Moon et al., 2015; Todd and Christoffersen, 2014). However, there is not always a clear relationship between mélange and terminus position (Carr et al., 2013; Sakakibara and Sugiyama, 2019). Other work suggests that there is a relationship between seasonal terminus retreat and the timing and duration of meltwater runoff (Fried et al., 2018), or relatedly, above-freezing air temperatures (Carr et al., 2013), as this runoff may drive terminus-face melting through subglacial upwelling and undercutting (Wood et al., 2021), or enhance hydrofracture-induced calving (Nick et al., 2010; Sohn et al., 1998) However, other studies have found a weaker or no relationship between seasonal terminus positions and runoff or its proxies such as air temperature (Joughin et al., 2008a; Moon et al., 2015; Schild and Hamilton, 2013).

Glacier flow is highly sensitive to changes at the terminus (Joughin et al., 2008b; Meier and Post, 1987; Nick et al., 2009; Schoof, 2007; Howat et al., 2008), so short-term terminus position variability may influence longer-term trends in glacier dynamics and, consequently, ice-sheet mass balance. Omitting terminus seasonality from numerical models can lead to both over- and under-estimated mass change projections on decadal time scales for individual glaciers, depending primarily on the magnitude of terminus seasonality (Felikson et al., 2022). Therefore, it is important that the terminus seasonality of individual glaciers be well-characterized.

To maintain a tight focus, we limit this investigation primarily to characterizing seasonal terminus-position variability for marine-terminating outlet glaciers around the entire Greenland Ice Sheet. Thus, given the number of processes contributing to seasonal variability (e.g., surface melt, ocean temperatures, and mélange) a detailed investigation of the causes of seasonal variability is beyond the scope of this paper. Our methods capitalize on the capabilities of the Sentinel-1A/B synthetic aperture radar (SAR) satellites, which typically imaged Greenland at a repeat interval of six days

when both satellites were operating. For the period from January 2015 through December 2021, we manually digitized monthly terminus positions for 199 glaciers around Greenland, and six-day terminus positions for an additional 20 glaciers in central-west and northwest Greenland. We use these terminus position data to characterize the magnitude and trends of seasonal terminus-position variability, and to estimate the frequency and seasonality of glacier retreat events at a six-day level.

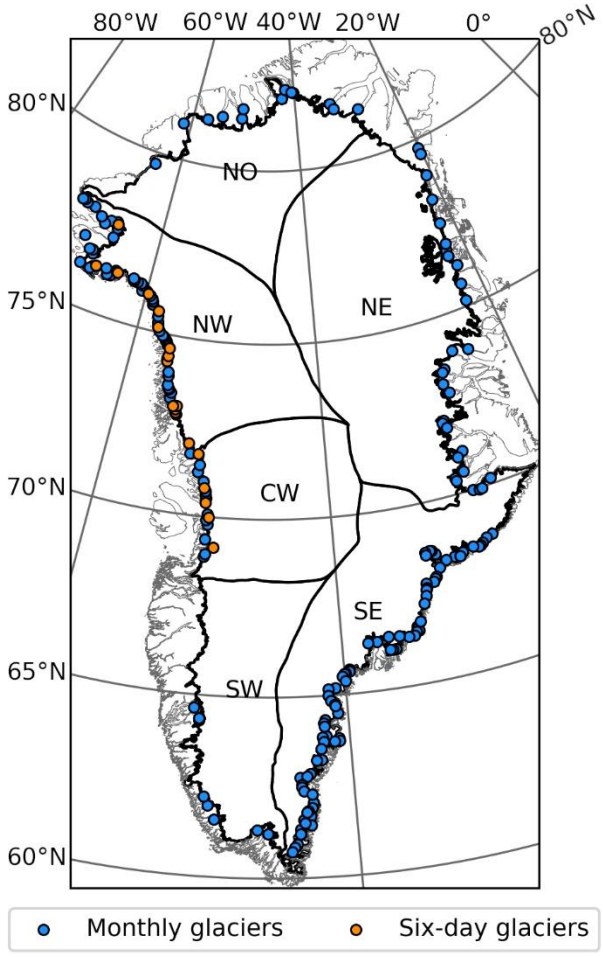

Figure 4.1: Map of glaciers and ice-sheet regions.
Map of glaciers covered in this study. Glaciers digitized at monthly resolution are in blue, and glaciers digitized at six-day resolution are in orange. The regions outlined are southwest (SW), central-west (CW), northwest (NW), north (NO), northeast (NE), and southeast (SE) Greenland.

4.2 Data

We used a total of 373 Sentinel-1A/B SAR mosaics (Joughin, 2020) to digitize glacier terminus positions at monthly and six-day intervals from January 2015 through December 2021. We chose this time period based on the availability of Sentinel-1 mosaics at the time that we digitized the glacier termini (late 2021 and early 2022) and in order to capture complete years of data. The monthly glaciers are located around the full margin of the ice sheet, while the six-day glaciers are concentrated in central-west and northwest Greenland (Figure 4.1).

4.2.1 Satellite images

SAR mosaics of the Greenland Ice Sheet were generated from images taken by the Sentinel-1A/B satellite pair (Joughin, 2020). These satellites are able to image the ice-sheet surface regardless of cloud conditions or solar illumination, making them valuable for capturing changes in glacier behavior throughout the year. Since Version 3, the SAR mosaic product has 25 m image resolution; earlier versions had 50 m resolution. The mosaics cover 12-day intervals from 1 January 2015 through 27 September 2016, during which time only Sentinel-1A was in orbit. After the launch of Sentinel-1B, the mosaics cover six-day intervals, up until the failure of Sentinel-1B on 23 December 2021, after which the mosaics returned to 12-day intervals. Occasionally, missed acquisitions produce intermittent spatial gaps (missing swaths) in the SAR mosaics, with corresponding temporal gaps in terminus position data for the affected glaciers.

4.2.2 Terminus positions

We manually digitized glacier terminus positions from Sentinel-1A/B SAR mosaics using ArcGIS. All digitizing was performed by a single analyst to reduce potential differences in interpretation of imagery. The error associated with these manually digitized terminus positions is typically

comparable to the image resolution (*i.e.*, 25 m for most SAR mosaics used in this study) (Moon et al., 2015) and often results from difficult interpretation conditions arising from poor image contrast, such as extensive proglacial mélange cover.

We digitized terminus positions for a total of 219 marine-terminating outlet glaciers (Figure 4.1), 199 of which were digitized at monthly intervals (Table C. 1), and 20 of which were digitized at six-day intervals (Table C. 2). For the monthly glaciers, we used the first SAR mosaic entirely within each month (*e.g.*, for the month of May, we may use 5–10 May, but not 29 April–4 May), from January 2015 through December 2021. For the 20 six-day glaciers , we chose to focus on central-west and northwest Greenland, where outlet glaciers have been changing rapidly (Black and Joughin, 2022; King et al., 2020), and selected glaciers with clear seasonal variations in the monthly data that we wanted to capture at higher temporal resolution. As part of this set, we selected all five glaciers in Upernavik Icefjord to include a local grouping of glaciers. For comparison to those with clear seasonal variations, we included one glacier (Yngvar Nielson Gletsjer, no. 65) that did not show strong seasonal variability in the monthly data. For these six-day glaciers, we digitized terminus positions in all available SAR mosaics from January 2015 through December 2021 at 12-day intervals before October 2016 and six-day intervals thereafter. For simplicity, we refer to metrics associated with this dataset as "six-day" (*e.g.*, "six-day glaciers").

4.3 Methods

We digitized 23,333 glacier terminus positions representing January 2015 through December 2021, with an average of 82 per glacier for the monthly glaciers and 353 per glacier for the six-day glaciers. We calculated glacier area and length change and used these data to identify the significance, timing, and magnitude of terminus position seasonality for each glacier. We also

summarized these characteristics for all glaciers around the ice sheet, as well as for individual regions of the ice sheet (IMBIE, 2022; Rignot and Mouginot, 2012). Finally, we identified the timing and magnitude of individual retreat events for the six-day glaciers.

4.3.1 Glacier area and length change

We used the box method (Moon and Joughin, 2008) to calculate glacier area over time. For each glacier, we defined an open-ended reference box with sides approximately parallel to ice flow and the back perpendicular to ice flow and upstream of the range of observed terminus positions. The box may be complex in shape (*i.e.*, composed of more than three line segments) as it follows glacier flow around obstacles and up fjords, particularly if the glacier has retreated substantially. Each terminus position intersects both sides of the box, forming a polygon from which we calculate the area. We calculated a proxy length over time by dividing each area measurement by the mean box width at the terminus, following the methods of Black and Joughin (2022).

4.3.2 Presence of terminus position seasonality

In characterizing terminus-position variability, one of our main objectives was to determine if there is a seasonal component to the pattern of terminus variation. To do this, we used the Lomb-Scargle periodogram, a tool for detecting periodicity in unevenly sampled data (Lomb, 1976; Scargle, 1982; VanderPlas, 2018). We chose this method due to the random temporal gaps in our time series associated with occasional missed satellite image acquisitions. For each glacier's set of terminus positions, we computed the length time series, linearly detrended the length, and calculated the Lomb-Scargle periodogram for the detrended time series. We determined the power for cycles with a period of one year and compared this to the Lomb-Scargle false-alarm level at p=0.05. This is the level at which, if there were no periodic signal in the data, there could still be

a peak at this frequency 5% of the time. If a glacier's length periodogram had a peak at annual frequency that exceeded the false-alarm level (*i.e.*, $p<0.05$), we declared it to have significant annual terminus position seasonality. Note that this classification only applies during our observation period (January 2015 through December 2021) as terminus position seasonality can change over time (*e.g.*, Joughin et al., 2008a).

4.3.3 Timing and magnitude of terminus position seasonality

For glaciers with significant annual terminus position seasonality (as determined with the Lomb-Scargle periodogram), we identified peaks and troughs in the glacier length time series to determine the timing and magnitude of seasonality (see example in Figure C. 1). We first used a peak-finding algorithm to identify all peaks and troughs in the length data, then detrended the data and found the resulting detrended length at each peak and trough. Then we found the date and detrended length of the highest peak and lowest trough for each year. In cases where retreat continued into the following year, we paired the associated trough with the peak in the previous year (*i.e.*, the peak from which the retreat initiated). We differenced the peak and trough lengths to find the magnitude of the terminus position seasonality for each year. Finally, for each glacier, we determined the median annual dates of greatest advance and retreat, the median duration of retreat, and the median magnitude of terminus position seasonality. We used these values to compute the Greenland-wide and regional timing and magnitude of terminus position seasonality.

4.3.4 Timing and magnitude of retreat events

For the six-day glaciers, we used each glacier's length time series to determine the timing and magnitude of retreat events (integrated over six days) for individual glaciers and cumulatively for the entire group of six-day glaciers. To do this, we differenced the glacier length time series to find

all potential retreat events (negative differences). To exclude small events within the range of terminus digitization uncertainty, we filtered the retreat events to retain only those with magnitudes greater than a threshold value of 50 m. In this process we do not account for glacier velocities, and so this method does not capture any retreat events that are smaller than the advance that occurred in the same time frame, *i.e.*, cases where there is net advance that is smaller than would be expected based on glacier velocity.

4.4 Results

Figure 4.2 shows the relative monthly glacier length as a function of time for each of the 219 glaciers in our study. A pattern of annual cycling between relatively advanced terminus positions (blue) and relatively retreated terminus positions (red) is visible for many glaciers, illustrating terminus position seasonality. The overall shift from blue to red over the entire duration illustrates an interannual retreat trend. Selected length time series are shown in Figure C. 2 and Figure C. 3 to illustrate what terminus position seasonality (or lack thereof) can look like for a subset of glaciers, including all of the six-day glaciers.

4.4.1 Prevalence of terminus position seasonality

To better isolate the annual signals in glacier length, we computed Lomb-Scargle periodograms for the detrended data for each glacier to identify significant annual peaks. We found that between 2015 and 2021, 73.5% (n=161) of Greenland's marine-terminating outlet glaciers exhibited significant annual terminus position seasonality at the 95% confidence level. For many of the other glaciers, annual peaks were visible in the Lomb-Scargle periodograms but below the 95% confidence level, suggesting some weak seasonal variability may be present.

Table 4.1 illustrates that glaciers with pronounced seasonality are more common in western Greenland (80.9 to 94.1%) and slightly less so in the east (64 to 69.3%). Seasonality is least common in the north (46.2%), where several glaciers have floating ice tongues, such as Petermann (no. 93) and Ryder (no. 96).

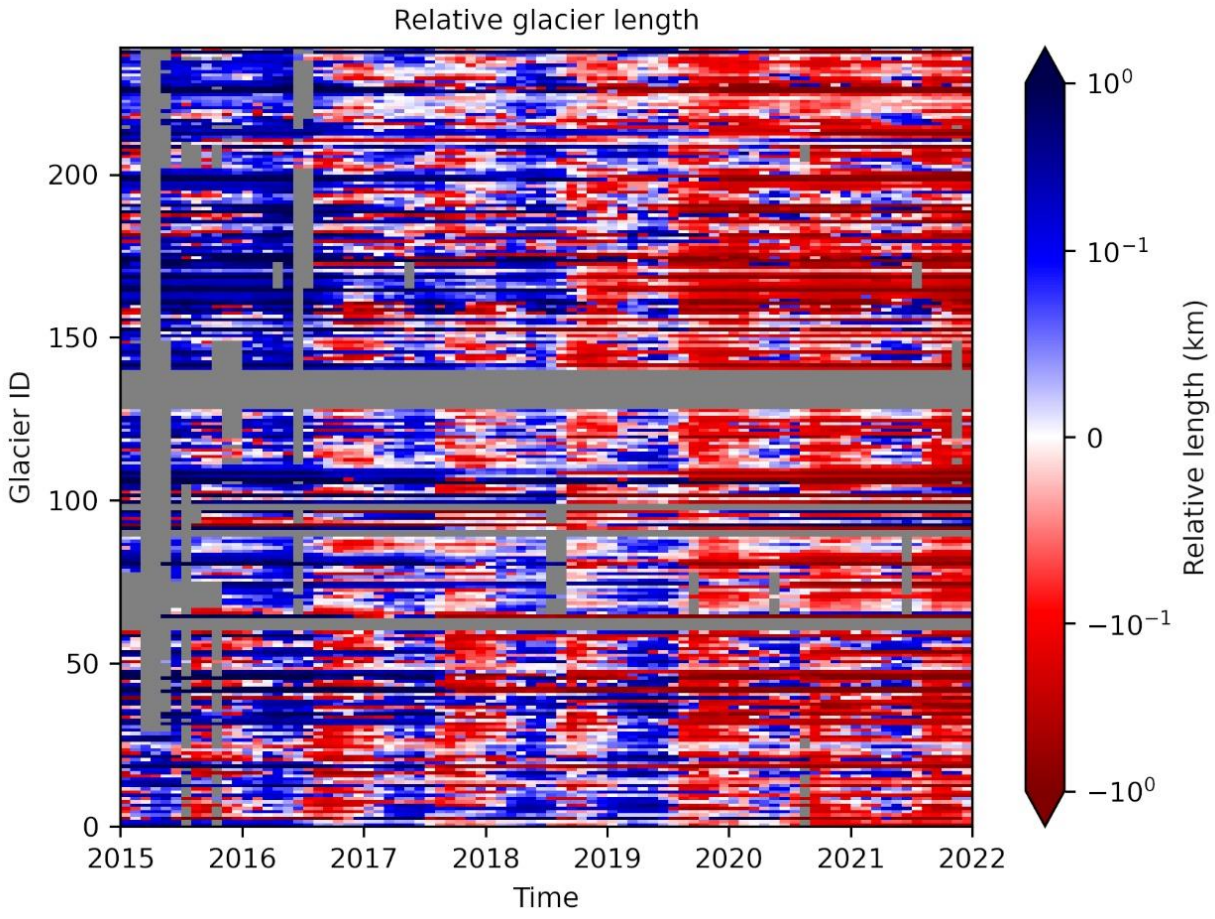

Figure 4.2: Glacier length relative to mean 2015–2021 length.
Glacier length relative to mean 2015–2021 length for each glacier. The Glacier ID system is derived from MEaSUREs glacier data (Joughin et al., 2015) and is detailed in Table C. 1 and Table C. 2. Terminus positions that are advanced relative to the mean length appear in blue, and terminus positions that are retreated relative to the mean length appear in red. No-data values are gray and are due to either spatial or temporal gaps in the SAR mosaics used for digitizing terminus positions.

Table 4.1: Regional quantification of terminus position seasonality.
Regional breakdown of the number and percentage of glaciers with significant ($p<0.05$) terminus position seasonality.

Region	Significant glaciers	Total glaciers	Percent significant
Southwest (SW)	7	8	87.5%
Central west (CW)	16	17	94.1%
Northwest (NW)	55	68	80.9%
North (NO)	6	13	46.2%
Northeast (NE)	16	25	64.0%
Southeast (SE)	61	88	69.3%
Greenland	**161**	**219**	**73.5%**

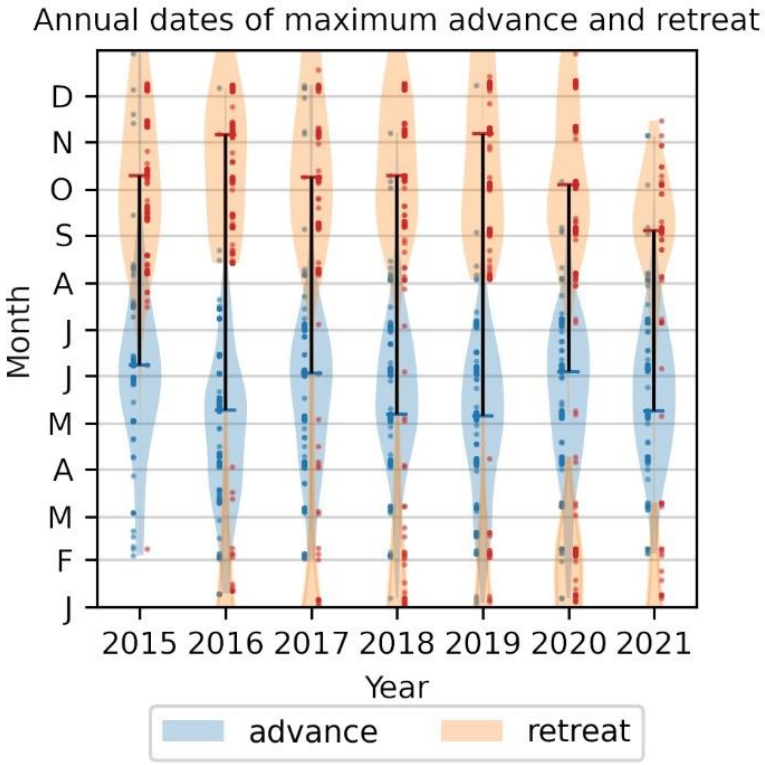

Figure 4.3: Timing of annual terminus position advance and retreat.
Distribution of the annual timing of maximum terminus position advance (blue) and maximum terminus position retreat (orange) for all seasonally-varying glaciers in the study. Horizontal bars show the median date of maximum advance or retreat for each year, and dots show the dates for individual glaciers. Vertical black bars show the duration of the retreat period each year, between the median dates of maximum advance and retreat. Retreat timing distributions in the early months of a year are continuations of the retreat timing distributions from the previous year.

4.4.2 Timing and magnitude of terminus position seasonality for all glaciers

We characterized the timing of terminus seasonality for the glaciers that had significant seasonality by finding the peaks and troughs in each glacier's length time series as described above. Figure 4.3 shows that these seasonally-varying glaciers tended to be at their most advanced state in late spring to early summer, and their most retreated state in autumn. Across all of these seasonally-varying glaciers, the median date of maximum advance ranged between May 6 and June 8, with a median of May 12. Retreat initiated immediately after the time of greatest advance, and the median date of maximum retreat ranged between September 4 and November 6, with a median of October 8. After this time, the glaciers began advancing again. The duration of the ice-sheet-wide retreat period, the time between the median dates of greatest advance and retreat, varied between 118 and 184 days, with an average of 145 days.

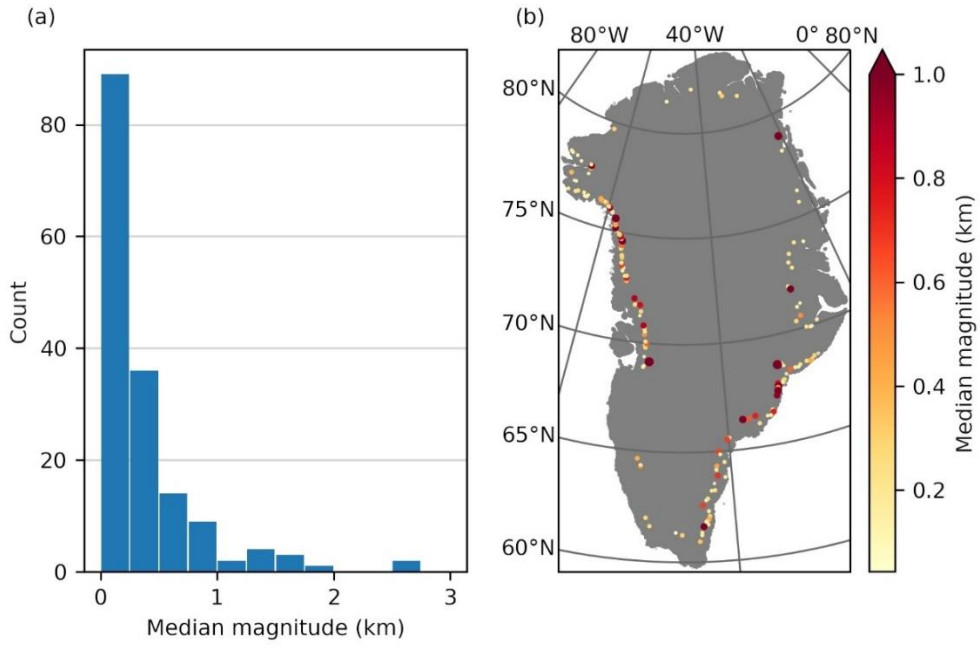

Figure 4.4: Magnitude of terminus position seasonality.
(a) Histogram and (b) map of the distribution of the median magnitude of terminus position seasonality for all seasonally-varying glaciers in the study. In (b) both the color and size of the points represent the magnitude of terminus position seasonality.

We calculated the amplitude of the seasonal signal in order to determine the typical annual range in detrended terminus positions. For the 161 glaciers with significant terminus seasonality, the magnitude of the terminus position seasonality is the difference between its detrended lengths at the dates of greatest advance and retreat. Figure 4.4a shows a histogram of the magnitude of terminus position seasonality. Across all of Greenland, the average annual range in terminus positions was 388 m, while the median was 221 m. Just over half of the glaciers had a magnitude of terminus position seasonality of less than 250 m. Lower magnitudes, however, should not necessarily be interpreted as evidence of weak seasonality, as some glaciers with relatively low magnitudes showed very clear seasonal cycles. For example, Eqip Sermia (no. 5) had a magnitude of about 290 m and showed very clear terminus position seasonality (Figure C. 3) (Kneib-Walter et al., 2021). Glaciers with particularly high magnitudes of terminus position seasonality include Kangerlussuaq (no. 153; 2.65 km seasonal magnitude), Sermeq Kujalleq (Jakobshavn Isbræ, no. 3; 2.59 km), Zachariae Isstrøm (no. 107; 1.76 km), and Sverdrup (no. 46; 1.72 km). Figure 4.4b indicates that these glaciers with a strong seasonal variation are distributed around the ice sheet.

To look at regional variations, we organized the glaciers into six groups defined by the regional drainage basins shown in Figure 4.1. Table 4.2 shows that the timing and magnitude of terminus position seasonality vary regionally. In the western regions of Greenland, the median dates of greatest advance and retreat tend to get later with increasing latitude. However, in the eastern regions the dates of greatest advance and retreat occur earlier in the north than in the south. The median magnitude of terminus position seasonality is highest in the southwest and central-west and is lowest in the north and northeast. The timing and magnitude of terminus position seasonality for individual glaciers is presented in Table C. 3.

Table 4.2: Regional timing and magnitude of terminus position seasonality.
Regional breakdown of the timing and magnitude of terminus position seasonality. All reported values are medians across the set of glaciers in a given region. To contextualize the magnitudes, note that the terminus digitization uncertainty is typically ~25 m.

Region	Peak advance	Peak retreat	Retreat duration (days)	Magnitude (m)
Southwest (SW)	April 20	September 7	156	273
Central west (CW)	May 1	September 9	153	225
Northwest (NW)	May 20	October 7	143	221
North (NO)	June 4	September 14	108	203
Northeast (NE)	May 6	October 5	148	201
Southeast (SE)	May 25	November 13	177	221
Greenland	**May 12**	**October 8**	**154**	**221**

4.4.3 Timing and magnitude of retreat events for six-day glaciers

We digitized 20 glaciers in central-west and northwest Greenland at six-day resolution rather than monthly resolution (Table C. 2). The greater temporal resolution of the six-day dataset allowed us to explore the number and magnitude of retreat events for this subset of glaciers in northwest and central-west Greenland. Note that we use the term ‘retreat events’ rather than ‘calving events’ because our method cannot detect calving that did not offset advance between observations, and because the calving that we did detect is integrated over a six-day period. Figure 5 shows that both the number and the magnitude of retreat events were greatest in July and August, and were lowest in January, February, and March. The timing and magnitude of retreat events for these 20 glaciers, individually and combined together, are shown in Figure C. 4 and Figure C. 5.

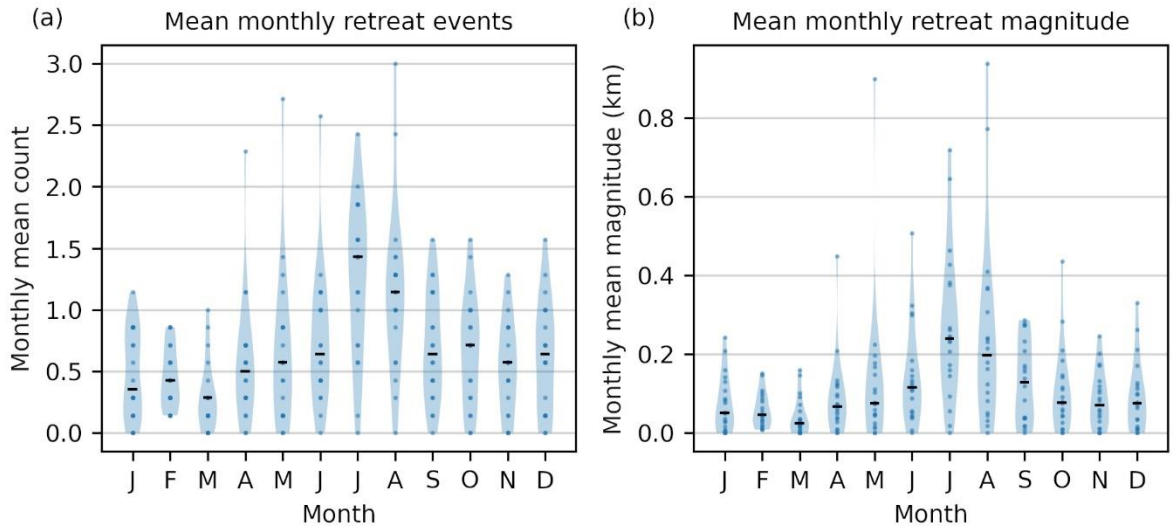

Figure 4.5: Number and magnitude of retreat events at six-day glaciers.
Distribution of the monthly (a) number and (b) magnitude of retreat events for each of the six-day glaciers. Horizontal black bars show the median for each month, and blue dots show the values for individual glaciers.

4.5 Discussion

The data reveal several interesting points about the prevalence (Table 4.1), timing (Figure 4.3), and magnitude (Figure 4.4) of terminus position seasonality around the Greenland Ice Sheet, its regions (Table 4.2), and at individual glaciers (Table C. 3).

4.5.1 Prevalence of terminus position seasonality

Our observations show that terminus position seasonality is widespread throughout Greenland (Figure 4.4b), and is especially common in western regions of the ice sheet (Table 4.1). We expect that the presence or absence of terminus position seasonality is related to ice velocity because advection of ice is necessary for the advance phase of the seasonal terminus position cycle. For instance, a glacier flowing at 50 m a^{-1} is unlikely to have annual terminus position seasonality of larger than 50 m, because it is not flowing fast enough to replenish the ice lost each year and

complete the seasonal cycle. To estimate representative velocities, we calculated the mean velocity along the most-retreated terminus position for each glacier, using a 2020 annual velocity map (Joughin, 2021; Joughin et al., 2010). We chose the most-retreated terminus position to ensure that it would be covered in the velocity map. Glaciers with significant terminus position seasonality tended to have a much higher velocity (median velocity of 840 m a^{-1}) than glaciers without significant terminus position seasonality (median velocity of 200 m a^{-1}). For a glacier flowing at an average of 840 m a^{-1}, a seasonal retreat of 220 m (the median magnitude of terminus position seasonality) represents removal of a quarter of the annual advection. Applying this relationship to the median velocity of glaciers for which we did not detect significant terminus position seasonality, we find that these glaciers could have a magnitude of terminus position seasonality of about 50 m, which would be difficult to detect in the Sentinel-1 SAR mosaics that we used.

We also explored whether our classification of the presence or absence of terminus position seasonality aligned with other classifications of glaciers in Greenland. Vijay et al. (2021) classified glaciers based on their seasonal velocity patterns following Moon et al. (2014), which may indicate variations in subglacial hydrology. Their classification includes glaciers that both speed up and slow down during the melt season ("type 2"), glaciers with high winter and spring velocities and a longer period of slowing ("type 3"), and glaciers with no classification. We compared our terminus position seasonality classification with their seasonal velocity classification and found that most glaciers in most velocity categories showed significant terminus position seasonality. We also compared our seasonality classification with the classification of Wood et al. (2021), who sorted glaciers into six categories based on their bathymetry at the terminus (*e.g.*, calving on a ridge, or calving in deep fjords). Again, we found that most glaciers in most bathymetry categories showed significant terminus position seasonality. Thus, the lack of a clear relationship with these

classifications suggests that, while the presence of terminus position seasonality may be related to mean annual velocity, it is likely not related to seasonal velocity variations. Similarly, the types of bathymetry analyzed by Wood et al. (2021) do not seem to influence whether or not terminus position seasonality occurs. However, we have not established whether seasonal velocity variations or terminus bathymetry have an effect on the magnitude of terminus position seasonality.

4.5.2 Timing of terminus position seasonality

We established that, ice sheet-wide, seasonal glacier advance tends to peak (and retreat begins) in May or early June each year, and retreat tends to peak (and advance begins) in October or early November (Figure 4.3), with variations in timing in different regions of the ice sheet (Table 4.2). The timing of peak advance and retreat that we observe is generally consistent with regional studies of glacier terminus seasonality (Fried et al., 2018; Carr et al., 2013; Seale et al., 2011). In cases where there are differences in the timing of terminus position seasonality, it appears to be related to the number of glaciers sampled (Sakakibara and Sugiyama, 2019). The only difference in Greenland-wide compilations is with King et al. (2018), who found that ice-sheet-wide retreat commenced about a month earlier (early April through late September) than our findings (mid-May through early October; Table 2). However, in calculating the timing of retreat, King et al. (2018) weighted each glacier by its contribution to total discharge; some of the highest-discharge glaciers begin retreating earlier in the year, which would bias the weighted timing of retreat earlier in the year as well. We do find that the number and magnitude of retreat events, which typically peaked in July and August (Figure 4.5), matches well with the seasonal peak discharge in mid-July reported by King et al. (2018).

The duration of the retreat period varies from year to year (Figure 4.3), with 2019 and 2016 having the longest retreat periods (180 to 184 days) and 2020, 2015, and 2017 having the shortest retreat periods (122 to 128 days); 2018 was in the middle with a retreat duration of 156 days. We do not include 2021 here because retreat can continue into the following year, and we have not digitized data for 2022, so our retreat duration for 2021 may be truncated. In the years with the longest retreat periods, retreat both started earlier (early May) and ended later (early November) than in the years with shorter retreat periods (early June through early October); in 2018 retreat occurred from early May through early October. The earlier initiation of retreat for the years with longer retreat durations may be related to the timing of the onset of melt on the ice sheet. We examined cumulative annual melt area (Mote, 2014; Mote and Anderson, 1995) and found that melt started relatively early (mid-April) in 2016, 2018, and 2019, and relatively late (early May) in 2015 and 2017. The 2020 result appears to be an outlier as early-season melt followed a similar trajectory to 2018 and 2019, but 2020 had the shortest observed retreat period. The timing of the onset of melt may control the initiation and duration of retreat through the effects of increased melt on early mélange breakup, hydrofracture-induced calving, and terminus undercutting through enhanced subglacial discharge. The timing of the onset of melt appears to be more important to retreat duration than the total melt, as 2015 and 2020 ultimately had moderate cumulative melt (more than 2017 and 2018), but also had the shortest retreat durations in our record. The duration of the retreat period also does not appear to correspond strongly with annual net mass balance or surface mass balance (Shepherd et al., 2020; Simonsen et al., 2021; Fettweis et al., 2017).

Our findings about the timing and magnitude of terminus position seasonality provide some insights into previous studies. Fried et al. (2018) found that glaciers with terminus position seasonality of a magnitude less than 500 m tended to be more sensitive to runoff. We found that

78% of glaciers in our study had a seasonal magnitude less than 500 m (Figure 4.4), so it is possible that runoff dominates seasonality for most glaciers in Greenland. However, a number of the glaciers in our study start advancing very late in the season (*e.g.*, December, January) and/or start retreating very early in the season (*e.g.*, February, March) (Figure 4.3), which suggests that the timing of their seasonality is not entirely controlled by runoff. Instead, the timing of seasonality for these glaciers seems more likely to be controlled by the formation of proglacial mélange, which tends to lag the end of runoff and can facilitate glacier advance (Carr et al., 2013; Howat et al., 2010; Joughin et al., 2008a; Kehrl et al., 2017; Kneib-Walter et al., 2021; Todd and Christoffersen, 2014), and by mid-winter episodes of mélange clearing, which can help initiate early glacier retreat (Cassotto et al., 2015; Joughin et al., 2008a). The conditions under which each mechanism may dominate remain unclear.

4.5.3 Magnitude of terminus position seasonality

The magnitude of seasonal terminus variations tends to be small relative to the multi-decadal retreat, with 55% of glaciers having a magnitude less than 250 m, and only 22% having a magnitude greater than 500 m (Figure 4.4). Many prior studies of glacier terminus seasonality used MODIS daily imagery to capture terminus positions at a higher temporal resolution than we could achieve with Sentinel-1 (Joughin et al., 2008b; Schild and Hamilton, 2013; Seale et al., 2011). However, the spatial resolution of MODIS imagery at best is limited to 250 m, so the terminus position seasonality of many glaciers in Greenland would not be detectable in MODIS imagery. Studies using higher-resolution imagery have been focused on western Greenland (Carr et al., 2013; Fried et al., 2018; Moon et al., 2015). Fried et al. (2018) found seasonal terminus position cycles ranging in magnitude from 150 to 1000 m in central-west Greenland, which is consistent with our findings for the same subset of glaciers, with magnitudes ranging from 80 to 880 m. The

only glacier in central-west Greenland with a larger magnitude was Sermeq Kujalleq (Jakobshavn Isbræ, no. 3), with a magnitude of 2600 m, but this glacier was not included in Fried et al. (2018). In northwestern Greenland, previous estimates of magnitudes of terminus position seasonality ranged from 600 to 800 m (Carr et al., 2013; Moon et al., 2015), which is three to four times higher than our median magnitude of 220 m for this region. These studies looked at small subsets of glaciers in northwestern Greenland; applying approximately the same subsets to our data, we found median magnitudes ranging from 340 to 470 m and mean magnitudes between 530 and 550 m, which are still below the previously reported magnitudes. These differences in magnitude may reflect differences in methodology, as we remove the interannual length trend before calculating the magnitude of the terminus position seasonality. Alternatively, the differences between our study and previously reported values could reflect the evolution of terminus position seasonality over time, as the data from Carr et al. (2013) were taken from 2004 through 2012, and those from Moon et al. (2015) were from 2009 through 2014, both of which predate our study period (2015–2021).

Some previous studies have found a strong relationship between the magnitude of terminus position seasonality and glacier width (Schild and Hamilton, 2013; Seale et al., 2011). We examined the relationship between magnitude and width for the glaciers in our study and found that, while there was a significant correlation ($p=0.004$), width alone did not explain much of the variance in the data ($R^2=0.051$). This correlation was improved somewhat ($p=0.000$, $R^2=0.178$) by removing Sermersuaq (Humboldt Glacier, no. 92), which at ~32 km wide was a substantial outlier (Figure C. 6). Seale et al. (2011) also found that glaciers with magnitudes of terminus position seasonality of less than 1 km were typically less than 2 km wide. However, we found that of 148

glaciers with magnitudes of terminus position seasonality less than 1 km, 107 were actually wider than 2 km.

We instead found a stronger correlation between the magnitude of terminus position seasonality and mean annual glacier velocity ($p=0.000$, $R^2=0.479$; Figure C. 7). The stronger correlation between terminus position seasonality and glacier velocity makes sense when considering how much a glacier would have to calve to balance its velocity. For instance, at a glacier that is flowing at several kilometers per year at the terminus, our median magnitude of terminus position seasonality of 221 m would be a relatively small signal. However, above we showed that this terminus position seasonality would remove a quarter of the annual advection for a glacier flowing at the median observed annual velocity. Because our data are detrended, the magnitude of terminus position seasonality is separated from interannual terminus position trends. Our measured magnitude of terminus position seasonality also only captures the period of seasonal retreat and does not include calving events that may happen outside of that period. Therefore, there is likely to be additional retreat each year to offset the annual advection and generate the widespread interannual retreat that has been observed.

Table 4.3: Terminus position seasonality for select individual glaciers.
Timing and magnitude of terminus position seasonality for several individual glaciers for comparison with previous studies. All reported values are medians for the given glacier.

Glacier	Peak advance	Peak retreat	Retreat duration (days)	Magnitude (m)
Sermeq Kujalleq (Jakobshavn)	April 16	August 14	120	2590
Kangilliup Sermia (Rink)	June 4	September 22	110	810
Daugaard-Jensen	April 8	September 2	147	1330
Kangerlussuaq	July 2	December 26	177	2650
Helheim	April 7	September 24	170	1480

4.5.4 Comparisons with select individual glaciers

The spatial breadth of our study allows us to make comparisons to data on several individual large glaciers reported in previous studies (Table 4.3). At all of these glaciers, we find that the differences in the timing and magnitude of terminus position seasonality reported by our study compared to others are relatively small (approximately a month). These differences can likely be explained by interannual variations in terminus position seasonality and the different time periods covered by these studies.

At Sermeq Kujalleq (Jakobshavn Isbræ, no. 3), we found that the timing of retreat was generally consistent with Schild and Hamilton (2013), who found that retreat typically occurred from March through August in 2001 through 2010. Joughin et al. (2008a) found that retreat ended later, in late September, although those data were collected when the terminus was rapidly evolving following the disintegration of the ice tongue. However, our data did agree with Joughin et al. (2008a) in finding rapid calving at Jakobshavn Isbræ in the spring and summer and limited calving in the winter.

At Kangilliup Sermia (Rink Isbræ, no. 17), we also found that the timing of retreat was consistent with Schild and Hamilton (2013), who found that retreat typically occurred from late May through September. Howat et al. (2010) found that this glacier's magnitude of terminus position seasonality was about 1000 m, while we found a slightly smaller value of 810 m.

At Daugaard-Jensen (no. 120), we found that retreat began over a month earlier than Schild and Hamilton (2013), who found that retreat began in late May; however, our findings for the timing of the end of retreat in early September were comparable.

At Kangerlussuaq (no. 153), our findings for the timing of retreat are consistent with those of Kehrl et al. (2017), who found that it typically retreated from mid-July until December; however, Schild and Hamilton (2013) found that Kangerlussuaq instead retreats from July through late September. The data from Kehrl et al. (2017) are more recent (2008–2016), so they are more likely to be consistent with our results. The maximum retreat in December is notable in that it is several months later than the maximum retreat timing at the other large glaciers that we looked at (Table 4.3). Kehrl et al. (2017) also found that Kangerlussuaq had a magnitude of terminus position seasonality of ~3 km, which is comparable to our magnitude of 2.65 km, making it the largest-magnitude glacier in our study.

Finally, at Helheim, we found that the timing of the initiation of retreat was shifted a month earlier than Schild and Hamilton (2013) and Joughin et al. (2008b), who found that Helheim typically retreated and calved more from May through September. Kehrl et al. (2017) reported that Helheim reached its greatest advance in late winter and its greatest retreat in late summer, which may be more consistent with our timings of April and September, respectively.

4.6 Conclusions

We used Sentinel-1 SAR images to characterize terminus position seasonality for 219 marine-terminating glaciers around Greenland from January 2015 through December 2021. We found that terminus position seasonality is common, with 74% of glaciers expressing significant seasonality. The glaciers that do not have significant terminus position seasonality tend to have large floating tongues or relatively low ice velocities. Of the glaciers with significant terminus position seasonality, retreat typically begins in mid-May and advance typically begins in early October, with some variation in different years and in different regions of Greenland, and substantial variation among individual glaciers. The number and timing of retreat events peaks in July and

August and is lowest in January through March. The average annual peak-to-trough magnitude of terminus position seasonality is nearly 400 m, although this is skewed by a few glaciers with very large seasonal cycles; the median magnitude is about 220 m. We found a stronger relationship between the magnitude of terminus position seasonality and glacier velocity than between magnitude and glacier width. Because glacier dynamics are sensitive to conditions at the terminus, understanding terminus position seasonality is important for projecting future glacier change. This study provides an important step forward by extending characterizations of terminus seasonality from individual glaciers and regions to the entire ice sheet.

Chapter 5. Summary and future work

In the preceding chapters of this dissertation, I have investigated glacier terminus changes in Greenland and Alaska on decadal to weekly time scales. Here, I summarize those investigations and discuss suggestions for future work.

5.1 Identifying mechanisms driving multi-decadal glacier retreat in Greenland

In Chapter 2, I showed that in northwest and central-west Greenland, the retreat of marine-terminating glaciers accelerated from around 1996, and that this retreat was most sensitive to increases in meltwater runoff and ocean temperatures. Runoff and ocean temperatures can affect glacier terminus retreat through several mechanisms, including by enhancing terminus undercutting and by reducing mélange rigidity; runoff can also enhance retreat through hydrofracture-induced calving. It is likely that a combination of these mechanisms is responsible for the widespread retreat observed in this region of Greenland. One of the limiting factors of this study and many like it is the lack of spatiotemporally dense observations of fjord conditions, such as near-terminus temperatures, circulation, and mélange conditions. Sampling at least seasonally both within individual fjords and across many fjords would improve our ability to resolve the mechanisms driving glacier retreat.

5.2 Monitoring glacier change in Kenai Fjords National Park

In Chapter 3, I showed that most glaciers in Kenai Fjords National Park retreated between 1984 and 2021, and the exceptions were predominantly tidewater glaciers. The presence of glaciers in the park affects both terrestrial and marine ecosystems, and glacier retreat will result in changes to landcover that also influence their associated ecosystems. Glacier retreat is also expected to affect ecotourism in the park, as glaciers are one of the main attractions for park visitors. I recommend

that resource managers in Kenai Fjords National Park, and at similar sites, map the extent of glaciers in their jurisdiction at least annually to maintain an understanding of the current state of glacier change. Complementary to monitoring glacier change is monitoring associated ecosystem change; I recommend that resource managers thoroughly characterize the current state of near-glacier ecosystems (such as proglacial lakes and nearshore marine environments) in order to develop a baseline against which to compare future changes.

5.3 Characterizing terminus position seasonality in Greenland

In Chapter 4, I showed that terminus position seasonality is widespread in Greenland, with retreat typically occurring from mid-May through early October, and with the number and magnitude of retreat events typically peaking in July and August. The presence and magnitude of terminus position seasonality appears to be influenced by ice velocities, while the duration of the annual retreat period may be driven in part by the timing of the onset of ice-sheet surface melt. I generated a large database of glacier terminus positions for this work, and there are several interesting avenues that could be pursued with those data in combination with other datasets and models. The characterization of the timing and magnitude of retreat events does not account for glacier velocity, and doing so would allow for the further identification of smaller retreat events that are not large enough to entirely offset the advection that occurs during the six-day observation period. The terminus position data could also be combined with bathymetry and ice thickness to determine whether the seasonal retreat that occurs each year is constrained by topographic pinning points. Finally, the seasonality metrics that I generated, or the raw terminus position data themselves, can be incorporated into numerical models of glacier dynamics to explore how seasonal variations affect projections of future ice-sheet mass change.

5.4 Additional recommendations

This dissertation has relied on extensive manual digitization of glacier terminus positions, a process which is incredibly time- and labor-intensive. In recent years, machine-learning methods for the automated detection of glacier termini in satellite imagery have greatly improved in accuracy. However, these methods still require manually-digitized training data, especially in situations where the terminus is more difficult to discern, such as in shadowy images or in mélange-choked fjords. All of my terminus data have been formatted in a labeled manner that is suitable as machine-learning training data, based on conversations with machine-learning practitioners, and all of my terminus data have been or will be posted on public data archives. I suggest that these data be used as training data for automated detection of glacier termini in both optical and SAR imagery, in a variety of illumination and proglacial conditions, and for both water-terminating and land-terminating glaciers.

References

Adalgeirsdóttir, G., Echelmeyer, K. A., and Harrison, W. D.: Elevation and volume changes on the Harding Icefield, Alaska, Journal of Glaciology, 44, 570–582, https://doi.org/10.3189/S0022143000002082, 1998.

Amundson, J. M., Fahnestock, M., Truffer, M., Brown, J., Lüthi, M. P., and Motyka, R. J.: Ice mélange dynamics and implications for terminus stability, Jakobshavn Isbræ, Greenland, Journal of Geophysical Research: Earth Surface, 115, F01005, https://doi.org/10.1029/2009JF001405, 2010.

Arendt, A. and Rich, J. L.: Randolph Glacier Inventory, University of Alaska Fairbanks [dataset], 2013.

Arendt, A., Walsh, J., and Harrison, W.: Changes of Glaciers and Climate in Northwestern North America during the Late Twentieth Century, Journal of Climate, 22, 4117–4134, https://doi.org/10.1175/2009JCLI2784.1, 2009.

Arendt, A. A., Echelmeyer, K. A., Harrison, W. D., Lingle, C. S., and Valentine, V. B.: Rapid Wastage of Alaska Glaciers and Their Contribution to Rising Sea Level, Science, 297, 382–386, https://doi.org/10.1126/science.1072497, 2002.

Arimitsu, M. L., Piatt, J. F., Madison, E. N., Conaway, J. S., and Hillgruber, N.: Oceanographic gradients and seabird prey community dynamics in glacial fjords, Fisheries Oceanography, 21, 148–169, https://doi.org/10.1111/j.1365-2419.2012.00616.x, 2012.

Arimitsu, M. L., Piatt, J. F., and Mueter, F.: Influence of glacier runoff on ecosystem structure in Gulf of Alaska fjords, Marine Ecology Progress Series, 560, 19–40, https://doi.org/10.3354/meps11888, 2016.

Barclay, D. J., Wiles, G. C., and Calkin, P. E.: Holocene glacier fluctuations in Alaska, Quaternary Science Reviews, 28, 2034–2048, https://doi.org/10.1016/j.quascirev.2009.01.016, 2009.

Beamer, J. P., Hill, D. F., Arendt, A., and Liston, G. E.: High-resolution modeling of coastal freshwater discharge and glacier mass balance in the Gulf of Alaska watershed, Water Resources Research, 52, 3888–3909, https://doi.org/10.1002/2015WR018457, 2016.

Benn, D. I., Warren, C. R., and Mottram, R. H.: Calving processes and the dynamics of calving glaciers, Earth-Science Reviews, 82, 143–179, https://doi.org/10.1016/j.earscirev.2007.02.002, 2007.

Bevan, S. L., Luckman, A. J., and Murray, T.: Glacier dynamics over the last quarter of a century at Helheim, Kangerdlugssuaq and 14 other major Greenland outlet glaciers, The Cryosphere, 6, 923–937, https://doi.org/10.5194/tc-6-923-2012, 2012.

Bianchi, T. S., Arndt, S., Austin, W. E. N., Benn, D. I., Bertrand, S., Cui, X., Faust, J. C., Koziorowska-Makuch, K., Moy, C. M., Savage, C., Smeaton, C., Smith, R. W., and Syvitski, J.:

Fjords as Aquatic Critical Zones (ACZs), Earth-Science Reviews, 203, 103145, https://doi.org/10.1016/j.earscirev.2020.103145, 2020.

Bidlack, A. L., Bisbing, S. M., Buma, B. J., Diefenderfer, H. L., Fellman, J. B., Floyd, W. C., Giesbrecht, I., Lally, A., Lertzman, K. P., Perakis, S. S., Butman, D. E., D'Amore, D. V., Fleming, S. W., Hood, E. W., Hunt, B. P. V., Kiffney, P. M., McNicol, G., Menounos, B., and Tank, S. E.: Climate-Mediated Changes to Linked Terrestrial and Marine Ecosystems across the Northeast Pacific Coastal Temperate Rainforest Margin, BioScience, 71, 581–595, https://doi.org/10.1093/biosci/biaa171, 2021.

Bitz, C. M. and Battisti, D. S.: Interannual to Decadal Variability in Climate and the Glacier Mass Balance in Washington, Western Canada, and Alaska, Journal of Climate, 12, 3181–3196, https://doi.org/10.1175/1520-0442(1999)012<3181:ITDVIC>2.0.CO;2, 1999.

Bjørk, A. A., Kjær, K. H., Korsgaard, N. J., Khan, S. A., Kjeldsen, K. K., Andresen, C. S., Box, J. E., Larsen, N. K., and Funder, S.: An aerial view of 80 years of climate-related glacier fluctuations in southeast Greenland, Nature Geoscience, 5, 427–432, https://doi.org/10.1038/ngeo1481, 2012.

Bjørk, A. A., Kruse, L. M., and Michaelsen, P. B.: Brief communication : Getting Greenland's glaciers right – a new data set of all official Greenlandic glacier names, The Cryosphere, 9, 2215–2218, https://doi.org/10.5194/tc-9-2215-2015, 2015.

Black, T.: 2021_KEFJ_glaciers: v1.0, , https://doi.org/10.5281/zenodo.6331265, 2022.

Black, T. and Kurtz, D.: Satellite observations of maritime glacier terminus positions at Kenai Fjords National Park, Integrated Resource Management Applications (IRMA) [dataset], 2022a.

Black, T. E. and Joughin, I.: Multi-decadal retreat of marine-terminating outlet glaciers in northwest and central-west Greenland, The Cryosphere, 16, 807–824, https://doi.org/10.5194/tc-16-807-2022, 2022.

Black, T. E. and Kurtz, D.: Maritime glacier retreat and terminus area change in Kenai Fjords National Park, Alaska, between 1984 and 2021, Journal of Glaciology, https://doi.org/10.1017/jog.2022.55, 2022b.

Brinkerhoff, D., Truffer, M., and Aschwanden, A.: Sediment transport drives tidewater glacier periodicity, Nature Communications, 8, 8, https://doi.org/10.1038/s41467-017-00095-5, 2017.

Bunce, C., Carr, J. R., Nienow, P. W., Ross, N., and Killick, R.: Ice front change of marine-terminating outlet glaciers in northwest and southeast Greenland during the 21st century, Journal of Glaciology, 64, 1–13, https://doi.org/10.1017/jog.2018.44, 2018.

Calkin, P. E., Wiles, G. C., and Barclay, D. J.: Holocene coastal glaciation of Alaska, Quaternary Science Reviews, 20, 449–461, https://doi.org/10.1016/S0277-3791(00)00105-0, 2001.

Capps, D. M.: The role of glaciers and glacier research in the development of U. S. national parks, Earth Sciences History, 36, 337–358, https://doi.org/10.17704/1944-6178-36.2.337, 2017.

Carr, J. R., Vieli, A., and Stokes, C.: Influence of sea ice decline, atmospheric warming, and glacier width on marine-terminating outlet glacier behavior in northwest Greenland at seasonal to interannual timescales, Journal of Geophysical Research: Earth Surface, 118, 1210–1226, https://doi.org/10.1002/jgrf.20088, 2013.

Carr, J. R., Vieli, A., Stokes, C. R., Jamieson, S. S. R., Palmer, S. J., Christoffersen, P., Dowdeswell, J. A., Nick, F. M., Blankenship, D. D., and Young, D. A.: Basal topographic controls on rapid retreat of Humboldt Glacier, northern Greenland, Journal of Glaciology, 61, 137–150, https://doi.org/10.3189/2015JoG14J128, 2015.

Carr, J. R., Stokes, Chris. R., and Vieli, A.: Threefold increase in marine-terminating outlet glacier retreat rates across the Atlantic Arctic: 1992–2010, Annals of Glaciology, 58, 72–91, https://doi.org/10.1017/aog.2017.3, 2017.

Cassotto, R., Fahnestock, M., Amundson, J. M., Truffer, M., and Joughin, I.: Seasonal and interannual variations in ice melange and its impact on terminus stability, Jakobshavn Isbræ, Greenland, Journal of Glaciology, 61, 76–88, https://doi.org/10.3189/2015JoG13J235, 2015.

Catania, G. A., Stearns, L. A., Sutherland, D. A., Fried, M. J., Bartholomaus, T. C., Morlighem, M., Shroyer, E., and Nash, J.: Geometric Controls on Tidewater Glacier Retreat in Central Western Greenland, Journal of Geophysical Research: Earth Surface, 123, 2024–2038, https://doi.org/10.1029/2017JF004499, 2018.

Choi, Y., Morlighem, M., Rignot, E., and Wood, M.: Ice dynamics will remain a primary driver of Greenland ice sheet mass loss over the next century, Communications Earth & Environment, 2, 1–9, https://doi.org/10.1038/s43247-021-00092-z, 2021.

Christian, J. E., Robel, A. A., and Catania, G.: A probabilistic framework for quantifying the role of anthropogenic climate change in marine-terminating glacier retreats, The Cryosphere Discussions, 1–28, https://doi.org/10.5194/tc-2021-394, 2022.

Cook, S. J., Christoffersen, P., Truffer, M., Chudley, T. R., and Abellán, A.: Calving of a Large Greenlandic Tidewater Glacier has Complex Links to Meltwater Plumes and Mélange, Journal of Geophysical Research: Earth Surface, 126, e2020JF006051, https://doi.org/10.1029/2020JF006051, 2021.

Criscitiello, A. S., Kelly, M. A., and Tremblay, B.: The Response of Taku and Lemon Creek Glaciers to Climate, Arctic, Antarctic, and Alpine Research, 42, 34–44, https://doi.org/10.1657/1938-4246-42.1.34, 2010.

Echelmeyer, K. A., Valentine, V. B., and Zirnheld, S. L.: Airborne Surface Profiling of Alaskan Glaciers, Version 1, NSIDC: National Snow and Ice Data Center [dataset], https://doi.org/10.7265/N5RF5RZJ, 2002.

Enderlin, E. M., Howat, I. M., Jeong, S., Noh, M.-J., van Angelen, J. H., and van den Broeke, M. R.: An improved mass budget for the Greenland ice sheet, Geophysical Research Letters, 41, 866–872, https://doi.org/10.1002/2013GL059010, 2014.

Etherington, L. L., Hooge, P. N., Hooge, E. R., and Hill, D. F.: Oceanography of Glacier Bay, Alaska: Implications for biological patterns in a glacial fjord estuary, Estuaries and Coasts: J ERF, 30, 927–944, https://doi.org/10.1007/BF02841386, 2007.

Ettema, J., van den Broeke, M. R., van Meijgaard, E., van de Berg, W. J., Bamber, J. L., Box, J. E., and Bales, R. C.: Higher surface mass balance of the Greenland ice sheet revealed by high-resolution climate modeling, Geophysical Research Letters, 36, https://doi.org/10.1029/2009GL038110, 2009.

Fahrner, D., Lea, J. M., Brough, S., Mair, D. W. F., and Abermann, J.: Linear response of the Greenland ice sheet's tidewater glacier terminus positions to climate, J. Glaciol., 67, 1–11, https://doi.org/10.1017/jog.2021.13, 2021.

Felikson, D., Catania, G. A., Bartholomaus, T. C., Morlighem, M., and Noël, B. P. Y.: Steep Glacier Bed Knickpoints Mitigate Inland Thinning in Greenland, Geophysical Research Letters, 48, e2020GL090112, https://doi.org/10.1029/2020GL090112, 2021.

Felikson, D., Nowicki, S., Nias, I., Morlighem, M., and Seroussi, H.: Seasonal Tidewater Glacier Terminus Oscillations Bias Multi-Decadal Projections of Ice Mass Change, Journal of Geophysical Research: Earth Surface, 127, e2021JF006249, https://doi.org/10.1029/2021JF006249, 2022.

Fettweis, X., Box, J. E., Agosta, C., Amory, C., Kittel, C., Lang, C., van As, D., Machguth, H., and Gallée, H.: Reconstructions of the 1900–2015 Greenland ice sheet surface mass balance using the regional climate MAR model, The Cryosphere, 11, 1015–1033, https://doi.org/10.5194/tc-11-1015-2017, 2017.

Foga, S., Stearns, L. A., and van der Veen, C. J.: Application of Satellite Remote Sensing Techniques to Quantify Terminus and Ice Mélange Behavior at Helheim Glacier, East Greenland, Marine Technology Society Journal, 48, 81–91, https://doi.org/10.4031/MTSJ.48.5.3, 2014.

Forget, G., Campin, J.-M., Heimbach, P., Hill, C. N., Ponte, R. M., and Wunsch, C.: ECCO version 4: an integrated framework for non-linear inverse modeling and global ocean state estimation, Geoscientific Model Development, 8, 3071–3104, https://doi.org/10.5194/gmd-8-3071-2015, 2015.

Fried, M. J., Catania, G. A., Stearns, L. A., Sutherland, D. A., Bartholomaus, T. C., Shroyer, E., and Nash, J.: Reconciling Drivers of Seasonal Terminus Advance and Retreat at 13 Central West Greenland Tidewater Glaciers, Journal of Geophysical Research: Earth Surface, 123, 1590–1607, https://doi.org/10.1029/2018JF004628, 2018.

Gardner, A. S., Moholdt, G., Cogley, J. G., Wouters, B., Arendt, A. A., Wahr, J., Berthier, E., Hock, R., Pfeffer, W. T., Kaser, G., Ligtenberg, S. R. M., Bolch, T., Sharp, M. J., Hagen, J. O., Broeke, M. R. van den, and Paul, F.: A Reconciled Estimate of Glacier Contributions to Sea Level Rise: 2003 to 2009, Science, 340, 852–857, https://doi.org/10.1126/science.1234532, 2013.

Giffen, B. A., Hall, D. K., and Chien, J. Y. L.: Alaska: Glaciers of Kenai Fjords National Park and Katmai National Park and Preserve, in: Global Land Ice Measurements from Space, edited by:

Kargel, J. S., Leonard, G. J., Bishop, M. P., Kääb, A., and Raup, B. H., Springer, Berlin, Heidelberg, 241–261, https://doi.org/10.1007/978-3-540-79818-7_11, 2014.

Goliber, S., Black, T., Catania, G., Lea, J. M., Olsen, H., Cheng, D., Bevan, S., Bjørk, A., Bunce, C., Brough, S., Carr, J. R., Cowton, T., Gardner, A., Fahrner, D., Hill, E., Joughin, I., Korsgaard, N. J., Luckman, A., Moon, T., Murray, T., Sole, A., Wood, M., and Zhang, E.: TermPicks: a century of Greenland glacier terminus data for use in scientific and machine learning applications, The Cryosphere, 16, 3215–3233, https://doi.org/10.5194/tc-16-3215-2022, 2022.

Grant, U. S. and Higgins, D. F.: Coastal Glaciers of Prince William Sound and Kenai Peninsula, Alaska, U.S. Government Printing Office, United States, https://doi.org/10.3133/b526, 1913.

Hill, E. A., Carr, J. R., and Stokes, C. R.: A Review of Recent Changes in Major Marine-Terminating Outlet Glaciers in Northern Greenland, Frontiers in Earth Science, 4, 1–23, https://doi.org/10.3389/feart.2016.00111, 2017.

Hock, R., Bliss, A., Marzeion, B., Giesen, R. H., Hirabayashi, Y., Huss, M., Radić, V., and Slangen, A. B. A.: GlacierMIP – A model intercomparison of global-scale glacier mass-balance models and projections, Journal of Glaciology, 65, 453–467, https://doi.org/10.1017/jog.2019.22, 2019.

Holland, D. M., Thomas, R. H., de Young, B., Ribergaard, M. H., and Lyberth, B.: Acceleration of Jakobshavn Isbræ triggered by warm subsurface ocean waters, Nature Geoscience, 1, 659–664, https://doi.org/10.1038/ngeo316, 2008.

Holland, D. M., Voytenko, D., Christianson, K., Dixon, T. H., Mel, M. J., Parizek, B. R., Vaňková, I., Walker, R. T., Walter, J. I., Nicholls, K., and Holland, D.: An Intensive Observation of Calving at Helheim Glacier, East Greenland, Oceanography, 29, 46–61, https://doi.org/10.5670/oceanog.2016.98, 2016.

Hood, E. and Berner, L.: Effects of changing glacial coverage on the physical and biogeochemical properties of coastal streams in southeastern Alaska, Journal of Geophysical Research: Biogeosciences, 114, G03001, https://doi.org/10.1029/2009JG000971, 2009.

Hood, E. and Scott, D.: Riverine organic matter and nutrients in southeast Alaska affected by glacial coverage, Nature Geosci, 1, 583–587, https://doi.org/10.1038/ngeo280, 2008.

Hood, E., Fellman, J., Spencer, R. G. M., Hernes, P. J., Edwards, R., D'Amore, D., and Scott, D.: Glaciers as a source of ancient and labile organic matter to the marine environment, Nature, 462, 1044–1047, https://doi.org/10.1038/nature08580, 2009.

Hoover-Miller, A. and Armato, P.: Harbor seal use of glacier ice and terrestrial haul-outs in the Kenai Fjords, Alaska, Marine Mammal Science, 34, 616–644, https://doi.org/10.1111/mms.12470, 2018.

How, P., Schild, K. M., Benn, D. I., Noormets, R., Kirchner, N., Luckman, A., Vallot, D., Hulton, N. R. J., and Borstad, C.: Calving controlled by melt-under-cutting: detailed calving styles revealed

through time-lapse observations, Annals of Glaciology, 60, 1–12, https://doi.org/10.1017/aog.2018.28, 2019.

Howat, I. M. and Eddy, A.: Multi-decadal retreat of Greenland's marine-terminating glaciers, Journal of Glaciology, 57, 389–396, https://doi.org/10.3189/002214311796905631, 2011.

Howat, I. M., Joughin, I., Fahnestock, M., Smith, B. E., and Scambos, T. A.: Synchronous retreat and acceleration of southeast Greenland outlet glaciers 2000-06: Ice dynamics and coupling to climate, Journal of Glaciology, 54, 646–660, https://doi.org/10.3189/002214308786570908, 2008.

Howat, I. M., Box, J. E., Ahn, Y., Herrington, A., and McFadden, E. M.: Seasonal variability in the dynamics of marine-terminating outlet glaciers in Greenland, Journal of Glaciology, 56, 601–613, https://doi.org/10.3189/002214310793146232, 2010.

Hugonnet, R., McNabb, R., Berthier, E., Menounos, B., Nuth, C., Girod, L., Farinotti, D., Huss, M., Dussaillant, I., Brun, F., and Kääb, A.: Accelerated global glacier mass loss in the early twenty-first century, Nature, 592, 726–731, https://doi.org/10.1038/s41586-021-03436-z, 2021.

Hurrell, J. W., Hack, J. J., Shea, D., Caron, J. M., and Rosinski, J.: A New Sea Surface Temperature and Sea Ice Boundary Dataset for the Community Atmosphere Model, Journal of Climate, 21, 5145–5153, https://doi.org/10.1175/2008JCLI2292.1, 2008.

Huss, M. and Hock, R.: A new model for global glacier change and sea-level rise, Frontiers in Earth Science, 3, 1–22, https://doi.org/10.3389/feart.2015.00054, 2015.

ICES: ICES Dataset on Ocean Hydrography, The International Council for the Exploration of the Sea [dataset], 2014.

IMBIE: http://imbie.org/imbie-3/drainage-basins/, last access: 9 June 2022.

IPCC: Sea Level Rise and Implications for Low-Lying Islands, Coasts and Communities, Cambridge University Press, Cambridge, UK and New York, NY, USA, https://doi.org/10.1017/9781009157964.006, 2019.

Jekel, C. and Venter, G.: pwlf: A Python Library for Fitting 1D Continuous Piecewise Linear Functions, 2019.

Jenckes, J., Ibarra, D. E., and Munk, L. A.: Concentration-Discharge Patterns Across the Gulf of Alaska Reveal Geomorphological and Glacierization Controls on Stream Water Solute Generation and Export, Geophysical Research Letters, 49, e2021GL095152, https://doi.org/10.1029/2021GL095152, 2022.

Josberger, E. G., Bidlake, W. R., March, R. S., and Kennedy, B. W.: Glacier mass-balance fluctuations in the Pacific Northwest and Alaska, USA, Annals of Glaciology, 46, 291–296, https://doi.org/10.3189/172756407782871314, 2007.

Joughin, I.: MEaSUREs Greenland Image Mosaics from Sentinel-1A and 1B, Version 4, NASA National Snow and Ice Data Center Distributed Active Archive Center [dataset], https://doi.org/10.5067/J9PKP1B9HX6F, 2020.

Joughin, I.: MEaSUREs Greenland Annual Ice Sheet Velocity Mosaics from SAR and Landsat, Version 3, NASA National Snow and Ice Data Center Distributed Active Archive Center [dataset], https://doi.org/10.5067/C2GFA20CXUI4, 2021.

Joughin, I., Howat, I. M., Fahnestock, M., Smith, B., Krabill, W., Alley, R. B., Stern, H., and Truffer, M.: Continued evolution of Jakobshavn Isbrae following its rapid speedup, Journal of Geophysical Research: Earth Surface, 113, F04006, https://doi.org/10.1029/2008JF001023, 2008a.

Joughin, I., Howat, I., Alley, R. B., Ekstrom, G., Fahnestock, M., Moon, T., Nettles, M., Truffer, M., and Tsai, V. C.: Ice-front variation and tidewater behavior on Helheim and Kangerdlugssuaq Glaciers, Greenland, Journal of Geophysical Research: Earth Surface, 113, F01004, https://doi.org/10.1029/2007JF000837, 2008b.

Joughin, I., Smith, B. E., Howat, I. M., Scambos, T. A., and Moon, T.: Greenland flow variability from ice-sheet-wide velocity mapping, Journal of Glaciology, 56, 415–430, https://doi.org/10.3189/002214310792447734, 2010.

Joughin, I., Moon, T., Joughin, J., and Black, T.: MEaSUREs Annual Greenland Outlet Glacier Terminus Positions from SAR Mosaics, Version 1, NASA National Snow and Ice Data Center Distributed Active Archive Center [dataset], 2015.

Joughin, I., Smith, B. E., Howat, I. M., Moon, T., and Scambos, T. A.: A SAR record of early 21st century change in Greenland, Journal of Glaciology, 62, 62–71, https://doi.org/10.1017/jog.2016.10, 2016a.

Joughin, I., Smith, B., Howat, I., and Scambos, T.: MEaSUREs Multi-year Greenland Ice Sheet Velocity Mosaic, Version 1, NASA National Snow and Ice Data Center Distributed Active Archive Center [dataset], https://doi.org/10.5067/QUA5Q9SVMSJG, 2016b.

Joughin, I., Smith, B. E., and Howat, I. M.: A complete map of Greenland ice velocity derived from satellite data collected over 20 years, Journal of Glaciology, 64, 1–11, https://doi.org/10.1017/jog.2017.73, 2018a.

Joughin, I., Smith, B. E., and Howat, I.: Greenland Ice Mapping Project: ice flow velocity variation at sub-monthly to decadal timescales, The Cryosphere, 12, 2211–2227, https://doi.org/10.5194/tc-12-2211-2018, 2018b.

Joughin, I., Shean, D. E., Smith, B. E., and Floricioiu, D.: A decade of variability on Jakobshavn Isbræ: ocean temperatures pace speed through influence on mélange rigidity, The Cryosphere, 14, 211–227, https://doi.org/10.5194/tc-14-211-2020, 2020.

Kehrl, L. M., Joughin, I., Shean, D. E., Floricioiu, D., and Krieger, L.: Seasonal and interannual variabilities in terminus position, glacier velocity, and surface elevation at Helheim and

Kangerlussuaq Glaciers from 2008 to 2016, Journal of Geophysical Research: Earth Surface, 122, 1635–1652, https://doi.org/10.1002/2016JF004133, 2017.

Khazendar, A., Fenty, I. G., Carroll, D., Gardner, A., Lee, C. M., Fukumori, I., Wang, O., Zhang, H., Seroussi, H., Moller, D., Noël, B. P. Y., Broeke, M. R. van den, Dinardo, S., and Willis, J.: Interruption of two decades of Jakobshavn Isbrae acceleration and thinning as regional ocean cools, Nature Geoscience, 12, 277–283, https://doi.org/10.1038/s41561-019-0329-3, 2019.

King, M. D., Howat, I. M., Jeong, S., Noh, M. J., Wouters, B., Noël, B., and Broeke, M. R. van den: Seasonal to decadal variability in ice discharge from the Greenland Ice Sheet, The Cryosphere, 12, 3813–3825, https://doi.org/10.5194/tc-12-3813-2018, 2018.

King, M. D., Howat, I. M., Candela, S. G., Noh, M. J., Jeong, S., Noël, B. P. Y., van den Broeke, M. R., Wouters, B., and Negrete, A.: Dynamic ice loss from the Greenland Ice Sheet driven by sustained glacier retreat, Communications Earth & Environment, 1, 1–7, https://doi.org/10.1038/s43247-020-0001-2, 2020.

Kneib-Walter, A., Lüthi, M. P., Moreau, L., and Vieli, A.: Drivers of Recurring Seasonal Cycle of Glacier Calving Styles and Patterns, Front. Earth Sci., 9, https://doi.org/10.3389/feart.2021.667717, 2021.

Kulp, S. A. and Strauss, B. H.: New elevation data triple estimates of global vulnerability to sea-level rise and coastal flooding, Nat Commun, 10, 4844, https://doi.org/10.1038/s41467-019-12808-z, 2019.

Kurtz, D. and Baker, E.: Two hundred years of terminus retreat at Exit Glacier: 1815-2015, National Park Service, Fort Collins, Colorado, 2016.

Kurtz, D. and Wolken, G.: Risk and Recreation in a Glacial Environment: Understanding Glacial Lake Outburst Floods at Bear Glacier in Kenai Fjords National Park, Alaska Park Science, 18, 38–43, 2019.

Kutzner, D.: Environmental change, resilience, and adaptation in nature-based tourism: conceptualizing the social-ecological resilience of birdwatching tour operations, null, 27, 1142–1166, https://doi.org/10.1080/09669582.2019.1601730, 2019.

Laidre, K. L., Moon, T., Hauser, D. D. W., McGovern, R., Heide-Jørgensen, M. P., Dietz, R., and Hudson, B.: Use of glacial fronts by narwhals (Monodon monoceros) in West Greenland, Biology Letters, 12, 20160457, https://doi.org/10.1098/rsbl.2016.0457, 2016.

Lambert, E., Hunter, C., Pierce, G. J., and MacLeod, C. D.: Sustainable whale-watching tourism and climate change: towards a framework of resilience, Journal of Sustainable Tourism, 18, 409–427, https://doi.org/10.1080/09669581003655497, 2010.

Larsen, C. F., Motyka, R. J., Arendt, A. A., Echelmeyer, K. A., and Geissler, P. E.: Glacier changes in southeast Alaska and northwest British Columbia and contribution to sea level rise, Journal of Geophysical Research: Earth Surface, 112, F01007, https://doi.org/10.1029/2006JF000586, 2007.

Larsen, C. F., Burgess, E., Arendt, A. A., O'Neel, S., Johnson, A. J., and Kienholz, C.: Surface melt dominates Alaska glacier mass balance, Geophysical Research Letters, 42, 5902–5908, https://doi.org/10.1002/2015GL064349, 2015.

Larsen, S. H., Khan, S. A., Ahlstrøm, A. P., Hvidberg, C. S., Willis, M. J., and Andersen, S. B.: Increased mass loss and asynchronous behavior of marine-terminating outlet glaciers at Upernavik Isstrøm, NW Greenland, J. Geophys. Res. Earth Surf., 121, 241–256, https://doi.org/10.1002/2015JF003507, 2016.

Lomb, N. R.: Least-squares frequency analysis of unequally spaced data, Astrophys Space Sci, 39, 447–462, https://doi.org/10.1007/BF00648343, 1976.

Loso, M., Arendt, A., Larsen, C., Rich, J., and Murphy, N.: Alaskan national park glaciers - status and trends: Final report, National Park Service, Fort Collins, Colorado, 2014.

Luckman, A., Benn, D. I., Cottier, F., Bevan, S., Nilsen, F., and Inall, M.: Calving rates at tidewater glaciers vary strongly with ocean temperature, Nat Commun, 6, 8566, https://doi.org/10.1038/ncomms9566, 2015.

Lydersen, C., Assmy, P., Falk-Petersen, S., Kohler, J., Kovacs, K. M., Reigstad, M., Steen, H., Strøm, H., Sundfjord, A., Varpe, Ø., Walczowski, W., Weslawski, J. M., and Zajaczkowski, M.: The importance of tidewater glaciers for marine mammals and seabirds in Svalbard, Norway, Journal of Marine Systems, 129, 452–471, https://doi.org/10.1016/j.jmarsys.2013.09.006, 2014.

Mann, D. H.: Reliability of a Fjord Glacier's Fluctuations for Paleoclimatic Reconstructions, Quaternary Research, 25, 10–24, https://doi.org/10.1016/0033-5894(86)90040-2, 1986.

Maraldo, D. R.: Accelerated retreat of coastal glaciers in the Western Prince William Sound, Alaska, Arctic, Antarctic, and Alpine Research, 52, 617–634, https://doi.org/10.1080/15230430.2020.1837715, 2020.

McFadden, E. M., Howat, I. M., Joughin, I., Smith, B. E., and Ahn, Y.: Changes in the dynamics of marine terminating outlet glaciers in west Greenland (2000–2009), Journal of Geophysical Research: Earth Surface, 116, F02022, https://doi.org/10.1029/2010JF001757, 2011.

McGrath, D., Sass, L., O'Neel, S., Arendt, A., and Kienholz, C.: Hypsometric control on glacier mass balance sensitivity in Alaska and northwest Canada, Earth's Future, 5, 324–336, https://doi.org/10.1002/2016EF000479, 2017.

McNabb, R. W. and Hock, R.: Alaska tidewater glacier terminus positions, 1948–2012, Journal of Geophysical Research: Earth Surface, 119, 153–167, https://doi.org/10.1002/2013JF002915, 2014.

McNabb, R. W., Hock, R., and Huss, M.: Variations in Alaska tidewater glacier frontal ablation, 1985–2013, Journal of Geophysical Research: Earth Surface, 120, 120–136, https://doi.org/10.1002/2014JF003276, 2015.

McNeil, C., O'Neel, S., Loso, M., Pelto, M., Sass, L., Baker, E. H., and Campbell, S.: Explaining mass balance and retreat dichotomies at Taku and Lemon Creek Glaciers, Alaska, Journal of Glaciology, 66, 530–542, https://doi.org/10.1017/jog.2020.22, 2020.

Meier, M. F. and Post, A.: Fast tidewater glaciers, Journal of Geophysical Research: Solid Earth, 92, 9051–9058, https://doi.org/10.1029/JB092iB09p09051, 1987.

Meier, M. F., Rasmussen, L. A., Post, A., Brown, C. S., Sikonia, W. G., Bindschadler, R. A., Mayo, L. R., and Trabant, D. C.: Predicted timing of the disintegration of the lower reach of Columbia Glacier, Alaska, Open-File Report, U.S. Geological Survey, https://doi.org/10.3133/ofr80582, 1980.

Meier, W. N., Fetterer, F., Savoie, M., Mallory, S., Duerr, R., and Stroeve, J.: NOAA/NSIDC Climate Data Record of Passive Microwave Sea Ice Concentration, Version 3, NASA National Snow and Ice Data Center Distributed Active Archive Center [dataset], https://doi.org/10.7265/N59P2ZTG, 2017.

Meire, L., Mortensen, J., Meire, P., Juul-Pedersen, T., Sejr, M. K., Rysgaard, S., Nygaard, R., Huybrechts, P., and Meysman, F. J. R.: Marine-terminating glaciers sustain high productivity in Greenland fjords, Global Change Biology, 23, 5344–5357, https://doi.org/10.1111/gcb.13801, 2017.

Mercer, J. H.: The Response of Fjord Glaciers to Changes in the Firn Limit, Journal of Glaciology, 3, 850–858, https://doi.org/10.3189/S0022143000027222, 1961.

Milner, A. M.: Colonization and ecological development of new streams in Glacier Bay National Park, Alaska, Freshwater Biol, 18, 53–70, https://doi.org/10.1111/j.1365-2427.1987.tb01295.x, 1987.

Milner, A. M.: Exxon Valdez oil spill - fisheries and water quality investigations in Kenai Fjord National Park : draft, University of Alaska, Institute of Arctic Biology, Fairbanks, AK, 1990.

Milner, A. M. and Bailey, R. G.: Salmonid colonization of new streams in Glacier Bay National Park, Alaska, Aquaculture Res, 20, 179–192, https://doi.org/10.1111/j.1365-2109.1989.tb00343.x, 1989.

Milner, A. M. and Oswood, M.: Stream Community Development Following Glacial Recession in Coastal Alaska, University of Alaska Fairbanks, Institute of Arctic Biology, Anchorage, AK, 1990.

Milner, A. M., Fastie, C. L., Chapin III, F. S., Engstrom, D. R., and Sharman, L. C.: Interactions and Linkages among Ecosystems during Landscape Evolution, BioScience, 57, 237–247, https://doi.org/10.1641/B570307, 2007.

Molnia, B. F.: Late nineteenth to early twenty-first century behavior of Alaskan glaciers as indicators of changing regional climate, Global and Planetary Change, 56, 23–56, https://doi.org/10.1016/j.gloplacha.2006.07.011, 2007.

Moon, T. and Joughin, I.: Changes in ice front position on Greenland's outlet glaciers from 1992 to 2007, Journal of Geophysical Research: Earth Surface, 113, F02022, https://doi.org/10.1029/2007JF000927, 2008.

Moon, T., Joughin, I., Smith, B., and Howat, I.: 21st-Century Evolution of Greenland Outlet Glacier Velocities, Science, 336, 576–578, https://doi.org/10.1126/science.1219985, 2012.

Moon, T., Joughin, I., Smith, B. E., van den Broeke, M. R., van de Berg, W. J., Noël, B., and Usher, M.: Distinct patterns of seasonal Greenland glacier velocity, Geophysical Research Letters, 41, 7209–7216, https://doi.org/10.1002/2014GL061836, 2014.

Moon, T., Joughin, I., and Smith, B.: Seasonal to multiyear variability of glacier surface velocity, terminus position, and sea ice/ice mélange in northwest Greenland, Journal of Geophysical Research: Earth Surface, 120, 818–833, https://doi.org/10.1002/2015JF003494, 2015.

Moon, T., Sutherland, D. A., Carroll, D., Felikson, D., Kehrl, L., and Straneo, F.: Subsurface iceberg melt key to Greenland fjord freshwater budget, Nature Geosci, 11, 49–54, https://doi.org/10.1038/s41561-017-0018-z, 2018.

Morlighem, M., Bondzio, J., Seroussi, H., Rignot, E., Larour, E., Humbert, A., and Rebuffi, S.: Modeling of Store Gletscher's calving dynamics, West Greenland, in response to ocean thermal forcing, Geophysical Research Letters, 43, 2659–2666, https://doi.org/10.1002/2016GL067695, 2016.

Morlighem, M., Williams, C. N., Rignot, E., An, L., Arndt, J. E., Bamber, J. L., Catania, G., Chauché, N., Dowdeswell, J. A., Dorschel, B., Fenty, I., Hogan, K., Howat, I., Hubbard, A., Jakobsson, M., Jordan, T. M., Kjeldsen, K. K., Millan, R., Mayer, L., Mouginot, J., Noël, B. P. Y., O'Cofaigh, C., Palmer, S., Rysgaard, S., Seroussi, H., Siegert, M. J., Slabon, P., Straneo, F., van den Broeke, M. R., Weinrebe, W., Wood, M., and Zinglersen, K. B.: BedMachine v3: Complete Bed Topography and Ocean Bathymetry Mapping of Greenland From Multibeam Echo Sounding Combined With Mass Conservation, Geophys. Res. Lett., 44, 11,051-11,061, https://doi.org/10.1002/2017GL074954, 2017a.

Morlighem, M., Williams, C., Rignot, E., An, L., Arndt, J. E., Bamber, J., Catania, G., Chauché, N., Dowdeswell, J. A., Dorschel, B., Fenty, I., Hogan, K., Howat, I., Hubbard, A., Jakobsson, M., Jordan, T. M., Kjeldsen, K. K., Millan, R., Mayer, L., Mouginot, J., Noël, B., O'Cofaigh, C., Palmer, S. J., Rysgaard, S., Seroussi, H., Siegert, M. J., Slabon, P., Straneo, F., van den Broeke, M. R., Weinrebe, W., Wood, M., and Zinglersen, K.: IceBridge BedMachine Greenland, Version 3, NASA National Snow and Ice Data Center Distributed Active Archive Center [dataset], https://doi.org/10.5067/2CIX82HUV88Y, 2017b.

Morlighem, M., Wood, M., Seroussi, H., Choi, Y., and Rignot, E.: Modeling the response of northwest Greenland to enhanced ocean thermal forcing and subglacial discharge, The Cryosphere, 13, 723–734, https://doi.org/10.5194/tc-13-723-2019, 2019.

Mortensen, J., Rysgaard, S., Bendtsen, J., Lennert, K., Kanzow, T., Lund, H., and Meire, L.: Subglacial Discharge and Its Down-Fjord Transformation in West Greenland Fjords With an Ice

Mélange, Journal of Geophysical Research: Oceans, 125, e2020JC016301, https://doi.org/10.1029/2020JC016301, 2020.

Mote, T. L.: MEaSUREs Greenland Surface Melt Daily 25km EASE-Grid 2.0, Version 1, NASA National Snow and Ice Data Center Distributed Active Archive Center [dataset], https://doi.org/10.5067/MEASURES/CRYOSPHERE/nsidc-0533.001, 2014.

Mote, T. L. and Anderson, M. R.: Variations in snowpack melt on the Greenland ice sheet based on passive-microwave measurements, Journal of Glaciology, 41, 51–60, https://doi.org/10.3189/S0022143000017755, 1995.

Motyka, R. J., Hunter, L., Echelmeyer, K. A., and Connor, C.: Submarine melting at the terminus of a temperate tidewater glacier, LeConte Glacier, Alaska, U.S.A., Annals of Glaciology, 36, 57–65, https://doi.org/10.3189/172756403781816374, 2003a.

Motyka, R. J., O'Neel, S., Connor, C. L., and Echelmeyer, K. A.: Twentieth century thinning of Mendenhall Glacier, Alaska, and its relationship to climate, lake calving, and glacier run-off, Global and Planetary Change, 35, 93–112, https://doi.org/10.1016/S0921-8181(02)00138-8, 2003b.

Motyka, R. J., Truffer, M., Fahnestock, M., Mortensen, J., Rysgaard, S., and Howat, I.: Submarine melting of the 1985 Jakobshavn Isbræ floating tongue and the triggering of the current retreat, Journal of Geophysical Research: Earth Surface, 116, F01007, https://doi.org/10.1029/2009JF001632, 2011.

Motyka, R. J., Dryer, W. P., Amundson, J., Truffer, M., and Fahnestock, M.: Rapid submarine melting driven by subglacial discharge, LeConte Glacier, Alaska, Geophysical Research Letters, 40, 5153–5158, https://doi.org/10.1002/grl.51011, 2013.

Motyka, R. J., Cassotto, R., Truffer, M., Kjeldsen, K. K., van As, D., Korsgaard, N. J., Fahnestock, M., Howat, I., Langen, P. L., Mortensen, J., Lennert, K., and Rysgaard, S.: Asynchronous behavior of outlet glaciers feeding Godthåbsfjord (Nuup Kangerlua) and the triggering of Narsap Sermia's retreat in SW Greenland, Journal of Glaciology, 63, 288–308, https://doi.org/10.1017/jog.2016.138, 2017.

Mouginot, J., Rignot, E., Bjørk, A. A., van den Broeke, M., Millan, R., Morlighem, M., Noël, B., Scheuchl, B., and Wood, M.: Forty-six years of Greenland Ice Sheet mass balance from 1972 to 2018, PNAS, 116, 9239–9244, https://doi.org/10.1073/pnas.1904242116, 2019.

Murray, T., Scharrer, K., Selmes, N., Booth, A. D., James, T. D., Bevan, S. L., Bradley, J., Cook, S., Cordero Llana, L., Drocourt, Y., Dyke, L., Goldsack, A., Hughes, A. L., Luckman, A. J., and McGovern, J.: Extensive retreat of Greenland tidewater glaciers, 2000-2010, Arctic, Antarctic, and Alpine Research, 47, 427–447, https://doi.org/10.1657/AAAR0014-049, 2015.

National Snow and Ice Data Center: Glacier Photograph Collection, Version 1, National Snow and Ice Data Center/World Data Center for Glaciology [dataset], https://doi.org/10.7265/N5/NSIDC-GPC-2009-12, 2021.

Neal, E. G., Hood, E., and Smikrud, K.: Contribution of glacier runoff to freshwater discharge into the Gulf of Alaska, Geophysical Research Letters, 37, L06404, https://doi.org/10.1029/2010GL042385, 2010.

Nick, F. M., Vieli, A., Howat, I. M., and Joughin, I.: Large-scale changes in Greenland outlet glacier dynamics triggered at the terminus, Nature Geoscience, 2, 110–114, https://doi.org/10.1038/ngeo394, 2009.

Nick, F. M., van der Veen, C. J., Vieli, A., and Benn, D. I.: A physically based calving model applied to marine outlet glaciers and implications for the glacier dynamics, Journal of Glaciology, 56, 781–794, https://doi.org/10.3189/002214310794457344, 2010.

Nick, F. M., Vieli, A., Andersen, M. L., Joughin, I., Payne, A., Edwards, T. L., Pattyn, F., and van de Wal, R. S. W.: Future sea-level rise from Greenland's main outlet glaciers in a warming climate, Nature, 497, 235–238, https://doi.org/10.1038/nature12068, 2013.

NOAA National Centers for Environmental Information: 1991-2020 U.S. Climate Normals, 2021.

Nowacki, G. J., Spencer, P., Fleming, M., Brock, T., and Jorgenson, T.: Unified Ecoregions of Alaska: 2001, Unified Ecoregions of Alaska: 2001, Geological Survey (U.S.), https://doi.org/10.3133/ofr2002297, 2003.

O'Neel, S., Echelmeyer, K. A., and Motyka, R. J.: Short-term variations in calving of a tidewater glacier: LeConte Glacier, Alaska, U.S.A., Journal of Glaciology, 49, 587–598, https://doi.org/10.3189/172756503781830430, 2003.

O'Neel, S., Hood, E., Bidlack, A. L., Fleming, S. W., Arimitsu, M. L., Arendt, A., Burgess, E., Sergeant, C. J., Beaudreau, A. H., Timm, K., Hayward, G. D., Reynolds, J. H., and Pyare, S.: Icefield-to-Ocean Linkages across the Northern Pacific Coastal Temperate Rainforest Ecosystem, BioScience, 65, 499–512, https://doi.org/10.1093/biosci/biv027, 2015.

O'Neel, S., McNeil, C., Sass, L. C., Florentine, C., Baker, E. H., Peitzsch, E., McGrath, D., Fountain, A. G., and Fagre, D.: Reanalysis of the US Geological Survey Benchmark Glaciers: long-term insight into climate forcing of glacier mass balance, Journal of Glaciology, 65, 850–866, https://doi.org/10.1017/jog.2019.66, 2019.

Östrem, G.: Ice Melting under a Thin Layer of Moraine, and the Existence of Ice Cores in Moraine Ridges, Geografiska Annaler, 41, 228–230, https://doi.org/10.1080/20014422.1959.11907953, 1959.

Peng, G., Meier, W. N., Scott, D. J., and Savoie, M. H.: A long-term and reproducible passive microwave sea ice concentration data record for climate studies and monitoring, Earth System Science Data, 5, 311–318, https://doi.org/10.5194/essd-5-311-2013, 2013.

Pfeffer, W. T.: A simple mechanism for irreversible tidewater glacier retreat, Journal of Geophysical Research: Earth Surface, 112, https://doi.org/10.1029/2006JF000590, 2007.

Pfeffer, W. T., Arendt, A. A., Bliss, A., Bolch, T., Cogley, J. G., Gardner, A. S., Hagen, J.-O., Hock, R., Kaser, G., Kienholz, C., Miles, E. S., Moholdt, G., Mölg, N., Paul, F., Radić, V., Rastner, P., Raup, B. H., Rich, J., Sharp, M. J., and The Randolph Consortium: The Randolph Glacier Inventory: a globally complete inventory of glaciers, Journal of Glaciology, 60, 537–552, https://doi.org/10.3189/2014JoG13J176, 2014.

Pitman, K. J., Moore, J. W., Sloat, M. R., Beaudreau, A. H., Bidlack, A. L., Brenner, R. E., Hood, E. W., Pess, G. R., Mantua, N. J., Milner, A. M., Radić, V., Reeves, G. H., Schindler, D. E., and Whited, D. C.: Glacier Retreat and Pacific Salmon, BioScience, 70, 220–236, https://doi.org/10.1093/biosci/biaa015, 2020.

Pitman, K. J., Moore, J. W., Huss, M., Sloat, M. R., Whited, D. C., Beechie, T. J., Brenner, R., Hood, E. W., Milner, A. M., Pess, G. R., Reeves, G. H., and Schindler, D. E.: Glacier retreat creating new Pacific salmon habitat in western North America, Nat Commun, 12, 6816, https://doi.org/10.1038/s41467-021-26897-2, 2021.

Post, A.: Effects of the March 1964 Alaska earthquake on glaciers, U.S. Geological Survey, 1967.

Post, A.: Preliminary hydrography and historic terminal changes of Columbia Glacier, Alaska, Hydrologic Atlas, https://doi.org/10.3133/ha559, 1975.

Post, A.: Preliminary bathymetry of McCarty Fiord and Neoglacial changes of McCarty Glacier, Alaska, Preliminary bathymetry of McCarty Fiord and Neoglacial changes of McCarty Glacier, Alaska, https://doi.org/10.3133/ofr80424, 1980a.

Post, A.: Preliminary bathymetry of Northwestern Fiord and neoglacial changes of Northwestern Glacier, Alaska, Preliminary bathymetry of Northwestern Fiord and neoglacial changes of Northwestern Glacier, Alaska, U.S. Geological Survey, https://doi.org/10.3133/ofr80414, 1980b.

Post, A., O'Neel, S., Motyka, R. J., and Streveler, G.: A complex relationship between calving glaciers and climate, Eos Transactions, 92, 305–306, https://doi.org/10.1029/2011EO370001, 2011.

Radić, V. and Hock, R.: Glaciers in the Earth's Hydrological Cycle: Assessments of Glacier Mass and Runoff Changes on Global and Regional Scales, in: The Earth's Hydrological Cycle, vol. 46, edited by: Bengtsson, L., Bonnet, R.-M., Calisto, M., Destouni, G., Gurney, R., Johannessen, J., Kerr, Y., Lahoz, W. A., and Rast, M., Springer, Dordrecht, 813–837, https://doi.org/10.1007/978-94-017-8789-5_15, 2014.

Reeh, N., Thomsen, H. H., Higgins, A. K., and Weidick, A.: Sea ice and the stability of north and northeast Greenland floating glaciers, Annals of Glaciology, 33, 474–480, https://doi.org/10.3189/172756401781818554, 2001.

RGI Consortium: Randolph Glacier Inventory – A Dataset of Global Glacier Outlines: Version 4.0, https://doi.org/10.7265/N5-RGI-40, 2014.

Rignot, E. and Kanagaratnam, P.: Changes in the Velocity Structure of the Greenland Ice Sheet, Science, 311, 986–990, https://doi.org/10.1126/science.1121381, 2006.

Rignot, E. and Mouginot, J.: Ice flow in Greenland for the International Polar Year 2008–2009, Geophysical Research Letters, 39, https://doi.org/10.1029/2012GL051634, 2012.

Rignot, E., Koppes, M., and Velicogna, I.: Rapid submarine melting of the calving faces of West Greenland glaciers, Nature Geoscience, 3, 187–191, https://doi.org/10.1038/ngeo765, 2010.

Rignot, E., Fenty, I., Menemenlis, D., and Xu, Y.: Spreading of warm ocean waters around Greenland as a possible cause for glacier acceleration, Annals of Glaciology, 53, 257–266, https://doi.org/10.3189/2012AoG60A136, 2012.

Rignot, E., Fenty, I., Xu, Y., Cai, C., and Kemp, C.: Undercutting of marine-terminating glaciers in West Greenland, Geophysical Research Letters, 42, 5909–5917, https://doi.org/10.1002/2015GL064236, 2015.

Ritchie, J. B., Lingle, C. S., Motyka, R. J., and Truffer, M.: Seasonal fluctuations in the advance of a tidewater glacier and potential causes: Hubbard Glacier, Alaska, USA, Journal of Glaciology, 54, 401–411, https://doi.org/10.3189/002214308785836977, 2008.

Robel, A. A.: Thinning sea ice weakens buttressing force of iceberg mélange and promotes calving, Nature Communications, 8, 14596, https://doi.org/10.1038/ncomms14596, 2017.

Roe, G. H.: What do glaciers tell us about climate variability and climate change?, Journal of Glaciology, 57, 567–578, https://doi.org/10.3189/002214311796905640, 2011.

Roe, G. H. and O'Neal, M. A.: The response of glaciers to intrinsic climate variability: observations and models of late-Holocene variations in the Pacific Northwest, Journal of Glaciology, 55, 839–854, https://doi.org/10.3189/002214309790152438, 2009.

Roe, G. H. H., Baker, M. B. B., and Herla, F.: Centennial glacier retreat as categorical evidence of regional climate change, Nature Geoscience, 10, 95–99, https://doi.org/10.1038/ngeo2863, 2017.

Rounce, D. R., Hock, R., McNabb, R. W., Millan, R., Sommer, C., Braun, M. H., Malz, P., Maussion, F., Mouginot, J., Seehaus, T. C., and Shean, D. E.: Distributed Global Debris Thickness Estimates Reveal Debris Significantly Impacts Glacier Mass Balance, Geophysical Research Letters, 48, e2020GL091311, https://doi.org/10.1029/2020GL091311, 2021.

Royer, T. C.: Baroclinic transport in the Gulf of Alaska Part II. A fresh water driven coastal current, Journal of Marine Research, 39, 251–266, 1981.

Sakakibara, D. and Sugiyama, S.: Seasonal ice-speed variations in 10 marine-terminating outlet glaciers along the coast of Prudhoe Land, northwestern Greenland, J. Glaciol., 1–10, https://doi.org/10.1017/jog.2019.81, 2019.

Salim, E., Ravanel, L., Bourdeau, P., and Deline, P.: Glacier tourism and climate change: effects, adaptations, and perspectives in the Alps, Reg Environ Change, 21, 120, https://doi.org/10.1007/s10113-021-01849-0, 2021.

Sapiano, J. J., Harrison, W. D., and Echelmeyer, K. A.: Elevation, volume and terminus changes of nine glaciers in North America, Journal of Glaciology, 44, 119–135, https://doi.org/10.3189/S0022143000002410, 1998.

Scargle, J. D.: Studies in astronomical time series analysis. II - Statistical aspects of spectral analysis of unevenly spaced data, ApJ, 263, 835, https://doi.org/10.1086/160554, 1982.

Schild, K. M. and Hamilton, G. S.: Seasonal variations of outlet glacier terminus position in Greenland, Journal of Glaciology, 59, 759–770, https://doi.org/10.3189/2013JoG12J238, 2013.

Schoof, C.: Ice sheet grounding line dynamics: Steady states, stability, and hysteresis, Journal of Geophysical Research: Earth Surface, 112, F03S28, https://doi.org/10.1029/2006JF000664, 2007.

Seale, A., Christoffersen, P., Mugford, R. I., and O'Leary, M.: Ocean forcing of the Greenland Ice Sheet: Calving fronts and patterns of retreat identified by automatic satellite monitoring of eastern outlet glaciers, Journal of Geophysical Research: Earth Surface, 116, F03013, https://doi.org/10.1029/2010JF001847, 2011.

Shea, D., Hurrell, J., and Phillips, A.: Merged Hadley-OI sea surface temperature and sea ice concentration data set (1.0), https://doi.org/10.5065/R33V-SV91, 2020.

Shepherd, A., Ivins, E., Rignot, E., Smith, B., van den Broeke, M., Velicogna, I., Whitehouse, P., Briggs, K., Joughin, I., Krinner, G., Nowicki, S., Payne, T., Scambos, T., Schlegel, N., A, G., Agosta, C., Ahlstrøm, A., Babonis, G., Barletta, V. R., Bjørk, A. A., Blazquez, A., Bonin, J., Colgan, W., Csatho, B., Cullather, R., Engdahl, M. E., Felikson, D., Fettweis, X., Forsberg, R., Hogg, A. E., Gallee, H., Gardner, A., Gilbert, L., Gourmelen, N., Groh, A., Gunter, B., Hanna, E., Harig, C., Helm, V., Horvath, A., Horwath, M., Khan, S., Kjeldsen, K. K., Konrad, H., Langen, P. L., Lecavalier, B., Loomis, B., Luthcke, S., McMillan, M., Melini, D., Mernild, S., Mohajerani, Y., Moore, P., Mottram, R., Mouginot, J., Moyano, G., Muir, A., Nagler, T., Nield, G., Nilsson, J., Noël, B., Otosaka, I., Pattle, M. E., Peltier, W. R., Pie, N., Rietbroek, R., Rott, H., Sandberg Sørensen, L., Sasgen, I., Save, H., Scheuchl, B., Schrama, E., Schröder, L., Seo, K.-W., Simonsen, S. B., Slater, T., Spada, G., Sutterley, T., Talpe, M., Tarasov, L., van de Berg, W. J., van der Wal, W., van Wessem, M., Vishwakarma, B. D., Wiese, D., Wilton, D., Wagner, T., Wouters, B., and Wuite, J.: Mass balance of the Greenland Ice Sheet from 1992 to 2018, Nature, 579, 233–239, https://doi.org/10.1038/s41586-019-1855-2, 2020.

Simonsen, S. B., Barletta, V. R., Colgan, W. T., and Sørensen, L. S.: Greenland Ice Sheet Mass Balance (1992–2020) From Calibrated Radar Altimetry, Geophysical Research Letters, 48, e2020GL091216, https://doi.org/10.1029/2020GL091216, 2021.

Slater, D. A., Nienow, P. W., Cowton, T. R., Goldberg, D. N., and Sole, A. J.: Effect of near-terminus subglacial hydrology on tidewater glacier submarine melt rates, Geophysical Research Letters, 42, 2861–2868, https://doi.org/10.1002/2014GL062494, 2015.

Slater, D. A., Nienow, P. W., Goldberg, D. N., Cowton, T. R., and Sole, A. J.: A model for tidewater glacier undercutting by submarine melting, Geophysical Research Letters, 44, 2360–2368, https://doi.org/10.1002/2016GL072374, 2017.

Slater, D. A., Straneo, F., Felikson, D., Little, C. M., Goelzer, H., Fettweis, X., and Holte, J.: Estimating Greenland tidewater glacier retreat driven by submarine melting, The Cryosphere, 13, 2489–2509, https://doi.org/10.5194/tc-13-2489-2019, 2019.

Slemmons, K. E. H., Saros, J. E., and Simon, K.: The influence of glacial meltwater on alpine aquatic ecosystems: a review, Environ. Sci.: Processes Impacts, 15, 1794–1806, https://doi.org/10.1039/C3EM00243H, 2013.

Sohn, H.-G., Jezek, K. C., and van der Veen, C. J.: Jakobshavn Glacier, west Greenland: 30 years of spaceborne observations, Geophysical Research Letters, 25, 2699–2702, https://doi.org/10.1029/98GL01973, 1998.

Straneo, F., Heimbach, P., Sergienko, O., Hamilton, G., Catania, G., Griffies, S., Hallberg, R., Jenkins, A., Joughin, I., Motyka, R., Pfeffer, W. T., Price, S. F., Rignot, E., Scambos, T., Truffer, M., and Vieli, A.: Challenges to Understanding the Dynamic Response of Greenland's Marine Terminating Glaciers to Oceanic and Atmospheric Forcing, Bull. Amer. Meteor. Soc., 94, 1131–1144, https://doi.org/10.1175/BAMS-D-12-00100.1, 2013.

Todd, J. and Christoffersen, P.: Are seasonal calving dynamics forced by buttressing from ice mélange or undercutting by melting? Outcomes from full-Stokes simulations of Store Glacier, West Greenland, The Cryosphere, 8, 2353–2365, https://doi.org/10.5194/tc-8-2353-2014, 2014.

Trabant, D., Krimmel, R. M., and Post, A.: A Preliminary Forecast of the Advance of Hubbard Glacier and Its Influence on Russell Fiord, Alaska, U.S. Department of the Interior, U.S. Geological Survey, 270 pp., 1991.

Truffer, M.: Ice thickness measurements on the Harding Icefield, Kenai Peninsula, Alaska, National Park Service, Fort Collins, Colorado, 2014.

Truffer, M., Motyka, R. J., Hekkers, M., Howat, I. M., and King, M. A.: Terminus dynamics at an advancing glacier: Taku Glacier, Alaska, Journal of Glaciology, 55, 1052–1060, https://doi.org/10.3189/002214309790794887, 2009.

Trüssel, B. L., Motyka, R. J., Truffer, M., and Larsen, C. F.: Rapid thinning of lake-calving Yakutat Glacier and the collapse of the Yakutat Icefield, southeast Alaska, USA, Journal of Glaciology, 59, 149–161, https://doi.org/10.3189/2013J0G12J081, 2013.

Trüssel, B. L., Truffer, M., Hock, R., Motyka, R. J., Huss, M., and Zhang, J.: Runaway thinning of the low-elevation Yakutat Glacier, Alaska, and its sensitivity to climate change, Journal of Glaciology, 61, 65–75, https://doi.org/10.3189/2015JoG14J125, 2015.

Urbanski, J. A., Stempniewicz, L., Węsławski, J. M., Dragańska-Deja, K., Wochna, A., Goc, M., and Iliszko, L.: Subglacial discharges create fluctuating foraging hotspots for sea birds in tidewater glacier bays, Sci Rep, 7, 43999, https://doi.org/10.1038/srep43999, 2017.

VanderPlas, J. T.: Understanding the Lomb–Scargle Periodogram, ApJS, 236, 16, https://doi.org/10.3847/1538-4365/aab766, 2018.

VanLooy, J., Forster, R., and Ford, A.: Accelerating thinning of Kenai Peninsula glaciers, Alaska, Geophysical Research Letters, 33, L21307, https://doi.org/10.1029/2006GL028060, 2006.

van der Veen, C. J.: Fracture mechanics approach to penetration of surface crevasses on glaciers, Cold Regions Science and Technology, 27, 31–47, https://doi.org/10.1016/S0165-232X(97)00022-0, 1998.

Vijay, S., King, M. D., Howat, I. M., Solgaard, A. M., Khan, S. A., and Noël, B.: Greenland ice-sheet wide glacier classification based on two distinct seasonal ice velocity behaviors, J. Glaciol., 1–8, https://doi.org/10.1017/jog.2021.89, 2021.

Weertman, J.: Can a water-filled crevasse reach the bottom surface of a glacier?, International Association of Scientific Hydrology, 139–145, 1973.

Whitney, E. J., Beaudreau, A. H., and Howe, E. R.: Using Stable Isotopes to Assess the Contribution of Terrestrial and Riverine Organic Matter to Diets of Nearshore Marine Consumers in a Glacially Influenced Estuary, Estuaries and Coasts, 41, 193–205, https://doi.org/10.1007/s12237-017-0260-z, 2018.

Wiles, G. C. and Calkin, P. E.: Late Holocene, high-resolution glacial chronologies and climate, Kenai Mountains, Alaska, GSA Bulletin, 106, 281–303, https://doi.org/10.1130/0016-7606(1994)106<0281:LHHRGC>2.3.CO;2, 1994.

Wiles, G. C., Calkin, P. E., and Post, A.: Glacier Fluctuations in the Kenai Fjords, Alaska, U.S.A.: An Evaluation of Controls on Iceberg-Calving Glaciers, Arctic and Alpine Research, 27, 234–245, https://doi.org/10.1080/00040851.1995.12003118, 1995.

Womble, J. N., Williams, P. J., McNabb, R. W., Prakash, A., Gens, R., Sedinger, B. S., and Acevedo, C. R.: Harbor Seals as Sentinels of Ice Dynamics in Tidewater Glacier Fjords, Front. Mar. Sci., 8, https://doi.org/10.3389/fmars.2021.634541, 2021.

Wood, M., Rignot, E., Fenty, I., An, L., Bjørk, A., van den Broeke, M., Cai, C., Kane, E., Menemenlis, D., Millan, R., Morlighem, M., Mouginot, J., Noël, B., Scheuchl, B., Velicogna, I., Willis, J. K., and Zhang, H.: Ocean forcing drives glacier retreat in Greenland, Sci. Adv., 7, eaba7282, https://doi.org/10.1126/sciadv.aba7282, 2021.

Wouters, B., Gardner, A. S., and Moholdt, G.: Global Glacier Mass Loss During the GRACE Satellite Mission (2002-2016), Front. Earth Sci., 7, https://doi.org/10.3389/feart.2019.00096, 2019.

Yang, R., Hock, R., Kang, S., Shangguan, D., and Guo, W.: Glacier mass and area changes on the Kenai Peninsula, Alaska, 1986–2016, J. Glaciol., 66, 603–617, https://doi.org/10.1017/jog.2020.32, 2020.

Zemp, M., Huss, M., Thibert, E., Eckert, N., McNabb, R., Huber, J., Barandun, M., Machguth, H., Nussbaumer, S. U., Gärtner-Roer, I., Thomson, L., Paul, F., Maussion, F., Kutuzov, S., and Cogley, J. G.: Global glacier mass changes and their contributions to sea-level rise from 1961 to 2016, Nature, 568, 382–386, https://doi.org/10.1038/s41586-019-1071-0, 2019.

Zhang, H., Menemenlis, D., and Fenty, I.: ECCO LLC270 Ocean-Ice State Estimate, 2018.

Appendix A

This appendix contains the supplementary material for Chapter 2, "Multi-decadal retreat of marine-terminating outlet glaciers in northwest and central-west Greenland".

A.1 Code and data availability

Data analysis and visualization code are available on GitHub (https://github.com/tarynblack/northwest_decadal_2021). The terminus positions are available on NSIDC as part of the MEaSUREs Annual Greenland Outlet Glacier Terminus Positions from SAR Mosaics dataset (https://nsidc.org/data/NSIDC-0642, Joughin et al., 2015). Bed topography is from BedMachine Greenland V3 (https://nsidc.org/data/idbmg4, Morlighem et al., 2017b). Ice-sheet velocity is from MEaSUREs Multi-year Greenland Ice Sheet Velocity Mosaic, Version 1 (https://nsidc.org/data/NSIDC-0670/versions/1, Joughin et al., 2016b). Landsat images were identified with GloVis (http://glovis.usgs.gov) and downloaded from Google Cloud Platform (https://console.cloud.google.com/storage/browser/gcp-public-data-landsat). Sentinel-1 images are from MEaSUREs Greenland Image Mosaics from Sentinel-1A and -1B, Version 3 (https://nsidc.org/data/nsidc-0723, Joughin, 2021). Ocean temperatures are from ECCO Version 5 (https://ecco-group.org, Forget et al., 2015; Zhang et al., 2018), the ICES Dataset on Ocean Hydrography (https://ocean.ices.dk/hydchem/hydchem.aspx, ICES, 2014), and the Merged Hadley-OI sea surface temperature and sea ice concentration data set (https://doi.org/10.5065/r33v-sv91, Hurrell et al., 2008; Shea et al., 2020). Sea-ice concentrations are from the Merged Hadley-OI data set and the NOAA/NSIDC Climate Data Record of Passive Microwave Sea Ice Concentration, Version 3 (https://nsidc.org/data/g02202, Meier et al., 2017;

Peng et al., 2013). Ice sheet climate data are from MAR v3.11 output over Greenland (ftp://ftp.climato.be/fettweis/MARv3.11/Greenland/ERA_1979-2020-6km/, Fettweis et al., 2017).

A.2 Ocean temperature correction

Wood et al. (2021) found biases in the ECCO ocean temperatures and applied corrections to the data, including a uniform 0.4 °C correction below 50m depth everywhere, and a linear trend to account for an initial 1 °C bias in Baffin Bay. Here we attempt to take advantage of those corrections by matching our data to those provided in the supplementary information of Wood et al. (2021).

We apply corrections to the deepwater ocean temperatures per each of our ocean points as follows:

1. Extract the temperatures for the bottom 60% of the water column at the given point
2. Determine the mean anomaly over the periods 1992-1997, 1998-2007, and 2008-2017 to match the supplementary data from Wood et al. (2021)
3. Compute the difference of the point data compared to Wood et al. (2021) supplementary data in the same region
4. Find a two-segment piecewise linear fit to the difference from (3), with endpoints at 1995, 2003, and 2013, using the python package scipy.optimize.curve_fit
5. Apply the output from (4) to all years (1992-2017) to compute a correction curve
6. Subtract the correction curve (5) from the original curve (1) to get a corrected temperature

By comparing our resulting means over the periods 1992-1997, 1998-2007, and 2008-2017 with those of Wood et al. (2021), we find that our corrected data agree well with theirs (Figure A. 6).

A.3 Supplementary tables

Table A. 1: Glacier ID, name, and geographic coordinates.
ID, name, and geographic coordinates for all glaciers in this study. Names provided are official names, with alternative or common name in parentheses, from Bjørk et al. (2015). Geographic coordinates are for a point feature on each glacier.

ID	Name	Geographic Coordinates
1	Saqqarliup Sermia	68.88° N, 50.31° W
2	Alanngorliup Sermia	68.94° N, 50.22° W
3	Sermeq Kujalleq (Jakobshavn Isbræ)	69.14° N, 49.58° W
4	Sermeq Avannarleq	69.37° N, 50.30° W
5	Eqip Sermia	69.79° N, 50.24° W
6	Kangilernata Sermia	69.91° N, 50.34° W
7	Sermeq Kujalleq (Alianaatsup Sermia)	69.99° N, 50.16° W
8	Sermeq Avannarleq	70.07° N, 50.31° W
9	Sermeq Kujalleq (Store Gletsjer)	70.40° N, 50.54° W
10	Sermeq Avannarleq (Lille Gletsjer)	70.53° N, 50.50° W
11	Sermilik	70.63° N, 50.62° W
12	Kangilleq	70.72° N, 50.63° W
13	Sermeq Silarleq	70.81° N, 50.79° W
14	Perlerfiup Sermia	70.99° N, 50.91° W
15	Kangerluarsuup Sermia	71.25° N, 51.48° W
16	Kangerlussuup Sermia	71.46° N, 51.38° W
17	Kangilliup Sermia (Rink Isbræ)	71.75° N, 51.61° W
18	Umiammakku Sermiat	71.74° N, 52.39° W
19	Salliarutsip Sermia (Inngia Isbræ)	72.03° N, 52.59° W
20		72.78° N, 54.22° W
21	Sermeq (Upernavik Isstrøm)	72.85° N, 54.31° W
22		72.94° N, 54.33° W
23		73.03° N, 54.30° W
24		73.00° N, 54.64° W
25	Naajarsuit Sermiat	73.23° N, 55.13° W
26		73.38° N, 55.03° W
27	(Kakivfait Sermia A)	73.46° N, 55.29° W
28	(Kakivfait Sermia B)	73.49° N, 55.43° W
29	Qeqertarsuup Sermia	73.59° N, 55.54° W
30	Sermeq Kujalleq (Ussingbraer A)	73.83° N, 55.59° W
31	Sermeq Avanarleq (Ussingbraer B)	73.94° N, 55.68° W
32	Ikissuup Sermersua (Cornell Gletsjer)	74.24° N, 56.05° W

ID	Name	Geographic Coordinates
33		74.30° N, 56.09° W
34	Illullip Sermia	74.40° N, 56.04° W
35	Nunatakassaap Sermia (Alison Glacier)	74.61° N, 56.06° W
36		74.70° N, 56.32° W
37		74.79° N, 56.53° W
38		74.87° N, 56.76° W
39		74.91° N, 56.91° W
40	Tuttulikassaap Sermia (Hayes Gletsjer)	74.94° N, 57.08° W
41		75.04° N, 57.53° W
42	Kjer Gletsjer	75.14° N, 57.78° W
43		75.20° N, 57.78° W
44	Sermersuaq (Steenstrup Gletsjer)	75.29° N, 57.91° W
45	Dietrichson Gletsjer	75.46° N, 58.03° W
46	Sverdrup Gletsjer	75.59° N, 58.12° W
47	Nansen Gletsjer	75.74° N, 58.89° W
48	Nordenskiöld Gletsjer	75.83° N, 59.04° W
49		75.89° N, 59.16° W
50		75.97° N, 59.49° W
51	Nuussuup Sermia (Kong Oscar Gletsjer)	76.01° N, 59.73° W
52		76.06° N, 59.96° W
53		76.08° N, 60.13° W
54	Issuusarsuit Sermiat (Peary Gletscher)	76.05° N, 60.63° W
55		76.21° N, 60.66° W
56	Rink Gletsjer	76.23° N, 60.92° W
57		76.25° N, 61.38° W
58	Qeqertat Timaanni Sermeq (Döcker Smith Gletsjer)	76.25° N, 61.78° W
59	Döcker Smith Gletsjer C	76.28° N, 61.91° W
60	Döcker Smith Gletsjer B	76.32° N, 61.97° W
61	Morell Gletsjer	76.30° N, 62.52° W
62	Innaqqissorsuup Oqquani Sermeq (Gade Gletsjer)	76.36° N, 62.84° W
63		76.43° N, 63.39° W
64		76.40° N, 63.55° W
65	Yngvar Nielsen Gletsjer	76.35° N, 64.08° W
66		76.37° N, 64.24° W
67		76.29° N, 64.61° W
68	Helland Gletsjer	76.19° N, 64.83° W
69	Savissuup Sermia	76.20° N, 65.24° W
70		76.34° N, 65.68° W

ID	Name	Geographic Coordinates
71		76.32° N, 66.84° W
72		76.26° N, 67.28° W
73		76.19° N, 67.48° W
74	Paakitsup Sermersua (Pituffik Gletsjer)	76.23° N, 68.79° W
75	Ullip Sermia (Harald Moltke Bræ)	76.59° N, 67.74° W
79	Leidy Gletsjer	77.26° N, 66.08° W
80	Qaqujaarsuup Sermia (Heilprin Gletsjer)	77.54° N, 66.00° W
81	Qeqertaarsuusarsuup Sermia (Tracy Gletsjer)	77.65° N, 66.05° W
82	Tuttulipaluup Sermia (Farquhar Gletsjer)	77.70° N, 66.25° W
83	Paarnarsuit Sermiat (Hart Gletsjer)	77.69° N, 67.14° W
84	Quinisut Sermiat (Hubbard Gletsjer)	77.54° N, 67.81° W
85	Kangerluarsuup Sermia (Bowdoin Gletsjer)	77.68° N, 68.60° W
86	Qinnguata Sermia (Verhoeff Gletsjer)	77.86° N, 69.89° W
87	Neqip Sermia (Morris Jesup Gletsjer)	77.89° N, 71.13° W
88	Arfalluarfiup Sermia (Diebitsch Gletsjer)	77.94° N, 71.60° W
89	Arfalluarfiup Sermia (Clements Markham Gletsjer)	77.93° N, 71.95° W
90	Bamse Gletsjer	78.02° N, 72.17° W

Table A. 2: Ocean sample point data.

Sample point numbers, region names, and geographic coordinates for locations from which ocean data were sampled.

Ocean Point	Region	Coordinates
1	Disko Bay	69.25° N, 52.25° W
2	Uummannaq Fjord	70.85° N, 54.25° W
3	Upernavik Icefjord and north	73.25° N, 58.00° W
4	South Melville Bay/Wilcox Head	74.50° N, 60.00° W
5	Central Melville Bay	75.50° N, 61.75° W
6	North Melville Bay/Cape York	75.75° N, 65.00° W
7	Wolstenholme Bay/Thule	76.25° N, 71.00° W
8	Inglefield Fjord	77.00° N, 72.50° W

Table A. 3: Measurements for individual glaciers.

Total number of observations, net area and equivalent length change since first observation, and breakpoint year for area and equivalent length. Significant area and length changes are indicated by an asterisk (*) after the value.

ID	Number of Observations	Net ΔArea (km^2)	Net ΔLength (km)	Breakpoint Year
1	43	-5.11*	-1.24*	2001
2	43	-1.34*	-0.61*	2000
3	43	-125.68*	-16.26*	1993
4	42	-6.76*	-2.73*	1996
5	41	-5.46*	-1.55*	1996
6	41	-9.16*	-2.88*	1997
7	39	-3.36	-0.77	N/A
8	38	-0.31	-0.07	1987
9	41	-0.12	-0.03	2002
10	40	-2.83*	-1.49*	1997
11	40	-0.81	-0.36	2004
12	40	0.06	0.04	2003
13	39	-16.77*	-5.27*	2000
14	39	-6.90*	-2.86*	2006
15	40	-3.01*	-1.41*	1997
16	40	0.46	0.13	1993
17	41	-1.92	-0.47	1984
18	42	-12.11*	-5.05*	1996
19	42	-26.52*	-8.49*	2003
20	41	-10.82*	-6.67*	1985
21	41	-2.08	-0.68	2013
22	42	-15.61*	-4.93*	2007
23	42	-40.62*	-8.42*	1997
24	43	-5.69*	-3.55*	2015
25	45	0.00	0.00	2012
26	43	-0.25	-0.15	1991
27	43	-4.79*	-1.44*	2009
28	42	-17.19*	-5.67*	2007
29	41	-5.02*	-1.35*	1999
30	41	-1.73*	-0.51*	2009
31	41	-3.45*	-0.76*	1994
32	40	-6.54*	-1.54*	2013
33	40	-3.28*	-1.50*	2002
34	41	-4.76*	-1.10*	2001

ID	Number of Observations	Net ΔArea (km^2)	Net ΔLength (km)	Breakpoint Year
35	40	-58.08*	14.31*	1996
36	40	-46.00*	-13.36*	2001
37	39	-21.03*	-5.42*	1984
38	39	-9.08*	-3.31*	1994
39	40	-5.66*	-2.00*	2008
40	40	-10.76*	-2.65*	1996
41	40	-8.19*	-1.20*	1997
42	43	-83.26*	-14.98*	2010
43	43	-23.55*	-7.51*	2013
44	43	-34.67*	-7.27*	1995
45	42	-7.11*	-2.78*	2006
46	41	-39.48*	-7.93*	2000
47	42	-28.35*	-4.83*	2014
48	42	-8.71*	-2.67*	2010
49	42	-1.74*	-0.64*	1993
50	42	-3.09*	-1.94*	1988
51	42	-10.84	-3.09	1989
52	43	-11.47*	-3.93*	2006
53	44	-8.36*	-3.49*	2011
54	46	-13.51*	-3.65*	2019
55	45	-1.63	-0.85	1992
56	44	-11.23*	-3.87*	1995
57	45	-1.90*	-0.97*	2002
58	46	-10.93*	-3.47*	1996
59	46	-15.36*	-9.22*	2001
60	46	-19.59*	-6.38*	1993
61	46	-16.46*	-5.38*	2005
62	46	-9.27*	-1.84*	1982
63	45	-8.65*	-3.17*	2012
64	45	-4.03*	-1.96*	1997
65	40	-16.14*	-7.01*	2013
66	39	-0.21	-0.12	N/A
67	38	-3.22*	-1.61*	1998
68	38	-4.36*	-1.43*	1996
69	39	-5.68*	-1.89*	1996
70	38	-23.86*	-5.69*	2001
71	39	-5.78*	-2.28*	1997
72	33	-7.71*	-3.27*	1998

ID	Number of Observations	Net ΔArea (km^2)	Net ΔLength (km)	Breakpoint Year
73	34	-18.44*	-5.19*	1992
74	33	-11.10*	-2.45*	1996
75	39	-33.54*	-6.10*	1999
79	44	-2.06*	-0.74*	1999
80	44	-6.12*	-1.78*	1996
81	44	-51.06*	-12.17*	1982
82	38	-7.28*	-3.83*	1998
83	45	-1.45*	-0.87*	2006
84	45	-2.10*	-1.01*	1994
85	43	-2.70*	-1.24*	2003
86	42	-0.83	-0.29	1997
87	42	-1.25	-0.42	1998
88	42	-5.11*	-1.72*	1997
89	38	-1.03*	-0.85*	1996
90	42	-1.27*	-0.80*	1997

A.4 Supplementary figures

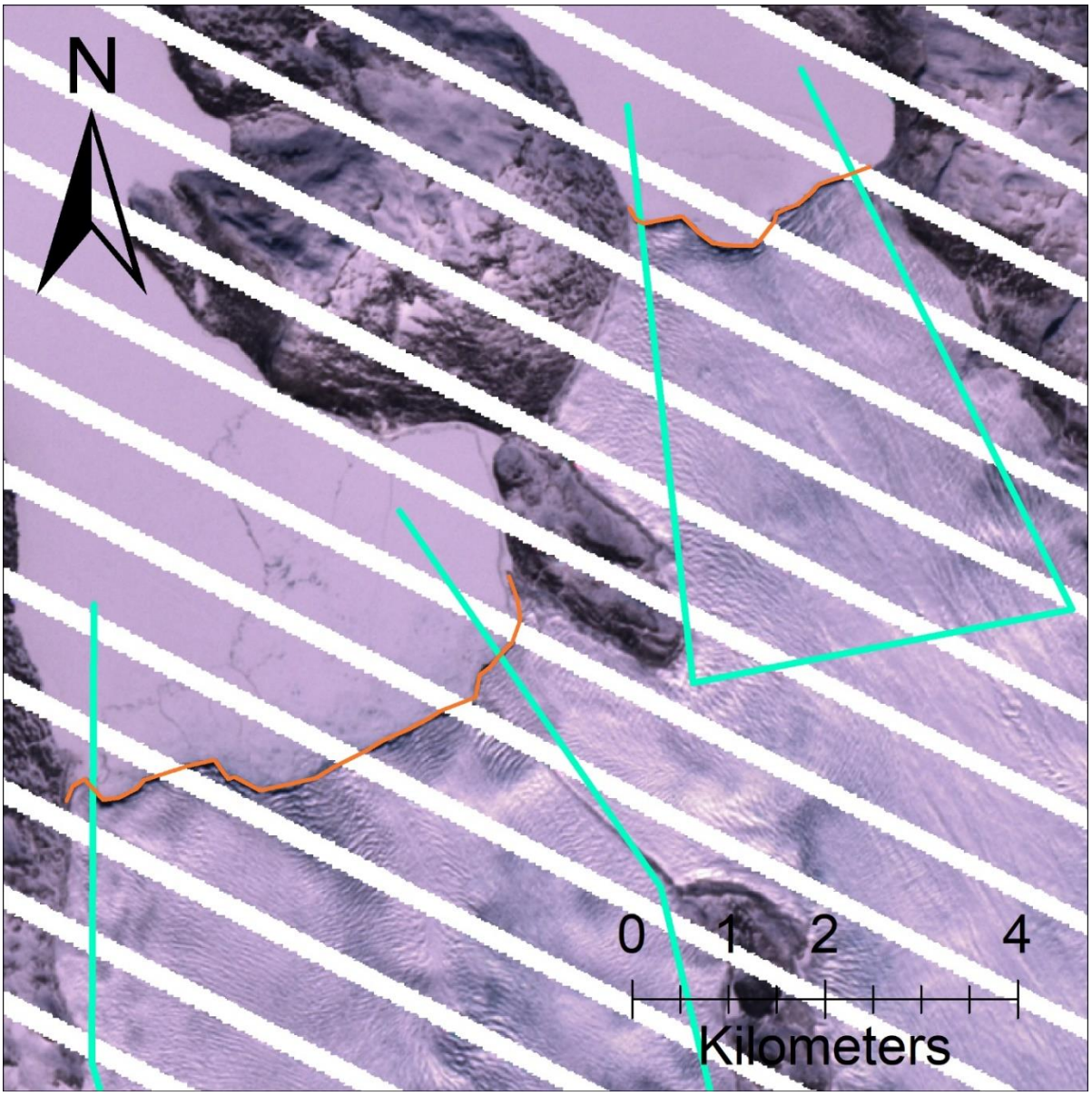

Figure A. 1: Landsat-7 scan-line corrector gaps.
Example of terminus digitization (red lines) across Landsat-7 scan-line corrector gaps, for glaciers #1 (Saqqarliup Sermia) and #2 (Alanngorliup Sermia). The base image is a Landsat-7 image from 25 April 2012. This image is typical of the images we used to digitize across scan-line corrector gaps.

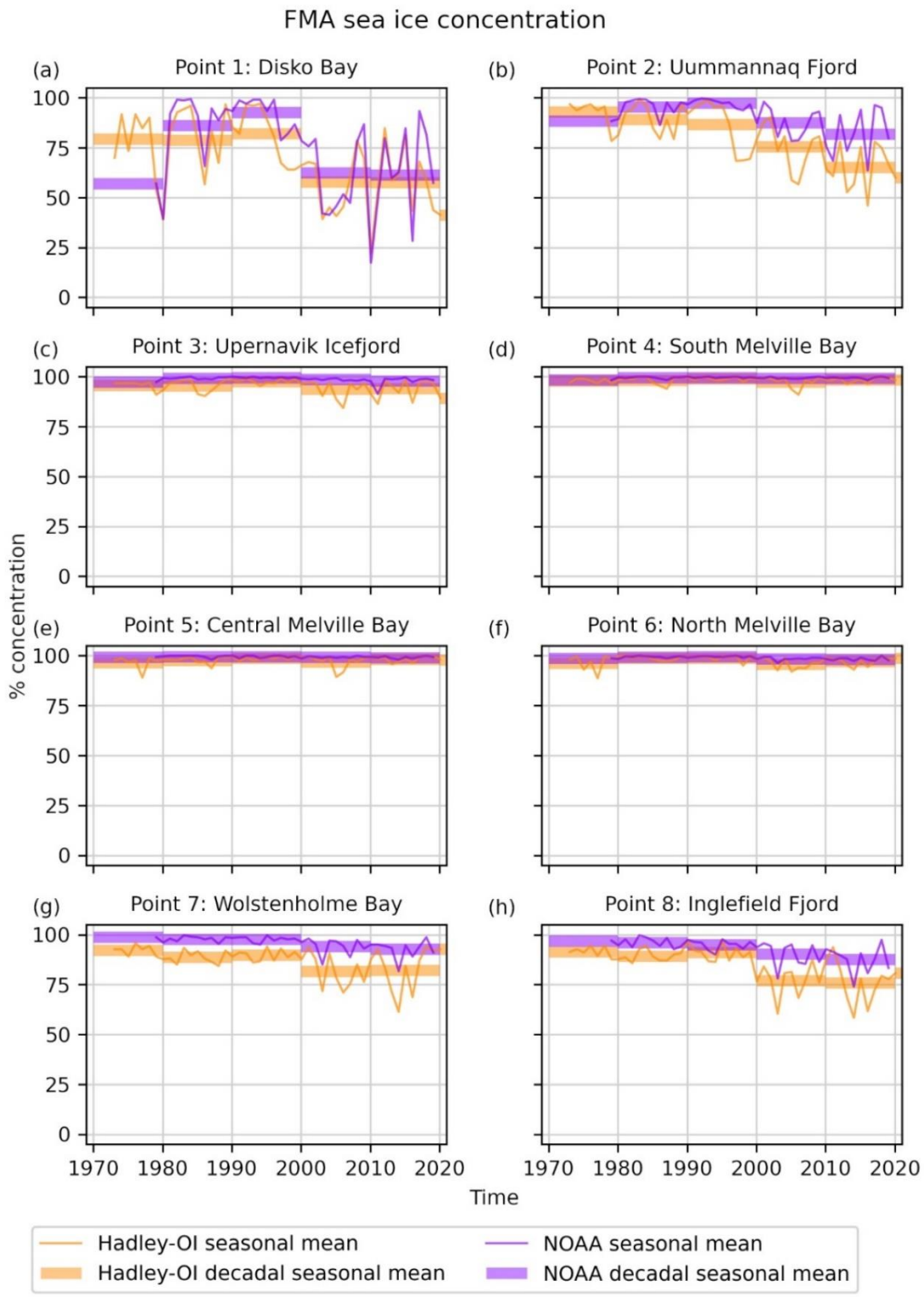

Figure A. 2: Annual and decadal February-April mean sea-ice concentration.
Annual and decadal February-April mean sea-ice concentration from Hadley-OI (orange) and NOAA (purple). Each panel corresponds with an ocean point in Figure 2.1.

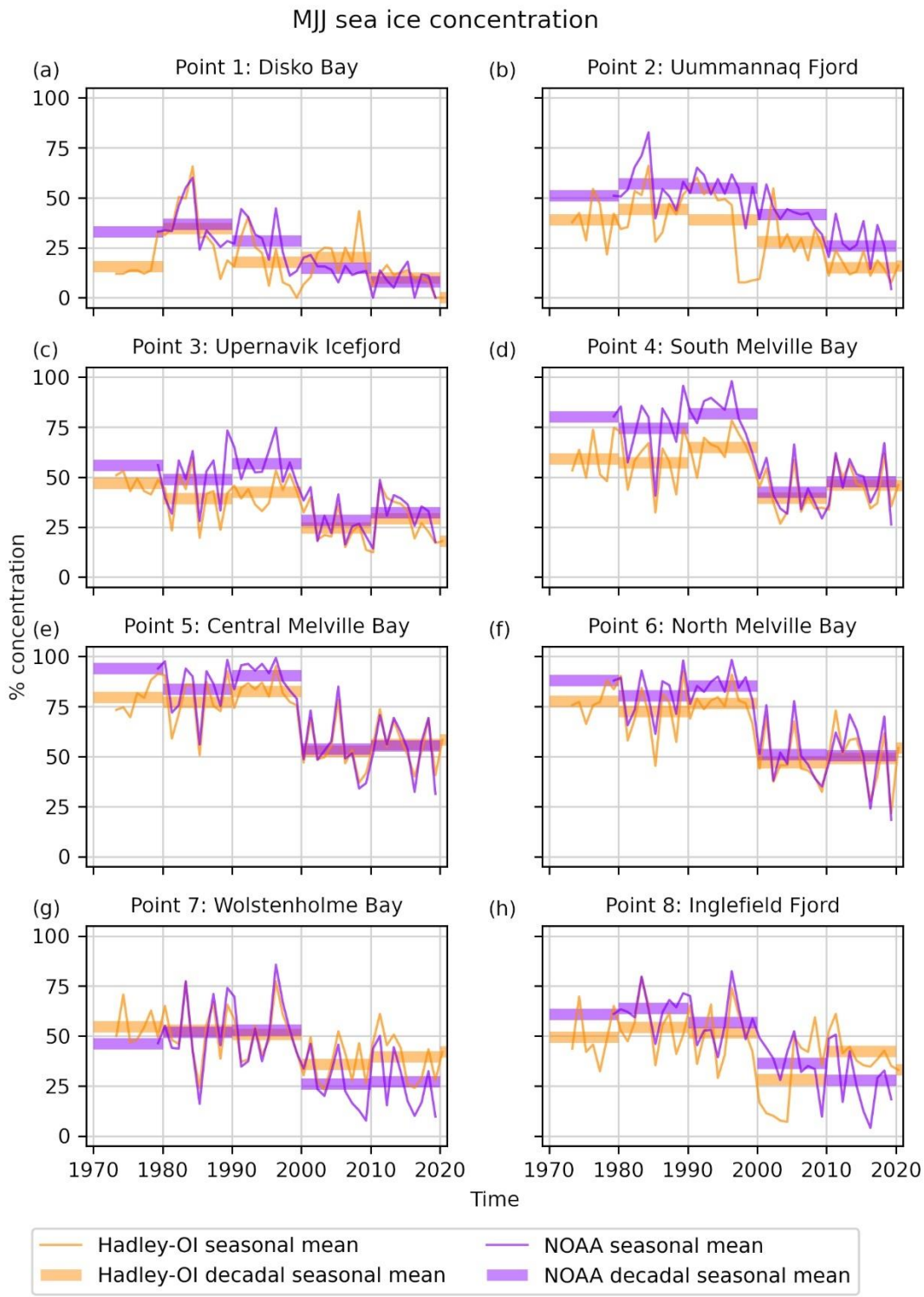

Figure A. 3: Annual and decadal May-July mean sea-ice concentration.
Annual and decadal May-July mean sea-ice concentration from Hadley-OI (orange) and NOAA (purple). Each panel corresponds with an ocean point in Figure 2.1.

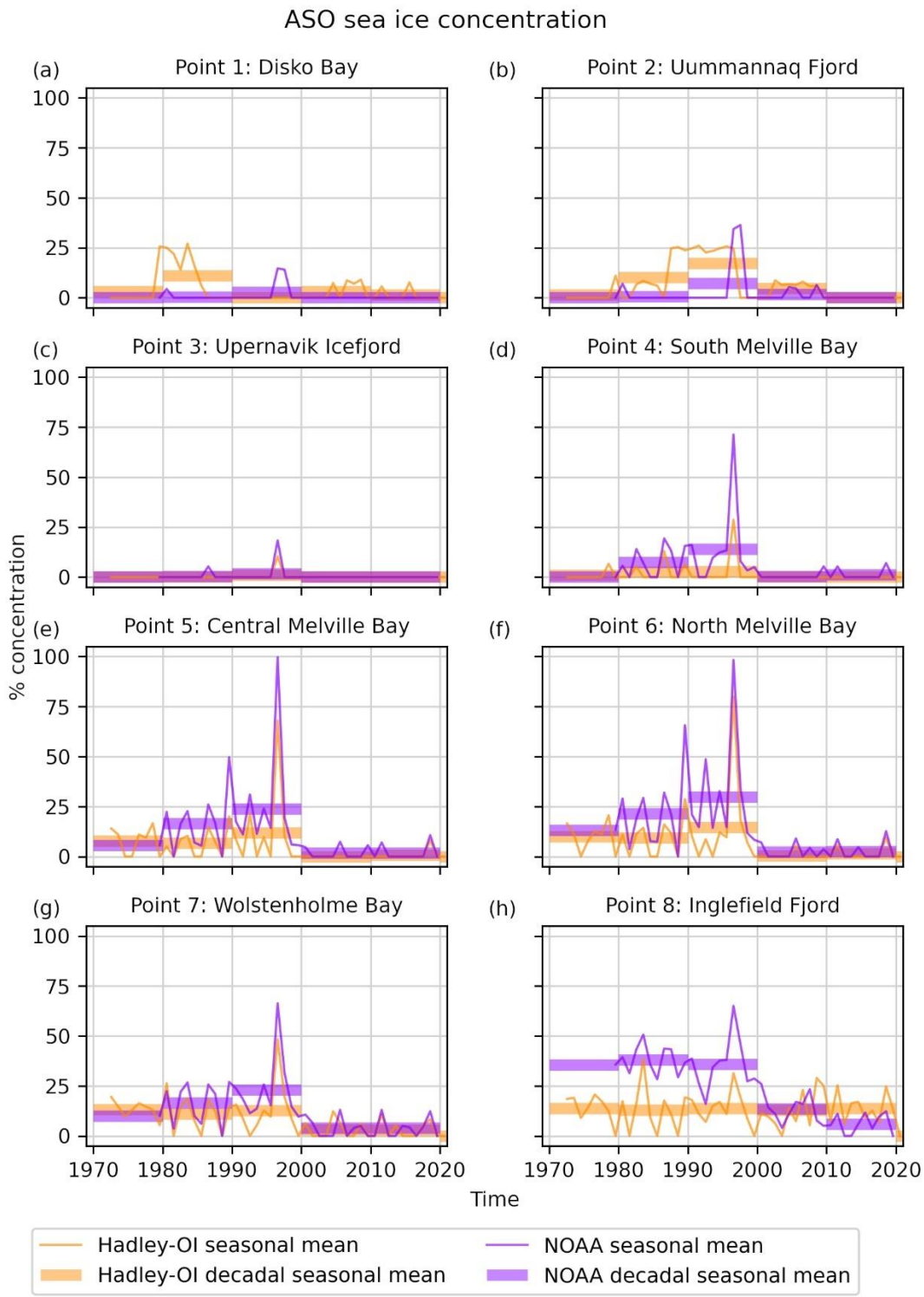

Figure A. 4: Annual and decadal August-October mean sea-ice concentration.
Annual and decadal August-October mean sea-ice concentration from Hadley-OI (orange) and NOAA (purple). Each panel corresponds with an ocean point in Figure 2.1.

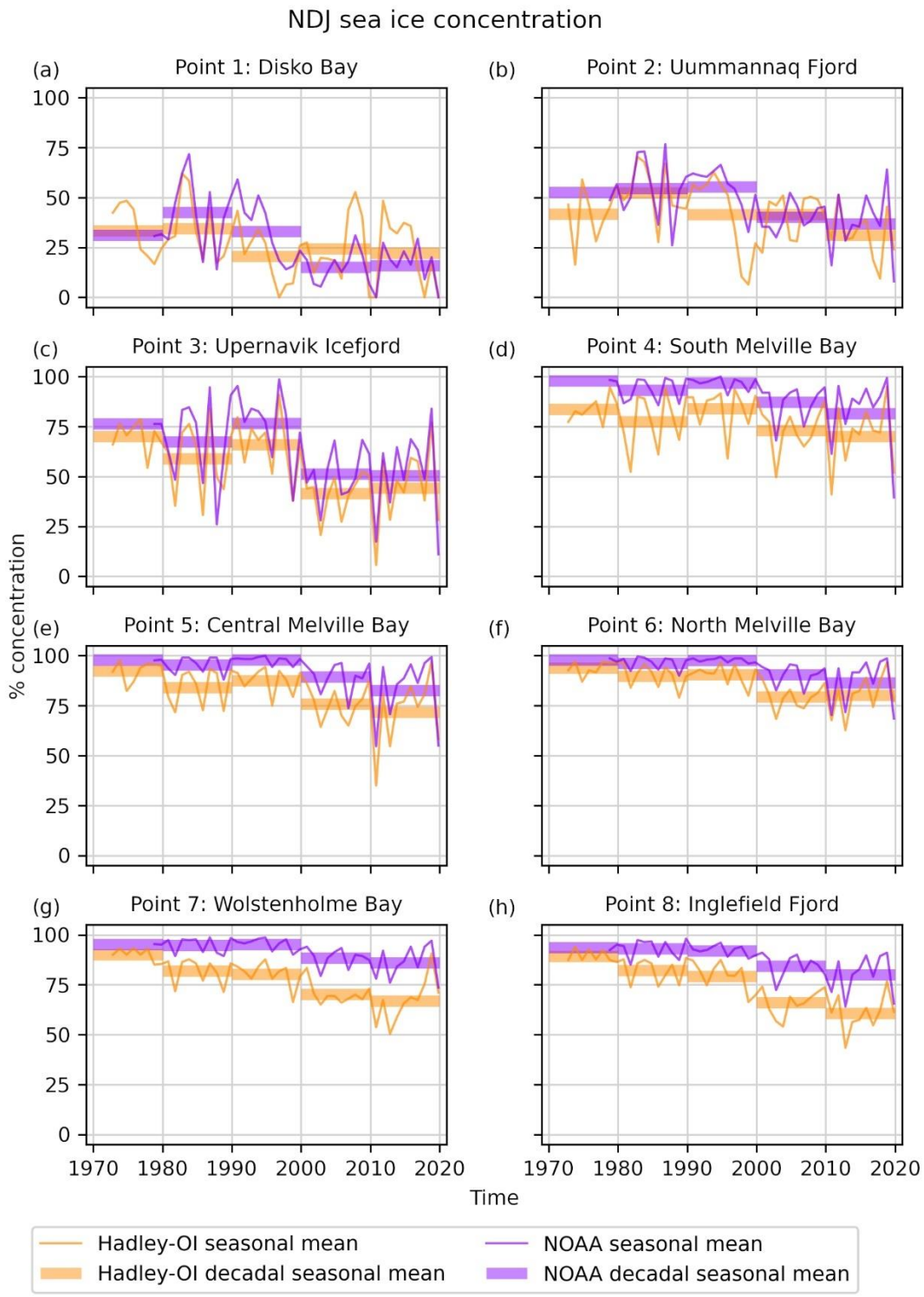

Figure A. 5: Annual and decadal November-January mean sea-ice concentration.
Annual and decadal November-January mean sea-ice concentration from Hadley-OI (orange) and NOAA (purple). Each panel corresponds with an ocean point in Figure 2.1.

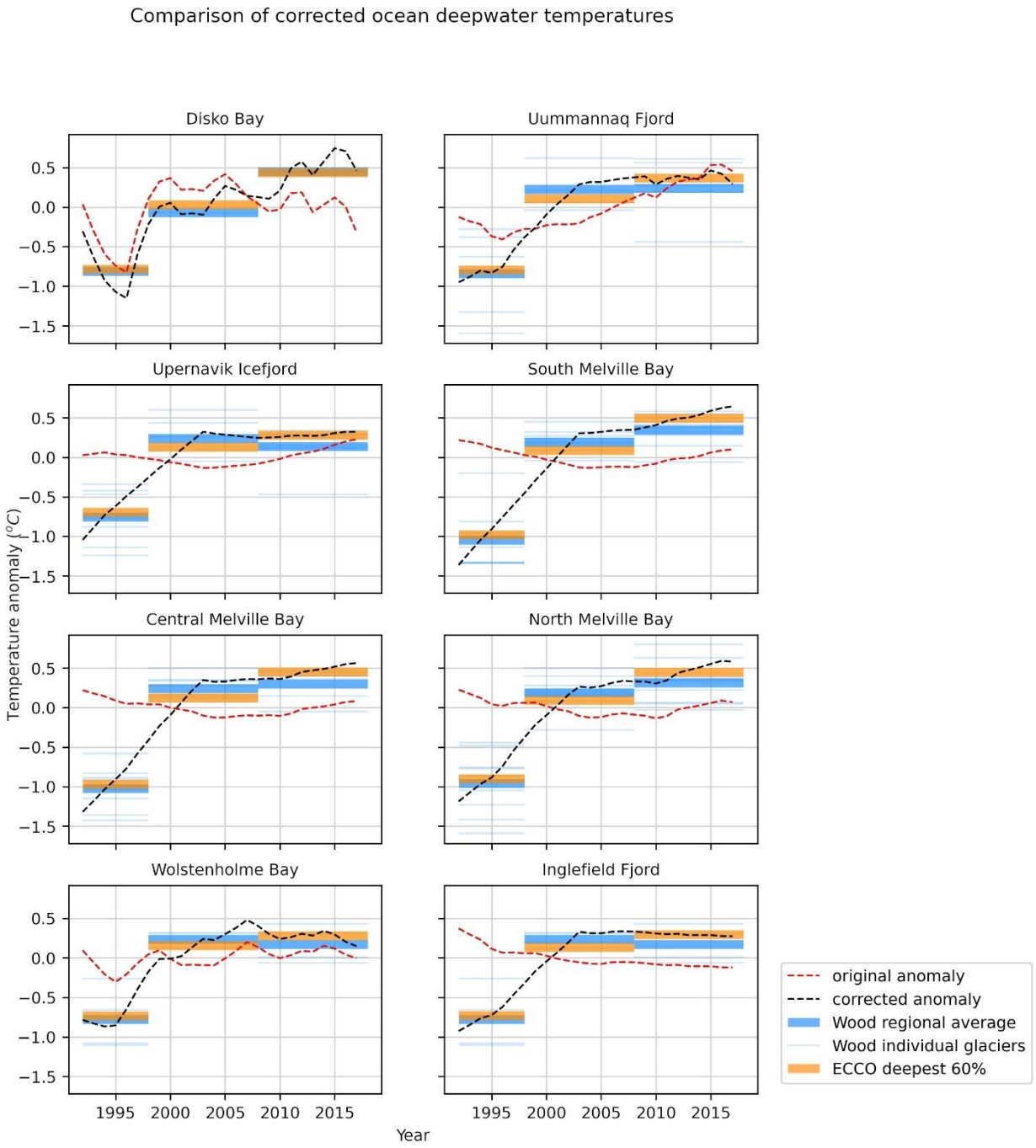

Figure A. 6: Ocean temperature correction.
Comparison of our uncorrected (red) and corrected (black) deepwater ocean temperatures and decadal means (orange) to the decadal means of Wood et al. (2021) (blue). Each panel corresponds with an ocean point in Figure 2.1.

Appendix B

This appendix contains the supplementary material for Chapter 3, “Maritime glacier retreat and terminus area change in Kenai Fjords National Park, Alaska, between 1984 and 2021”.

B.1 Data and code availability

The glacier termini digitized in this study are available on the US National Park Service Integrated Resource Management Applications (IRMA) Portal (https://irma.nps.gov/DataStore/Reference/Profile/2293309, Black and Kurtz, 2022a). The scripts used for image downloads and data analysis are available at https://doi.org/10.5281/zenodo.6331265 (Black, 2022). We acquired Landsat images from Google Cloud Platform (https://console.cloud.google.com/storage/browser/gcp-public-data-landsat), and glacier centerlines from IRMA (https://irma.nps.gov/DataStore/Reference/Profile/2221653, Arendt and Rich, 2013).

B.2 Supplementary tables

Table B. 1: Glacier length change rates.
Net and decadal length change rates for each glacier. All values are in m a^{-1}.

Glacier	Net dL/dt	1980s dL/dt	1990s dL/dt	2000s dL/dt	2010s dL/dt	2020s dL/dt
Bear Glacier	-139	-12	-146	-115	-172	-294
Aialik Glacier	-0	111	-53	-6	1	11
Pedersen Glacier	-86	3	-22	-70	-206	31
Holgate Glacier	13	57	-30	17	20	53
South Holgate Glacier - West	-10	6	-7	-8	-5	-97
South Holgate Glacier - East	-34	31	1	-55	-52	-164
Northeastern Glacier	-56	-44	-63	-46	-57	-83
Northwestern Glacier	-42	-6	-154	1	-0	7
Ogive Glacier	1	-10	5	4	-1	10
Anchor Glacier	-3	33	-2	5	-13	-75
Reconstitution Glacier	-8	10	-16	-15	-13	33
Southwestern Glacier	-42	-69	-7	-11	-57	-162
Sunlight Glacier	-16	-13	-13	-49	12	-65
Paguna Glacier	6	32	10	4	0	-11
McCarty Glacier	-20	18	-23	-46	-6	-25
Dinglestadt Glacier	-24	12	-11	-32	-27	-92
Split Glacier	-15	-60	9	-29	-12	-69
Yalik Glacier	-61	-50	-43	-58	-65	-158
Petrof Glacier	-28	-68	-22	-13	-35	-36

Table B. 2: Glacier area change rates.

Net and decadal area change rates for each glacier. All values are in $km^2\ a^{-1}$.

Glacier	Net dA/dt	1980s dA/dt	1990s dA/dt	2000s dA/dt	2010s dA/dt	2020s dA/dt
Bear Glacier	-0.463	-0.654	-0.383	-0.537	-0.378	-0.587
Aialik Glacier	-0.016	0.098	-0.063	-0.056	-0.009	0.052
Pedersen Glacier	-0.114	-0.077	-0.033	-0.202	-0.158	0.003
Holgate Glacier	0.006	0.070	-0.057	0.034	0.005	0.052
South Holgate Glacier - West	-0.006	0.004	-0.002	-0.014	-0.002	-0.034
South Holgate Glacier - East	-0.013	0.020	-0.013	-0.028	-0.009	-0.050
Northeastern Glacier	-0.066	-0.073	-0.063	-0.040	-0.074	-0.114
Northwestern Glacier	-0.044	0.012	-0.177	0.005	0.002	-0.020
Ogive Glacier	-0.002	0.005	-0.013	0.010	-0.002	-0.009
Anchor Glacier	-0.003	0.020	-0.003	0.001	-0.010	-0.038
Reconstitution Glacier	-0.011	0.008	-0.022	-0.017	-0.008	-0.001
Southwestern Glacier	-0.037	-0.043	-0.007	-0.034	-0.058	-0.061
Sunlight Glacier	-0.024	-0.079	-0.015	-0.047	-0.012	-0.003
Paguna Glacier	-0.001	0.011	0.007	-0.003	-0.002	-0.052
McCarty Glacier	-0.049	0.012	-0.001	-0.170	-0.036	-0.031
Dinglestadt Glacier	-0.020	0.007	-0.011	-0.031	-0.022	-0.050
Split Glacier	-0.018	-0.029	0.001	-0.032	-0.010	-0.112
Yalik Glacier	-0.185	-0.415	-0.093	-0.231	-0.176	-0.371
Petrof Glacier	-0.062	-0.084	-0.058	-0.061	-0.067	-0.047

B.3 Supplementary figures

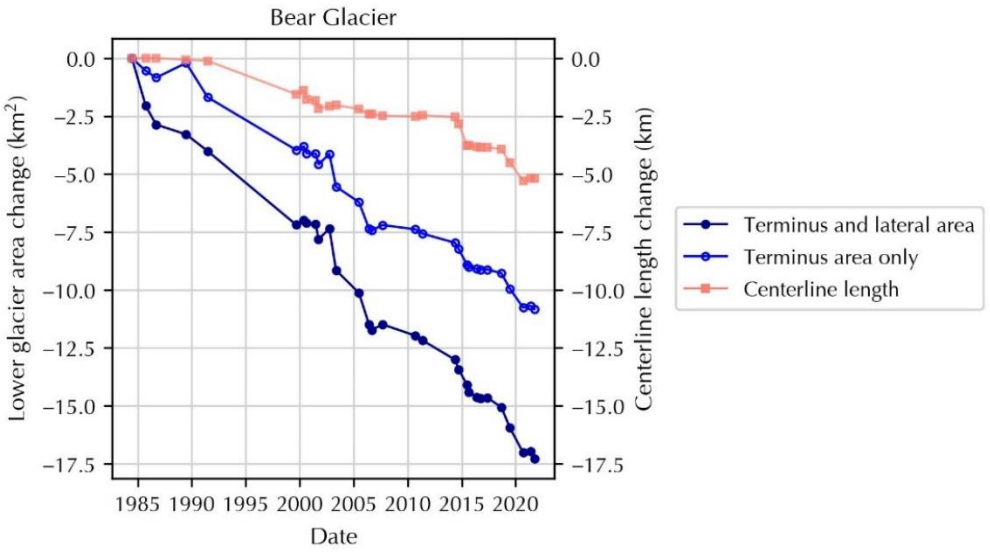

Figure B. 1: Bear Glacier.
Observed change in lower glacier area (dark blue, closed circles), terminus area (blue, open circles), and centerline length (pink, squares) at Bear Glacier.

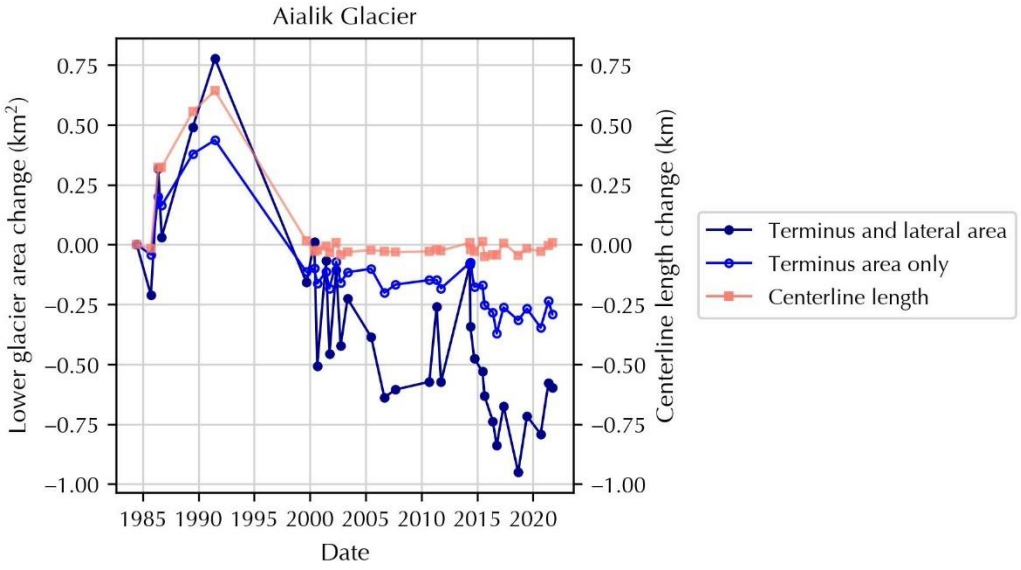

Figure B. 2: Aialik Glacier.
Observed change in lower glacier area (dark blue, closed circles), terminus area (blue, open circles), and centerline length (pink, squares) at Aialik Glacier.

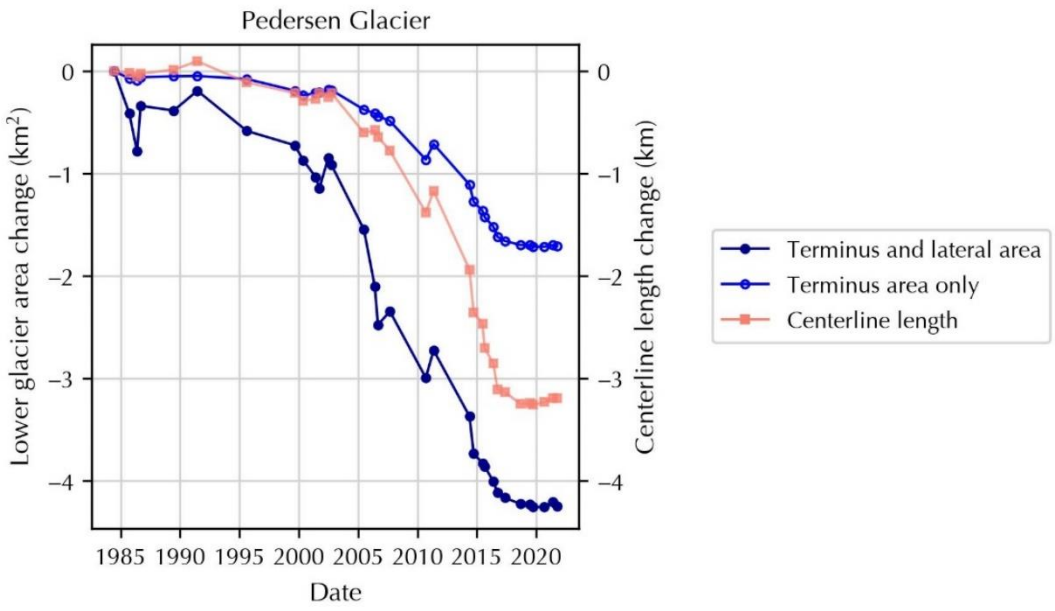

Figure B. 3: Pedersen Glacier.
Observed change in lower glacier area (dark blue, closed circles), terminus area (blue, open circles), and centerline length (pink, squares) at Pedersen Glacier.

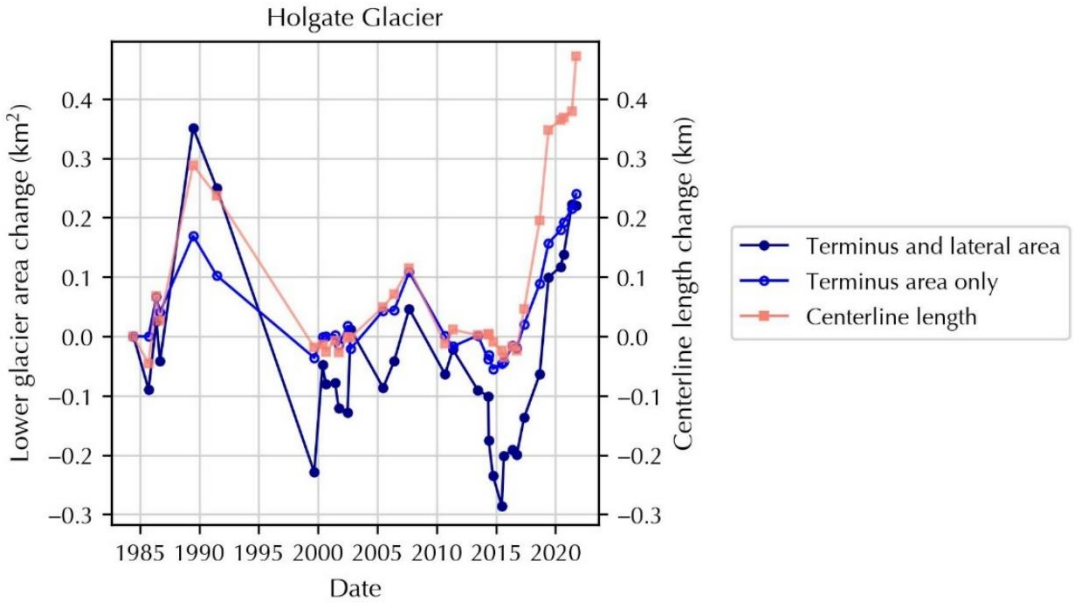

Figure B. 4: Holgate Glacier.
Observed change in lower glacier area (dark blue, closed circles), terminus area (blue, open circles), and centerline length (pink, squares) at Holgate Glacier.

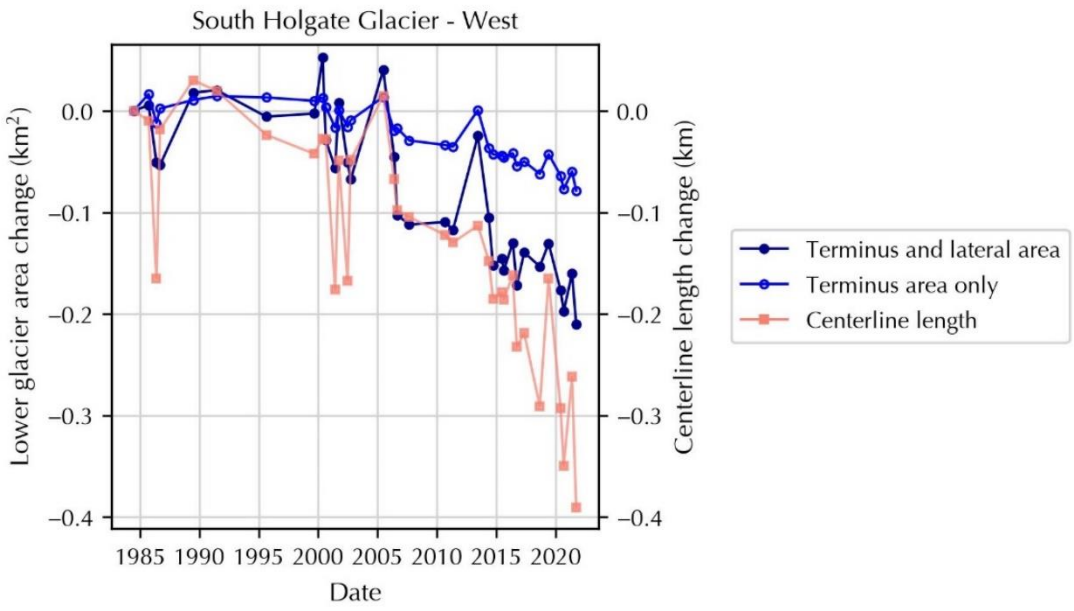

Figure B. 5: South Holgate Glacier – West.
Observed change in lower glacier area (dark blue, closed circles), terminus area (blue, open circles), and centerline length (pink, squares) at South Holgate Glacier – West.

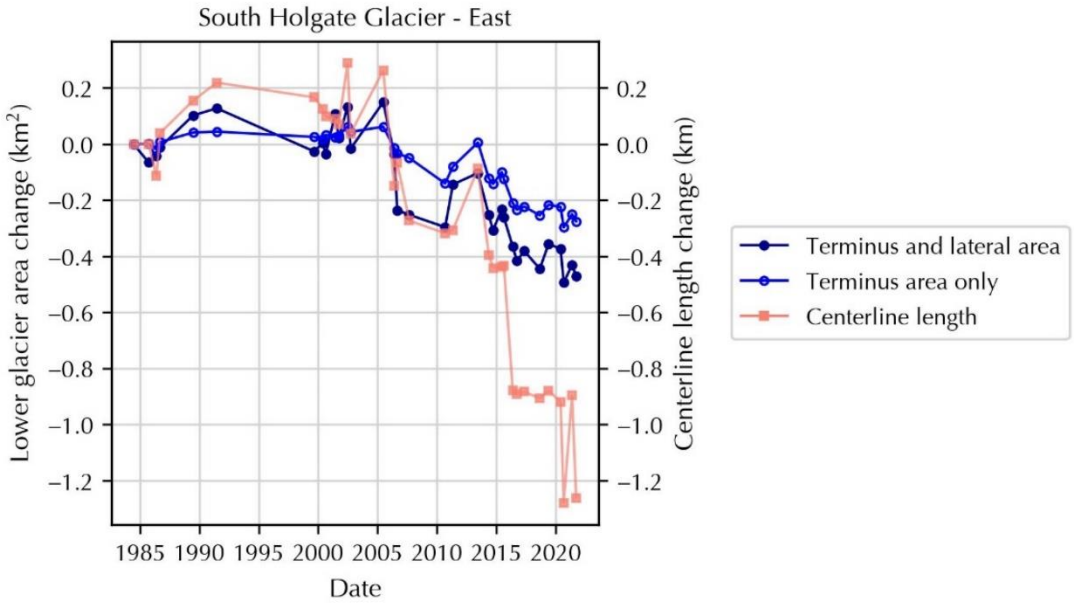

Figure B. 6: South Holgate Glacier – East.
Observed change in lower glacier area (dark blue, closed circles), terminus area (blue, open circles), and centerline length (pink, squares) at South Holgate Glacier – East.

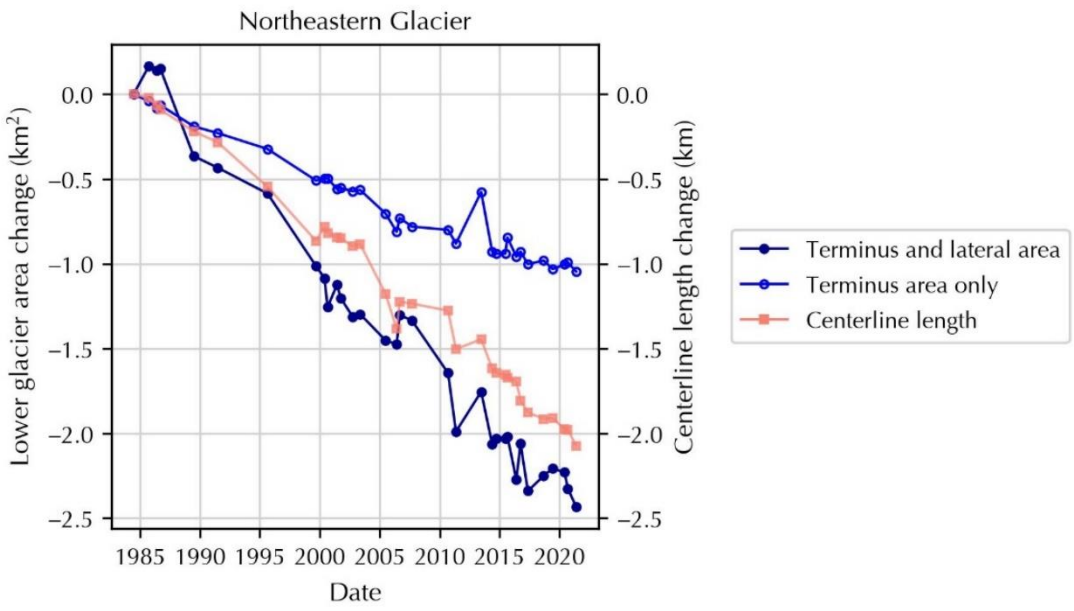

Figure B. 7: Northeastern Glacier.
Observed change in lower glacier area (dark blue, closed circles), terminus area (blue, open circles), and centerline length (pink, squares) at Northeastern Glacier.

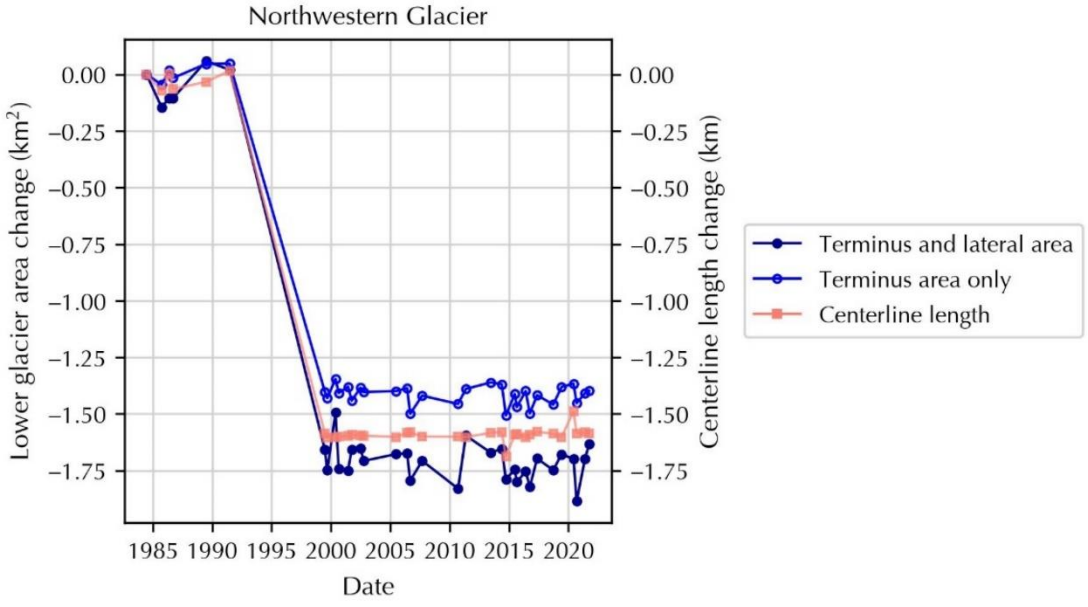

Figure B. 8: Northwestern Glacier.
Observed change in lower glacier area (dark blue, closed circles), terminus area (blue, open circles), and centerline length (pink, squares) at Northwestern Glacier.

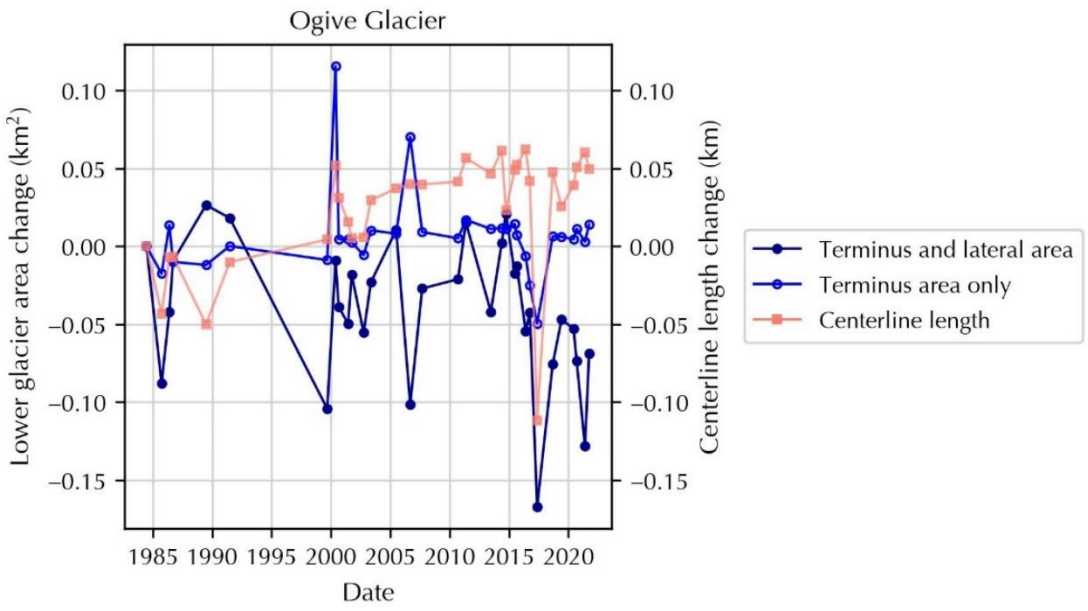

Figure B. 9: Ogive Glacier.
Observed change in lower glacier area (dark blue, closed circles), terminus area (blue, open circles), and centerline length (pink, squares) at Ogive Glacier.

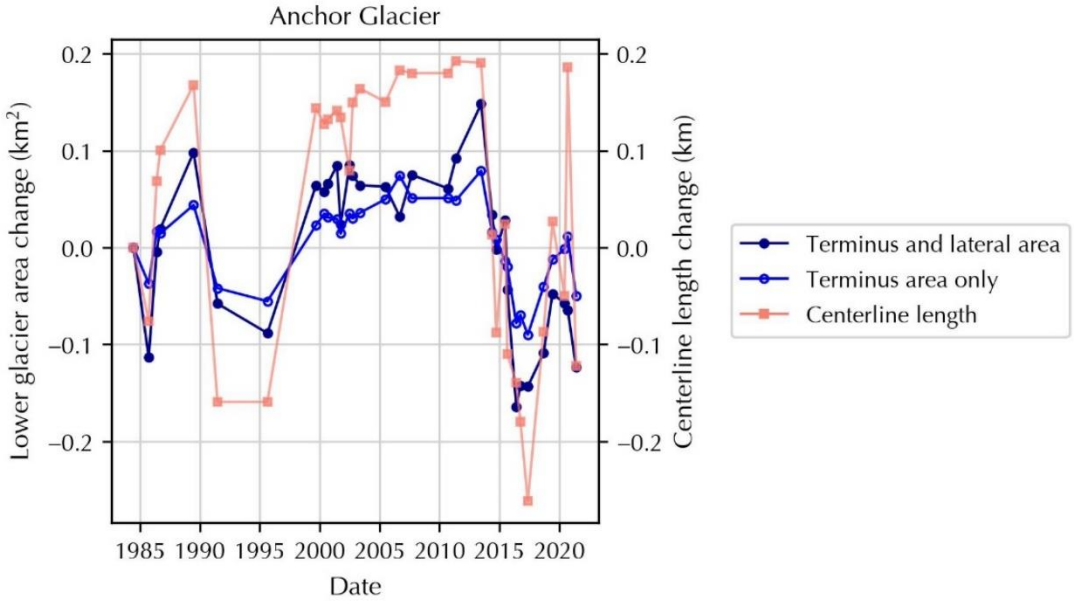

Figure B. 10: Anchor Glacier.
Observed change in lower glacier area (dark blue, closed circles), terminus area (blue, open circles), and centerline length (pink, squares) at Anchor Glacier.

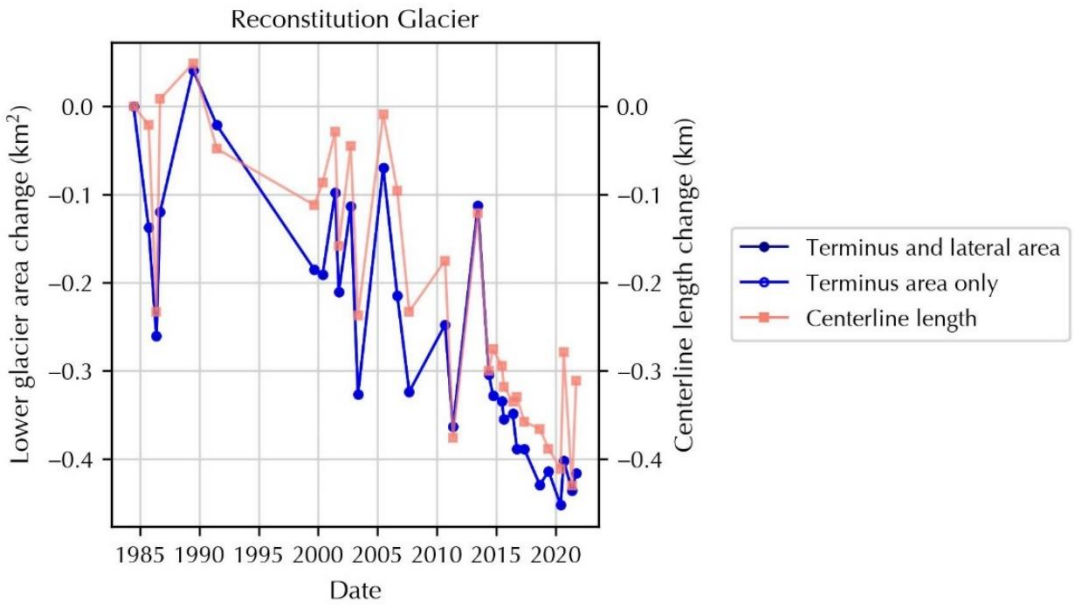

Figure B. 11: Reconstitution Glacier.
Observed change in lower glacier area (dark blue, closed circles), terminus area (blue, open circles), and centerline length (pink, squares) at Reconstitution Glacier.

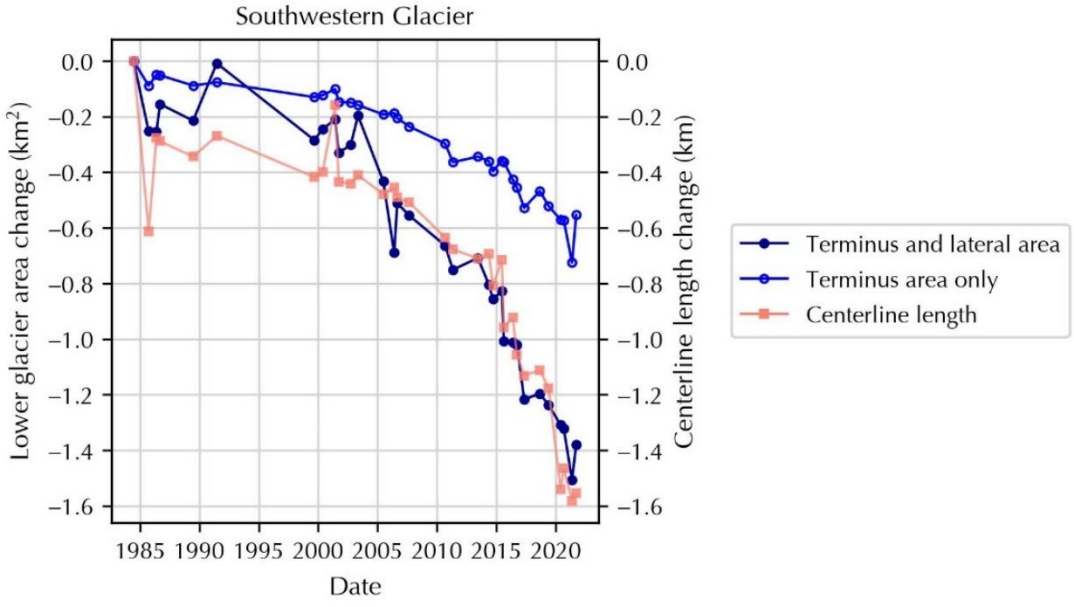

Figure B. 12: Southwestern Glacier.
Observed change in lower glacier area (dark blue, closed circles), terminus area (blue, open circles), and centerline length (pink, squares) at Southwestern Glacier.

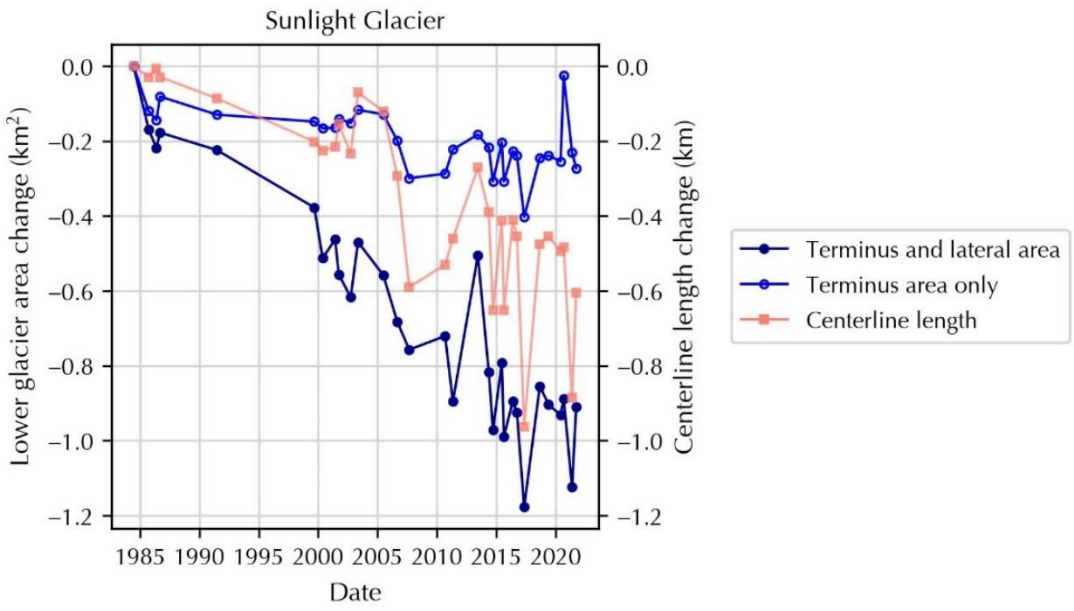

Figure B. 13: Sunlight Glacier.
Observed change in lower glacier area (dark blue, closed circles), terminus area (blue, open circles), and centerline length (pink, squares) at Sunlight Glacier.

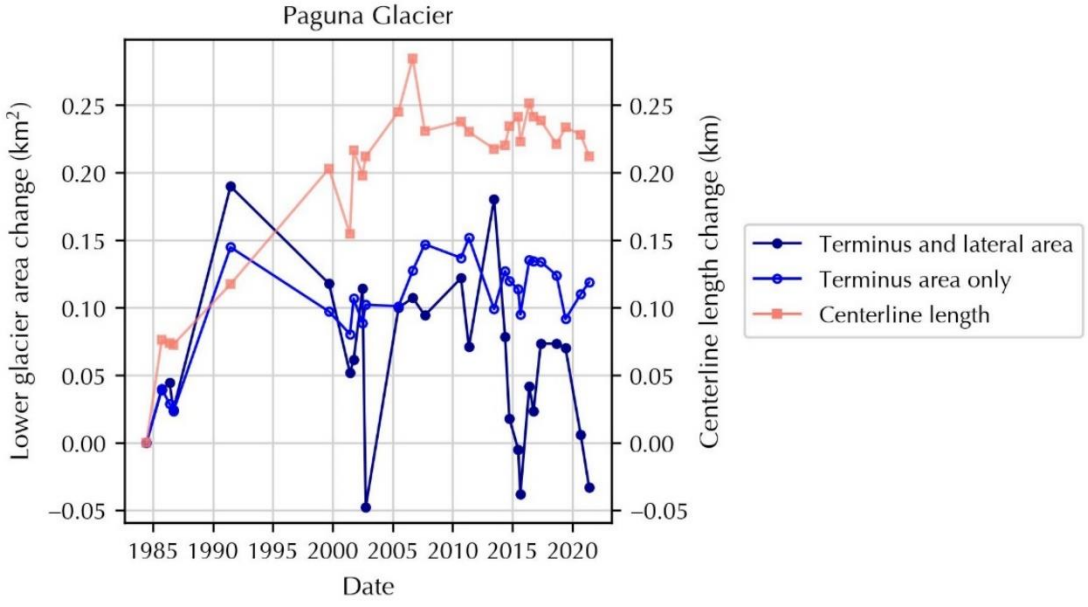

Figure B. 14: Paguna Glacier.
Observed change in lower glacier area (dark blue, closed circles), terminus area (blue, open circles), and centerline length (pink, squares) at Paguna Glacier.

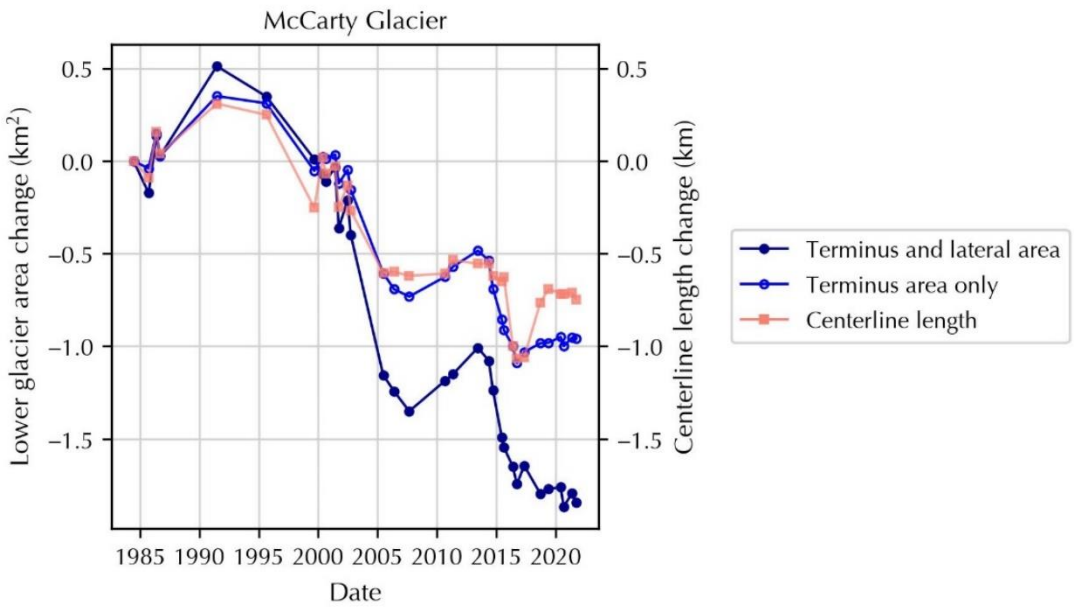

Figure B. 15: McCarty Glacier.
Observed change in lower glacier area (dark blue, closed circles), terminus area (blue, open circles), and centerline length (pink, squares) at McCarty Glacier.

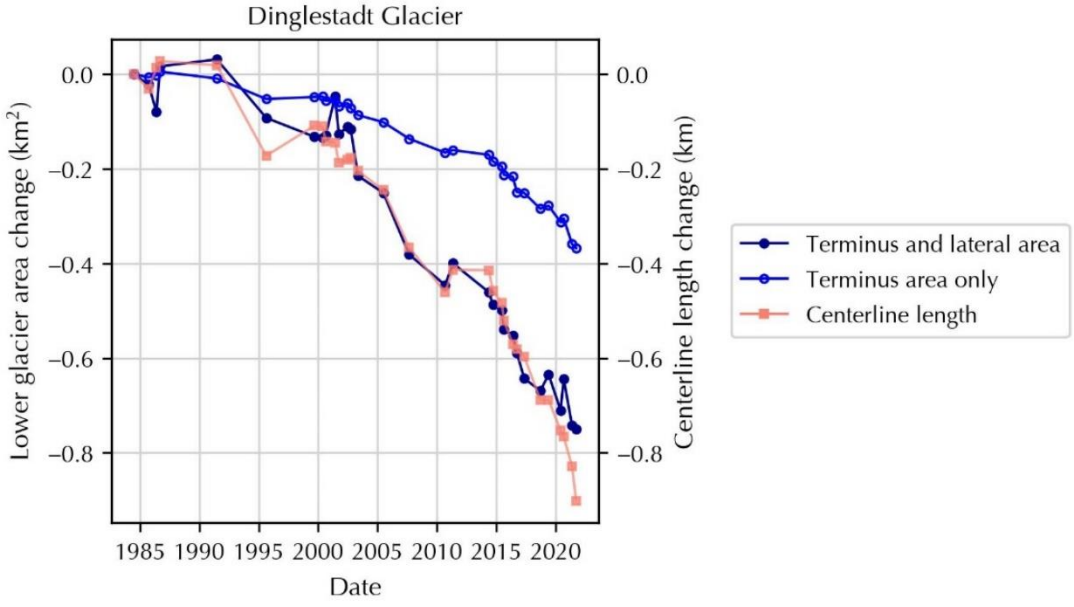

Figure B. 16: Dinglestadt Glacier.
Observed change in lower glacier area (dark blue, closed circles), terminus area (blue, open circles), and centerline length (pink, squares) at Dinglestadt Glacier.

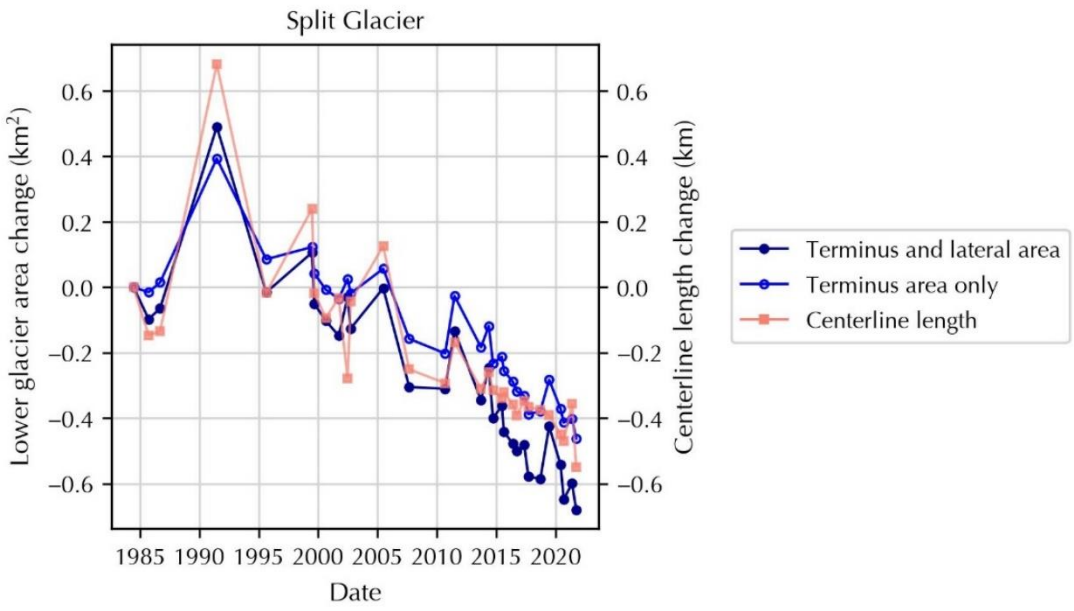

Figure B. 17: Split Glacier.
Observed change in lower glacier area (dark blue, closed circles), terminus area (blue, open circles), and centerline length (pink, squares) at Split Glacier.

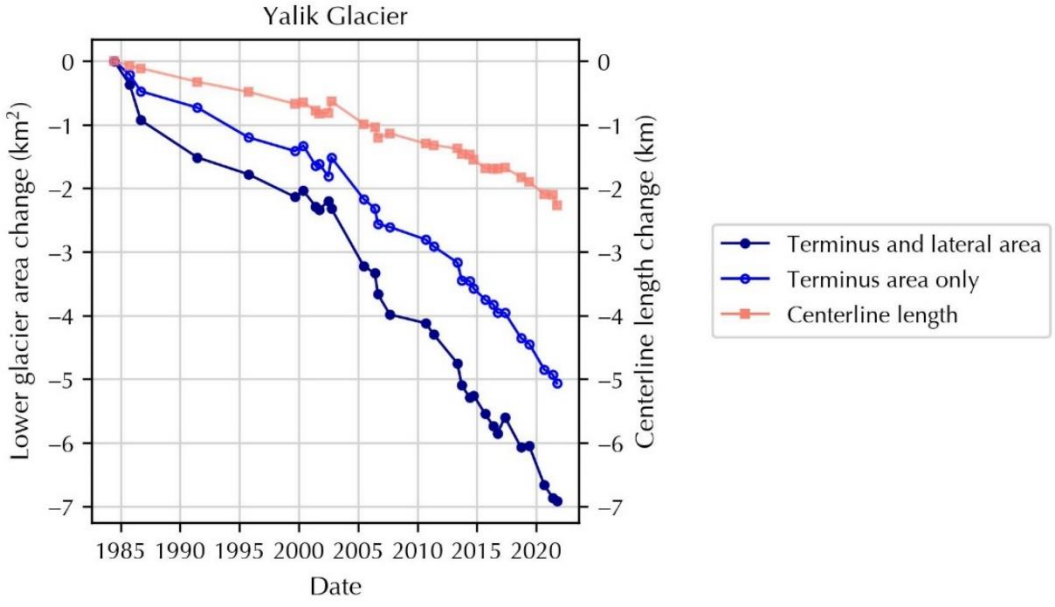

Figure B. 18: Yalik Glacier.
Observed change in lower glacier area (dark blue, closed circles), terminus area (blue, open circles), and centerline length (pink, squares) at Yalik Glacier.

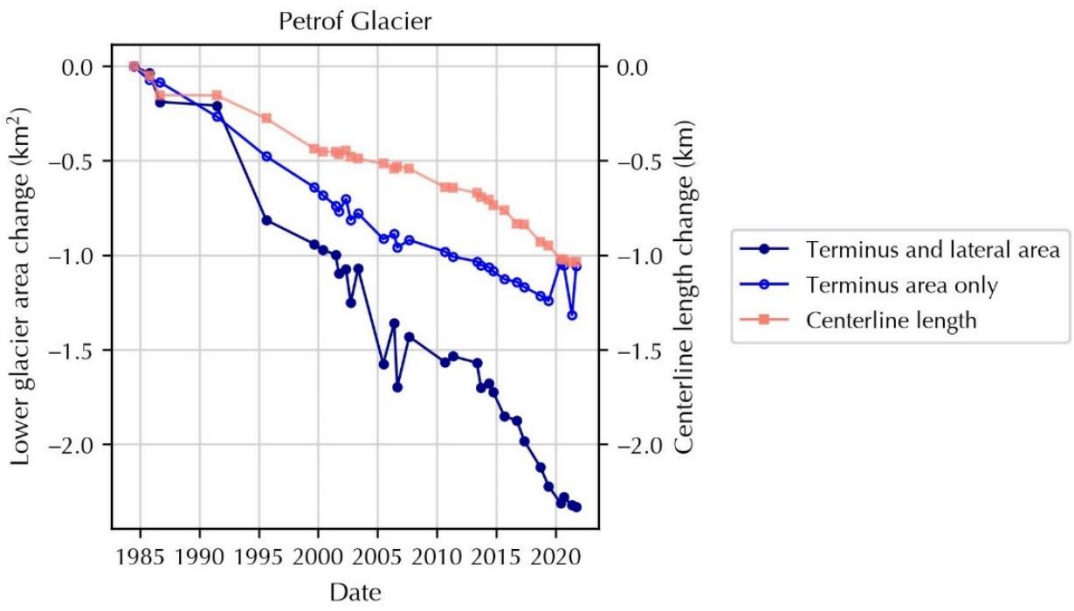

Figure B. 19: Petrof Glacier.
Observed change in lower glacier area (dark blue, closed circles), terminus area (blue, open circles), and centerline length (pink, squares) at Petrof Glacier.

Appendix C

This appendix contains the supplementary material for Chapter 4, "Weekly to monthly terminus variability of Greenland's marine-terminating outlet glaciers".

C.1 Supplementary tables

Table C. 1: List of glaciers digitized at monthly resolution.
List of glaciers digitized at monthly temporal resolution, including their database identification number, ice-sheet region, official name (and alternative common name), and terminus centroid coordinates. Identification numbers match those in Joughin et al. (2015). Regions listed are central-west (CW), northwest (NW), north (NO), northeast (NE), southeast (SE), and southwest (SW). Glacier names are those designated by Bjørk et al. (2015).

ID	Region	Glacier name	Terminus centroid coordinates
1	CW	Saqqarliup Sermia (Sarqardliup Sermia)	(68.899, -50.319)
2	CW	Alanngorliup Sermia (Alangordliup Sermia)	(68.953, -50.221)
4	CW	Sermeq Avannarleq (Sermeq Avannarleq A)	(69.361, -50.315)
5	CW	Eqip Sermia	(69.793, -50.226)
6	CW	Kangilernata Sermia (Kangilerngata Sermia)	(69.903, -50.341)
8	CW	Sermeq Avannarleq (Sermeq Avangnardleq B)	(70.051, -50.316)
10	CW	Sermeq Avannarleq (Lille Gletsjer)	(70.526, -50.511)
11	CW	Sermilik (Sermilik Isbræ)	(70.630, -50.649)
12	CW	Kangilleq (Kangilleq Kangigdleq Isbræ)	(70.717, -50.668)
14	CW	Perlerfiup Sermia (Perdlerfiup Sermia)	(70.984, -50.874)
15	CW	Kangerluarsuup Sermia (Kangerdluarssup Sermia)	(71.252, -51.485)
16	CW	Kangerlussuup Sermia (Kangerdlugssup Sermerssua)	(71.463, -51.407)
18	NW	Umiammakku Sermiat (Umiammakku Isbræ)	(71.727, -52.409)
25	NW	Naajarsuit Sermiat (Nunatakassaap Sermia)	(73.226, -55.158)
26	NW		(73.373, -55.046)
27	NW	Kakiffaat Sermiat A	(73.453, -55.317)
28	NW	Kakiffaat Sermiat B	(73.483, -55.359)
29	NW	Qeqertarsuup Sermia (Qeqertarssup Sermia)	(73.586, -55.581)
30	NW	Sermeq Kujalleq (Ussingbraer A)	(73.845, -55.618)
31	NW	Sermeq Avanarleq (Ussingbraer B)	(73.943, -55.745)
33	NW		(74.294, -56.093)
36	NW		(74.728, -56.355)
37	NW		(74.789, -56.600)
38	NW		(74.861, -56.773)

ID	Region	Glacier name	Terminus centroid coordinates
39	NW		(74.906, -56.927)
40	NW	Tuttulikassaap Sermia (Hayes Gletsjer)	(74.932, -57.087)
41	NW		(75.019, -57.611)
43	NW		(75.205, -57.731)
44	NW	Sermersuaq (Steenstrup Gletsjer)	(75.285, -57.939)
45	NW	Dietrichson Gletsjer	(75.461, -57.998)
47	NW	Nansen Gletsjer	(75.743, -58.893)
48	NW	Nordenskiöld Gletsjer	(75.839, -59.048)
49	NW		(75.877, -59.186)
50	NW		(75.975, -59.517)
52	NW		(76.070, -59.984)
53	NW		(76.079, -60.151)
54	NW	Issuusarsuit Sermiat (Peary Gletscher)	(76.049, -60.664)
55	NW		(76.191, -60.719)
56	NW	Rink Gletsjer	(76.236, -61.002)
57	NW		(76.237, -61.397)
58	NW	Qeqertat Timaanni Sermeq (Döcker Smith Gletsjer)	(76.252, -61.805)
59	NW	Döcker Smith Gletsjer C	(76.281, -61.893)
60	NW	Döcker Smith Gletsjer B	(76.316, -61.981)
66	NW		(76.357, -64.340)
67	NW		(76.283, -64.616)
68	NW	Helland Gletsjer	(76.193, -64.863)
69	NW	Savissuup Sermia (Savigssuaq Gletscher)	(76.197, -65.244)
70	NW		(76.330, -65.556)
72	NW		(76.257, -67.281)
73	NW		(76.194, -67.485)
74	NW	Paakitsup Sermersua (Pituffik Gletsjer)	(76.232, -68.803)
75	NW	Ullip Sermia (Harald Moltke Bræ)	(76.597, -67.759)
76	NW	Equutissaatsut Sermiat (Knud Rasmussen Gletsjer)	(76.703, -67.960)
77	NW	Naajat Sermiat (Chamberlin Gletsjer)	(76.691, -68.338)
78	NW	Berlingske Glacier	(76.998, -69.638)
79	NW	Leidy Gletsjer	(77.264, -66.111)
80	NW	Qaqujaarsuup Sermia (Heilprin Gletsjer)	(77.538, -66.038)
82	NW	Tuttulipaluup Sermia (Farquhar Gletsjer)	(77.698, -66.249)
83	NW	Paarnarsuit Sermiat (Hart Gletsjer)	(77.684, -67.136)
84	NW	Quinisut Sermiat (Hubbard Gletsjer)	(77.534, -67.832)
85	NW	Kangerluarsuup Sermia (Bowdoin Gletsjer)	(77.679, -68.615)
86	NW	Qinnguata Sermia (Verhoeff Gletsjer)	(77.848, -69.919)

ID	Region	Glacier name	Terminus centroid coordinates
87	NW	Neqip Sermia (Morris Jesup Gletsjer)	(77.887, -71.172)
88	NW	Arfalluarfiup Sermia (Diebitsch Gletsjer)	(77.940, -71.623)
89	NW	Arfalluarfiup Sermia (Clements Markham Gletsjer)	(77.928, -71.983)
92	NO	Sermersuaq (Humboldt Gletsjer)	(79.690, -64.369)
93	NO	Petermann Gletsjer	(80.969, -61.241)
94	NO	Newman Bugt	(81.330, -57.255)
95	NO	Steensby Gletsjer	(81.500, -54.603)
96	NO	Ryder Gletsjer	(81.512, -50.746)
97	NO	Ryder Gletsjer	(81.814, -50.683)
100	NO	Jungersen Gletsjer	(82.117, -42.689)
101	NO		(82.363, -42.007)
102	NO	Adams Gletsjer	(82.257, -40.147)
103	NO	Marie Sophie Gletsjer	(81.783, -32.801)
104	NO	Academy Gletsjer	(81.643, -32.340)
105	NO	Hagen Bræ	(81.439, -27.518)
106	NE	Spaltegletsjer	(79.763, -20.225)
107	NE	Zachariae Isstrøm	(78.896, -20.843)
108	NE	Kofoed-Hansen Bræ	(77.536, -21.792)
109	NE	Bredebræ	(76.706, -22.481)
110	NE	Soranerbræen	(76.208, -21.820)
111	NE	Heinkel Gletsjer	(75.167, -22.482)
112	NE	Waltershausen Gletsjer	(73.806, -24.213)
113	NE	Nunatakgletsjer	(73.947, -25.810)
114	NE	Gerard de Geer Gletsjer	(73.497, -27.250)
115	NE	Jættegletsjer	(73.453, -27.430)
116	NE	Nordenskiöld Gletsjer	(73.134, -27.714)
117	NE	Hisinger Gletsjer	(72.845, -27.435)
118	NE	F. Graae Gletscher	(72.105, -28.693)
119	NE	Charcot Gletscher	(72.051, -28.865)
120	NE	Daugaard-Jensen Gletsjer	(71.912, -28.576)
121	NE	Eielson Gletsjer	(71.130, -27.862)
122	NE	Rolige Bræ	(70.587, -28.273)
123	NE	Døde Bræ	(70.450, -29.115)
124	NE	Vestfjord Gletsjer	(70.390, -29.099)
125	SE		(70.007, -27.973)
126	SE	Kista Dan Gletsjer	(69.965, -27.422)
127	SE	Magga Dan Gletsjer	(69.972, -27.281)
128	SE	Sydbræ	(70.195, -26.306)

ID	Region	Glacier name	Terminus centroid coordinates
141	SE		(68.640, -27.514)
142	SE	Borggraven	(68.619, -28.073)
143	SE		(68.488, -28.474)
144	SE	Kronborg Gletsjer	(68.438, -28.656)
145	SE	Rosenborg Gletsjer	(68.420, -28.817)
146	SE		(68.462, -29.257)
147	SE	Christian IV Gletsjer	(68.405, -30.027)
148	SE	Sorgenfri Gletsjer	(68.296, -30.814)
149	SE	Frederiksborg Gletsjer	(68.274, -31.533)
150	SE	Courtauld Gletsjer	(68.504, -32.208)
151	SE	Styrtegletscher	(68.626, -32.444)
152	SE	Nordfjord Gletsjer	(68.636, -32.584)
153	SE	Kangerlussuaq Gletsjer	(68.601, -32.909)
154	SE		(68.099, -32.041)
155	SE	Apuliliip Apusiia (Polaric Gletsjer)	(67.870, -32.491)
156	SE		(67.843, -32.608)
157	SE		(67.774, -32.732)
158	SE	Søndre Parallelgletsjer	(67.752, -33.360)
159	SE		(67.627, -33.341)
160	SE		(67.569, -33.420)
161	SE	Unartit	(67.428, -33.551)
162	SE		(67.225, -33.741)
163	SE		(66.630, -34.558)
164	SE		(66.575, -34.545)
165	SE	K.J.V. Steenstrup Nordre Bræ	(66.512, -34.527)
166	SE	Sulussuulip Apusiia (K.J.V. Steenstrup Søndre)	(66.473, -34.676)
167	SE	Tuttiliip Kattertarpia (Tuttiliip Kattilersorpia)	(66.372, -34.891)
168	SE	Nigertuluup Kattilertarpia Oqqorteq	(66.375, -35.257)
169	SE	Kattilersorpia (Glacier de France)	(66.446, -35.961)
170	SE	Apuseeq (Knud Rasmussen Gletsjer)	(66.085, -36.327)
171	SE		(66.080, -36.565)
172	SE	Kaarali Gletsjer	(66.095, -36.673)
173	SE	Nigertiip Apusiia (Midgård Gletsjer)	(66.471, -36.690)
174	SE	Apuseerajik (Fenris Gletsjer)	(66.368, -37.546)
175	SE	Helheim Gletsjer	(66.364, -38.171)
176	SE		(65.693, -39.640)
177	SE		(65.621, -39.663)
178	SE		(65.589, -39.930)

ID	Region	Glacier name	Terminus centroid coordinates
179	SE		(65.558, -39.983)
180	SE	Ikertivaq	(65.504, -40.122)
181	SE		(65.193, -40.675)
182	SE		(65.160, -41.136)
183	SE		(64.974, -41.170)
184	SE		(64.875, -41.063)
185	SE		(64.748, -40.804)
186	SE		(64.493, -40.648)
187	SE	Gråulv	(64.328, -41.507)
188	SE		(64.265, -41.569)
189	SE	Sleipner	(63.892, -41.477)
190	SE	A.P. Bernstorff Gletsjer	(63.833, -41.706)
191	SE	Storebjørn	(63.712, -41.660)
192	SE	Apusiigajik (Skinfaxe)	(63.214, -41.839)
193	SE	Rimfaxe	(63.208, -42.170)
194	SE	Heimdal Gletsjer	(62.857, -42.586)
195	SE		(62.761, -43.212)
196	SE		(62.071, -42.455)
197	SE		(61.745, -42.893)
198	SE		(61.690, -42.642)
199	SE		(61.601, -43.094)
200	SE		(61.444, -42.656)
201	SE		(61.326, -43.254)
202	SE		(60.923, -43.468)
203	SW	Eqalorutsit Kangilliit Sermiat (Eqalorutsit Killiit)	(61.311, -45.783)
204	SW	Sermiligaarsuup Sermia (Sermiligaarsuk Bræ)	(61.585, -48.334)
205	SW	Uukkaasorsuaq (Sermilik Bræ)	(61.964, -48.760)
206	SW	Avannarleq Bræ	(62.196, -49.017)
207	SW	Kangiata Nunaata Sermia	(64.304, -49.622)
208	SW	Akullersuup Sermia (Akugdlerssup Sermia)	(64.346, -49.637)
209	SW	Narsap Sermia (Narssap Sermia)	(64.643, -49.975)
210	NO	Ekspedition Bræ	(82.283, -40.323)
211	NE		(79.558, -19.530)
212	NE	Blæsebræ	(78.215, -21.274)
213	NE		(76.855, -22.164)
214	NE		(76.529, -22.398)
215	SE		(68.272, -30.422)
216	SE		(68.560, -32.897)

ID	Region	Glacier name	Terminus centroid coordinates
217	SE		(66.696, -34.302)
218	SE		(65.371, -39.909)
219	SE		(64.726, -40.742)
220	SE		(64.166, -41.512)
221	SE	Gjallerbroen	(63.803, -40.639)
222	SE		(63.711, -40.675)
223	SE	Ydun Gletsjer	(63.690, -40.938)
224	SE	Thrym Gletsjer	(63.565, -41.763)
225	SE		(62.786, -42.730)
226	SE		(62.551, -43.095)
227	SE		(62.491, -43.075)
228	SE		(62.417, -43.003)
229	SE		(62.313, -42.549)
230	SE		(61.925, -42.566)
231	SE		(61.823, -42.775)
232	SE		(61.789, -42.831)
233	SE		(61.511, -42.964)
234	SE		(61.206, -43.214)
235	SE		(60.841, -43.589)
236	SW	Qooqqup Sermia	(61.195, -45.201)
237	NE	Stormgletsjer	(75.657, -22.222)
238	SE		(60.725, -43.801)
239	NE		(70.962, -28.311)

Table C. 2: List of glaciers digitized at six-day resolution.

List of glaciers digitized at six-day temporal resolution, including their database identification number, ice-sheet region (central-west, CW, or northwest, NW), official name (and alternative common name), and terminus centroid coordinates. Identification numbers match those in Joughin et al. (2015). Glacier names are those designated by Bjørk et al. (2015).

ID	Region	Glacier name	Terminus centroid coordinates
3	CW	Sermeq Kujalleq (Jakobshavn Isbræ)	(69.194, -49.651)
7	CW	Sermeq Kujalleq (Alianaatsup Sermia)	(69.999, -50.228)
9	CW	Sermeq Kujalleq (Store Gletsjer)	(70.383, -50.601)
13	CW	Sermeq Silarleq (Sermeq Silardleq)	(70.827, -50.757)
17	CW	Kangilliup Sermia (Rink Isbræ)	(71.736, -51.661)
19	NW	Salliarutsip Sermia (Inngia Isbræ)	(72.065, -52.545)
20	NW		(72.787, -54.233)

21	NW	Sermeq (Upernavik Isstrøm)	(72.848, -54.349)
22	NW		(72.937, -54.282)
23	NW		(73.024, -54.443)
24	NW		(72.999, -54.646)
32	NW	Ikissuup Sermersua (Cornell Gletsjer)	(74.228, -56.082)
34	NW	Illullip Sermia (Igdlugdlip Sermia)	(74.402, -56.092)
35	NW	Nunatakassaap Sermia (Alison Glacier)	(74.605, -56.025)
42	NW	Kjer Gletsjer	(75.132, -57.674)
46	NW	Sverdrup Gletsjer	(75.595, -58.096)
51	NW	Nuussuup Sermia (Kong Oscar Gletsjer)	(75.991, -59.794)
65	NW	Yngvar Nielsen Gletsjer	(76.364, -64.122)
71	NW		(76.313, -66.881)
81	NW	Qeqertaarsuusarsuup Sermia (Tracy Gletsjer)	(77.656, -66.038)

Table C. 3: Timing and magnitude of terminus position seasonality for individual glaciers. Timing and magnitude of terminus position seasonality for individual glaciers. Regions listed are central-west (CW), northwest (NW), north (NO), northeast (NE), southeast (SE), and southwest (SW). Glaciers that do not show significant terminus position seasonality have "N/A" reported for the timing and magnitude of terminus seasonality. All reported values are medians.

ID	Region	Peak advance	Peak retreat	Retreat duration (days)	Magnitude (m)
1	CW	April 5	September 10	158	170
2	CW	March 11	October 22	225	110
3	CW	April 16	August 14	120	2590
4	CW	May 8	September 3	118	80
5	CW	May 4	September 8	127	290
6	CW	June 3	September 7	96	230
7	CW	April 22	September 4	135	590
8	CW	March 23	September 3	164	180
9	CW	April 28	August 22	116	510
10	CW	May 5	December 7	216	120
11	CW	April 9	December 6	241	210
12	CW	March 11	September 9	182	220
13	CW	May 24	January 25	246	880
14	CW	N/A	N/A	N/A	N/A
15	CW	May 7	October 8	154	80
16	CW	May 5	October 4	152	280
17	CW	June 4	September 22	110	810
18	NW	April 4	September 5	154	270

ID	Region	Peak advance	Peak retreat	Retreat duration (days)	Magnitude (m)
19	NW	May 31	October 30	152	870
20	NW	June 3	December 5	185	180
21	NW	May 30	September 3	96	470
22	NW	May 5	December 5	214	780
23	NW	April 21	October 7	169	270
24	NW	March 8	October 7	213	120
25	NW	May 5	August 26	113	170
26	NW	May 6	September 3	120	110
27	NW	N/A	N/A	N/A	N/A
28	NW	May 6	September 24	141	680
29	NW	June 6	September 6	92	200
30	NW	June 6	October 7	123	330
31	NW	June 4	September 5	93	280
32	NW	April 19	September 20	154	320
33	NW	April 7	September 7	153	190
34	NW	June 17	October 27	132	590
35	NW	July 12	November 11	122	1480
36	NW	May 5	September 25	143	220
37	NW	June 19	November 9	143	850
38	NW	June 4	October 7	125	350
39	NW	August 6	December 5	121	270
40	NW	N/A	N/A	N/A	N/A
41	NW	April 5	September 7	155	170
42	NW	June 22	November 24	155	1080
43	NW	N/A	N/A	N/A	N/A
44	NW	May 20	October 3	136	440
45	NW	June 10	September 6	88	420
46	NW	July 5	October 18	105	1720
47	NW	N/A	N/A	N/A	N/A
48	NW	July 6	October 21	107	220
49	NW	June 6	September 18	104	120
50	NW	May 22	February 4	258	200
51	NW	June 18	October 10	114	920
52	NW	May 6	August 26	112	220
53	NW	June 6	September 8	94	160
54	NW	N/A	N/A	N/A	N/A
55	NW	July 4	November 6	125	520
56	NW	April 20	September 12	145	220

ID	Region	Peak advance	Peak retreat	Retreat duration (days)	Magnitude (m)
57	NW	April 21	September 7	139	160
58	NW	June 22	November 7	138	460
59	NW	N/A	N/A	N/A	N/A
60	NW	June 20	October 7	109	420
65	NW	N/A	N/A	N/A	N/A
66	NW	N/A	N/A	N/A	N/A
67	NW	June 5	September 15	102	120
68	NW	April 24	September 9	138	140
69	NW	May 7	October 24	170	90
70	NW	May 22	January 7	230	160
71	NW	May 18	October 29	164	230
72	NW	May 9	November 8	183	220
73	NW	N/A	N/A	N/A	N/A
74	NW	May 8	November 10	186	180
75	NW	N/A	N/A	N/A	N/A
76	NW	May 7	September 27	143	110
77	NW	April 9	November 9	214	50
78	NW	May 12	November 8	180	370
79	NW	March 10	October 7	211	80
80	NW	May 9	September 10	124	370
81	NW	July 10	December 4	147	1020
82	NW	March 10	September 25	199	190
83	NW	N/A	N/A	N/A	N/A
84	NW	N/A	N/A	N/A	N/A
85	NW	April 28	September 22	147	110
86	NW	March 14	November 5	236	130
87	NW	June 6	October 6	122	130
88	NW	May 22	November 8	170	110
89	NW	N/A	N/A	N/A	N/A
92	NO	May 9	October 6	150	310
93	NO	N/A	N/A	N/A	N/A
94	NO	N/A	N/A	N/A	N/A
95	NO	N/A	N/A	N/A	N/A
96	NO	June 22	September 6	76	130
97	NO	N/A	N/A	N/A	N/A
100	NO	June 4	October 5	123	180
101	NO	N/A	N/A	N/A	N/A
102	NO	N/A	N/A	N/A	N/A

ID	Region	Peak advance	Peak retreat	Retreat duration (days)	Magnitude (m)
103	NO	June 3	September 3	92	180
104	NO	July 3	September 21	80	310
105	NO	April 4	September 6	155	220
106	NE	N/A	N/A	N/A	N/A
107	NE	June 23	November 5	135	1760
108	NE	N/A	April 3	N/A	N/A
109	NE	N/A	N/A	N/A	N/A
110	NE	June 5	October 5	122	120
111	NE	N/A	N/A	N/A	N/A
112	NE	June 6	October 4	120	120
113	NE	May 11	October 7	149	200
114	NE	May 5	September 18	136	250
115	NE	N/A	N/A	N/A	N/A
116	NE	May 6	October 1	148	220
117	NE	May 6	October 5	152	200
118	NE	N/A	N/A	N/A	N/A
119	NE	May 18	January 3	230	180
120	NE	April 8	September 2	147	1330
121	NE	April 7	November 7	214	90
122	NE	May 25	November 6	165	510
123	NE	N/A	N/A	N/A	N/A
124	NE	May 4	September 4	123	290
125	SE	June 4	November 6	155	180
126	SE	June 5	November 7	155	180
127	SE	June 4	December 5	184	70
128	SE	June 4	October 3	121	160
141	SE	June 4	January 27	237	50
142	SE	June 5	November 24	172	300
143	SE	July 3	November 9	129	180
144	SE	May 6	November 6	184	360
145	SE	June 4	November 7	156	440
146	SE	May 7	December 6	213	230
147	SE	May 6	October 8	155	220
148	SE	May 20	October 7	140	160
149	SE	May 7	October 8	154	600
150	SE	May 4	September 20	139	70
151	SE	May 14	October 6	145	220
152	SE	N/A	N/A	N/A	N/A

ID	Region	Peak advance	Peak retreat	Retreat duration (days)	Magnitude (m)
153	SE	July 2	December 26	177	2650
154	SE	June 3	December 9	189	70
155	SE	June 12	November 10	151	260
156	SE	May 18	November 4	170	290
157	SE	July 1	January 19	202	140
158	SE	July 15	November 10	118	790
159	SE	July 15	December 20	158	1720
160	SE	June 2	October 22	142	410
161	SE	July 11	December 9	151	1660
162	SE	June 4	December 7	186	960
163	SE	May 9	December 4	209	160
164	SE	May 4	November 19	199	280
165	SE	May 5	December 5	214	750
166	SE	N/A	N/A	N/A	N/A
167	SE	July 4	February 4	215	150
168	SE	May 3	November 19	200	110
169	SE	N/A	N/A	N/A	N/A
170	SE	May 14	November 10	180	230
171	SE	N/A	N/A	N/A	N/A
172	SE	N/A	N/A	N/A	N/A
173	SE	May 4	October 2	151	750
174	SE	April 7	August 10	125	620
175	SE	April 7	September 24	170	1480
176	SE	N/A	N/A	N/A	N/A
177	SE	N/A	N/A	N/A	N/A
178	SE	June 8	February 23	260	200
179	SE	April 6	August 12	128	220
180	SE	April 9	November 13	218	680
181	SE	N/A	N/A	N/A	N/A
182	SE	N/A	N/A	N/A	N/A
183	SE	May 8	October 9	154	670
184	SE	April 23	October 6	166	140
185	SE	N/A	N/A	N/A	N/A
186	SE	May 8	January 9	246	210
187	SE	May 29	November 9	164	450
188	SE	N/A	N/A	N/A	N/A
189	SE	May 25	November 10	185	220
190	SE	N/A	N/A	N/A	N/A

ID	Region	Peak advance	Peak retreat	Retreat duration (days)	Magnitude (m)
191	SE	N/A	N/A	N/A	N/A
192	SE	May 9	November 10	185	220
193	SE	April 6	August 28	144	180
194	SE	April 10	August 16	128	270
195	SE	N/A	N/A	N/A	N/A
196	SE	June 7	December 23	199	310
197	SE	N/A	N/A	N/A	N/A
198	SE	June 5	December 8	186	190
199	SE	September 6	February 13	160	1270
200	SE	N/A	N/A	N/A	N/A
201	SE	May 12	December 8	210	200
202	SE	July 8	January 21	197	340
203	SW	May 4	March 8	308	100
204	SW	April 20	September 7	140	250
205	SW	February 4	August 24	201	270
206	SW	N/A	N/A	N/A	N/A
207	SW	May 20	September 18	121	540
208	SW	May 6	September 21	138	150
209	SW	March 22	September 7	169	410
210	NO	N/A	N/A	N/A	N/A
211	NE	N/A	N/A	N/A	N/A
212	NE	May 3	October 6	156	140
213	NE	N/A	N/A	N/A	N/A
214	NE	N/A	N/A	N/A	N/A
215	SE	July 4	January 6	186	110
216	SE	N/A	N/A	N/A	N/A
217	SE	N/A	N/A	N/A	N/A
218	SE	N/A	N/A	N/A	N/A
219	SE	N/A	N/A	N/A	N/A
220	SE	April 7	October 10	186	180
221	SE	May 7	September 22	138	150
222	SE	N/A	N/A	N/A	N/A
223	SE	N/A	N/A	N/A	N/A
224	SE	May 12	November 24	196	50
225	SE	June 7	February 7	245	110
226	SE	August 11	March 24	225	670
227	SE	N/A	N/A	N/A	N/A
228	SE	N/A	N/A	N/A	N/A

ID	Region	Peak advance	Peak retreat	Retreat duration (days)	Magnitude (m)
229	SE	May 8	December 8	214	170
230	SE	May 25	January 8	228	410
231	SE	May 9	September 24	138	220
232	SE	June 8	December 11	186	40
233	SE	N/A	N/A	N/A	N/A
234	SE	June 8	December 7	182	170
235	SE	N/A	N/A	N/A	N/A
236	SW	April 4	September 7	156	290
237	NE	April 3	October 6	186	160
238	SE	N/A	N/A	N/A	N/A
239	NE	June 3	September 23	112	160

C.2 Supplementary figures

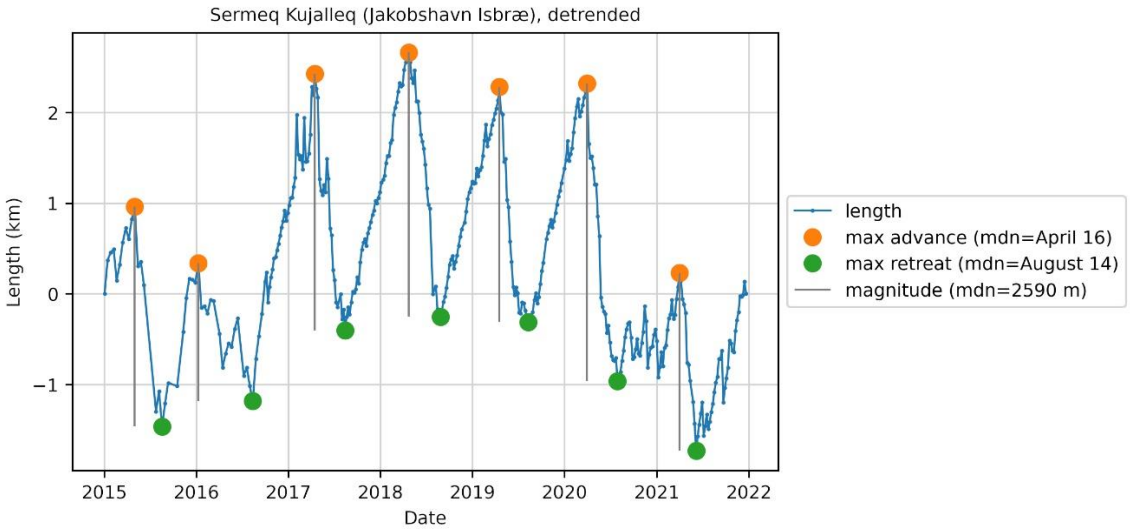

Figure C. 1: Illustration of how dates of greatest advance and retreat are determined. Illustration of the process of determining the annual dates of greatest advance (orange dots) and greatest retreat (green dots) and the annual magnitude of retreat (gray vertical line), demonstrated for Sermeq Kujalleq (Jakobshavn Isbræ, no. 3). The dates of greatest advance and retreat are identified in the original time series, then the time series is detrended and the dates are plotted on the detrended time series. The detrended length at the date of greatest retreat is subtracted from the detrended length at the date of greatest advance to calculate an annual magnitude of retreat. The median dates of greatest advance and retreat and the median magnitude of retreat are reported in the legend.

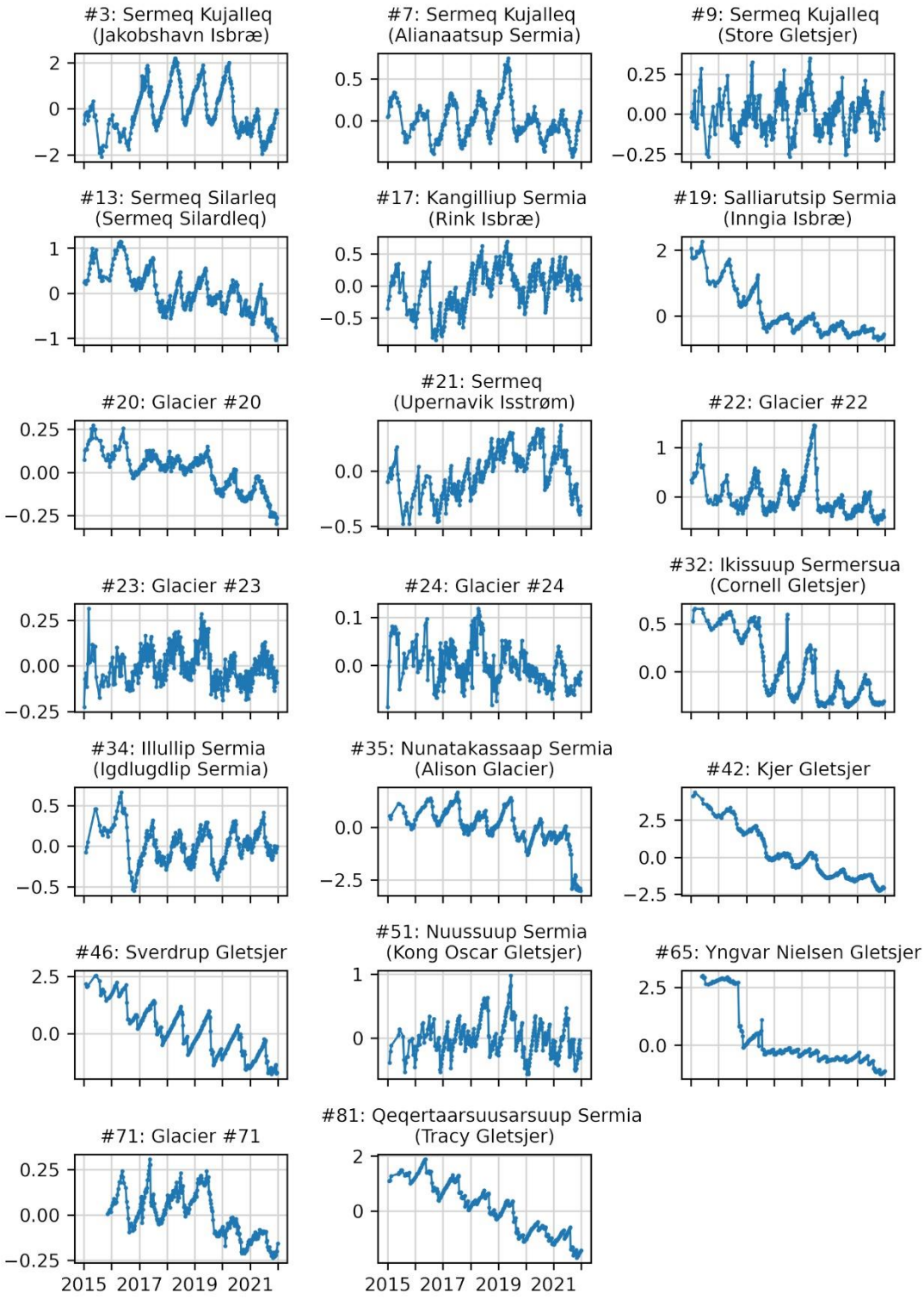

Figure C. 2: Length time series for six-day glaciers.

Length time series for the 20 glaciers digitized at six-day resolution. All lengths are given in kilometers.

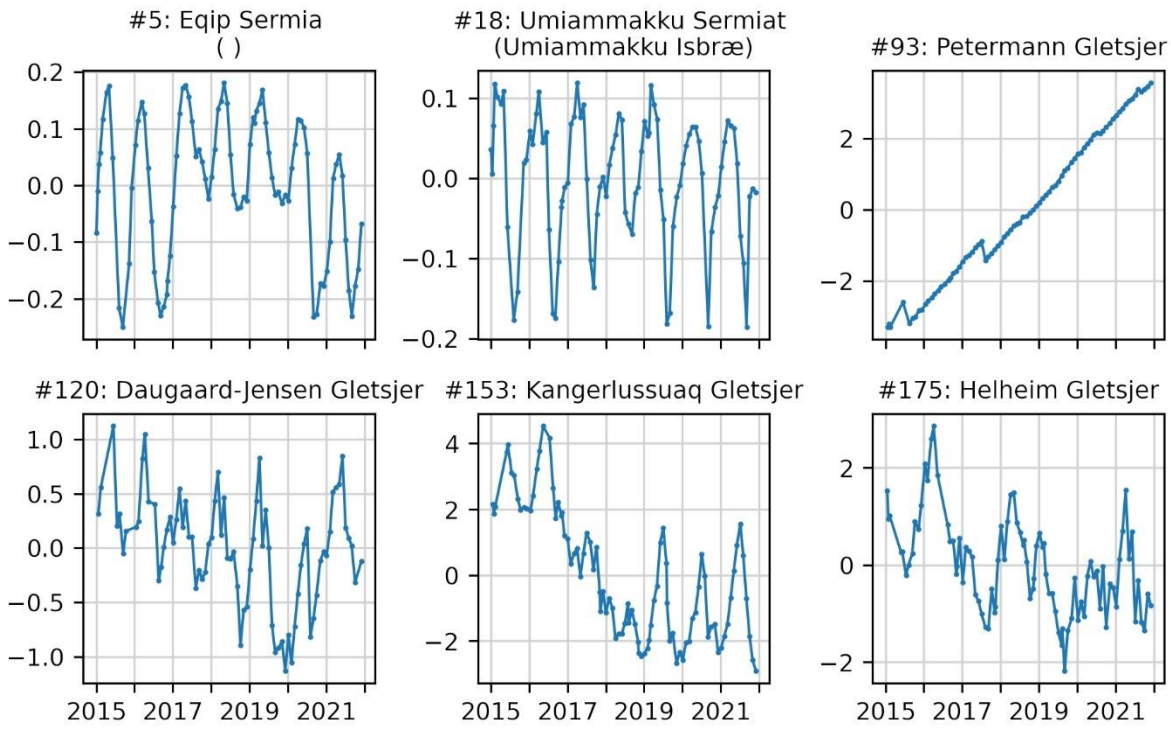

Figure C. 3: Length time series for selected monthly glaciers.
Length time series for selected glaciers digitized at monthly resolution. One glacier from each ice-sheet region is represented. All lengths are given in kilometers.

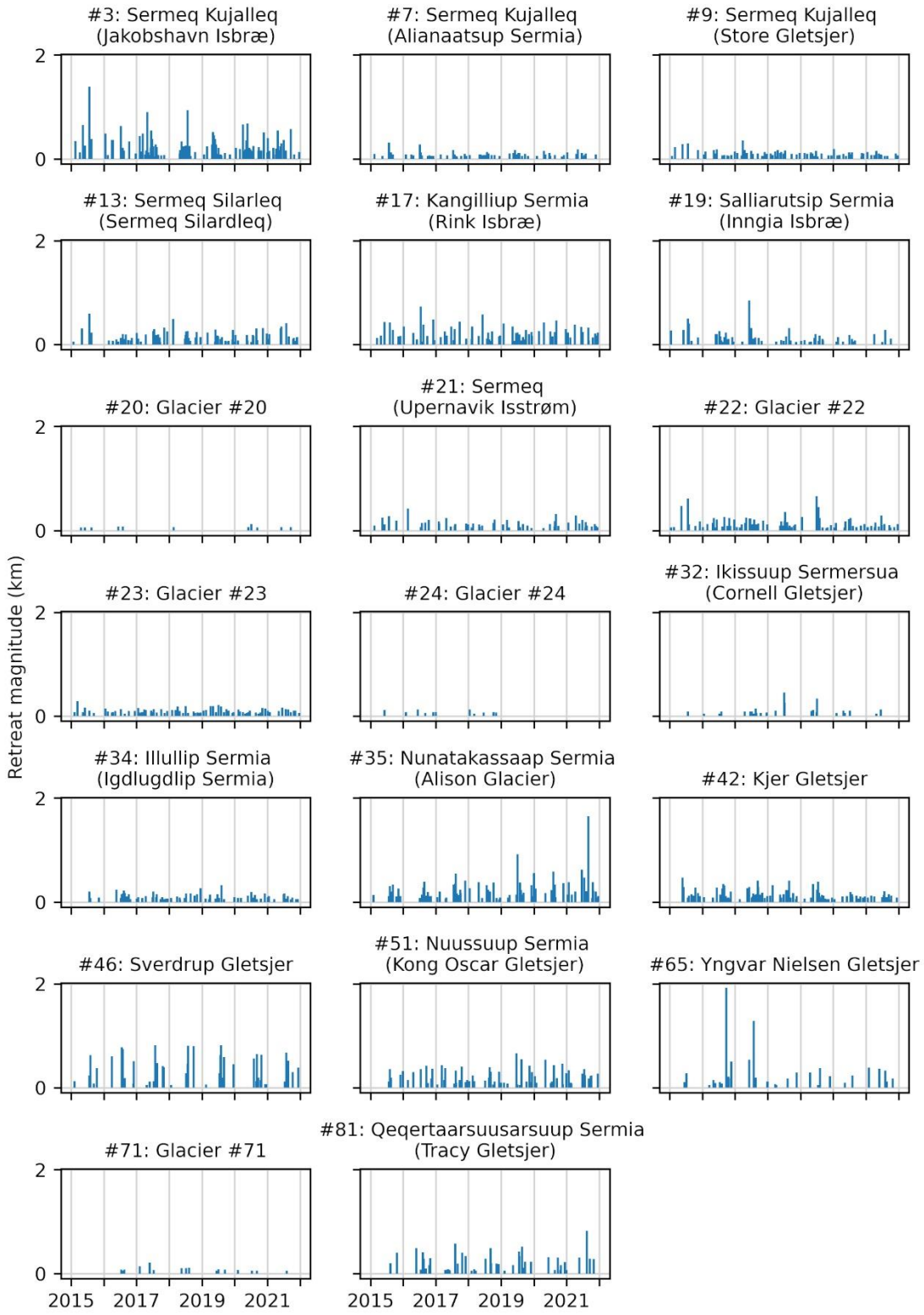

Figure C. 4: Timing and magnitude of retreat events at individual glaciers.
Timing and magnitude of individual retreat events at the 20 six-day glaciers.

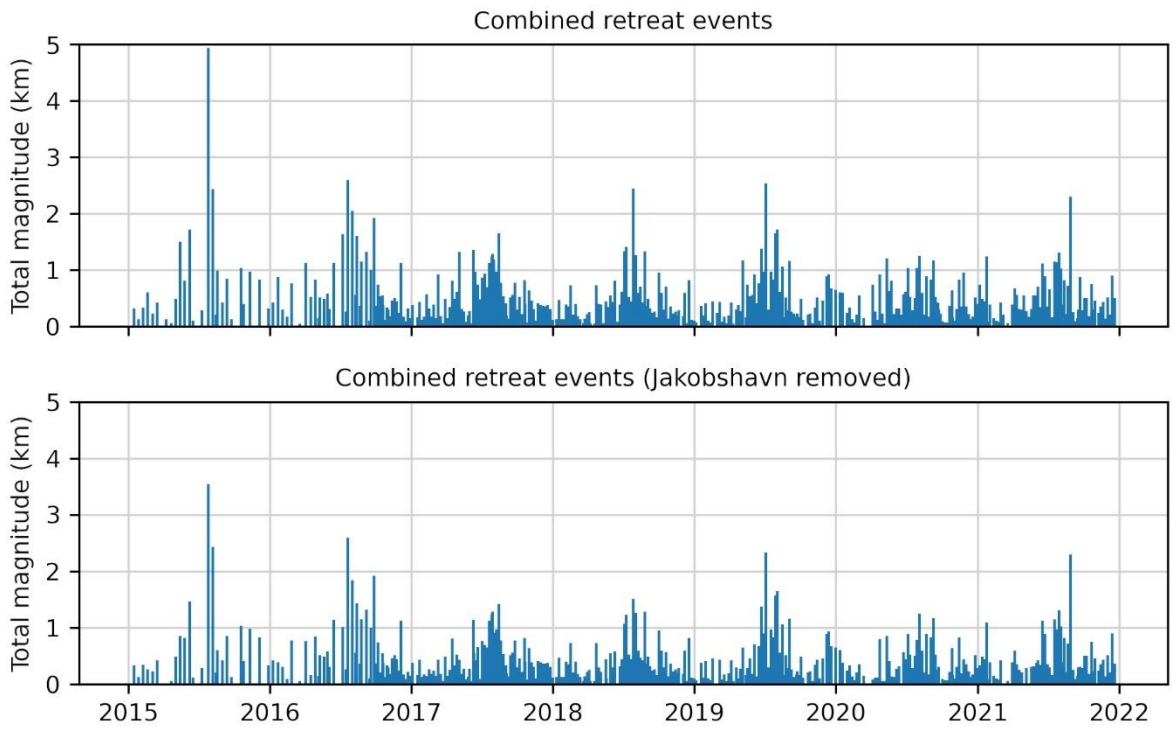

Figure C. 5: Combined timing and magnitude of retreat events.
Timing and magnitude of retreat events combined across the 20 six-day glaciers. If multiple retreat events occur at different glaciers on a single day, their retreat magnitudes are added together. In the lower plot, Sermeq Kujalleq (Jakobshavn Isbræ, no. 3) is removed to show that it is not solely driving the seasonality in retreat events.

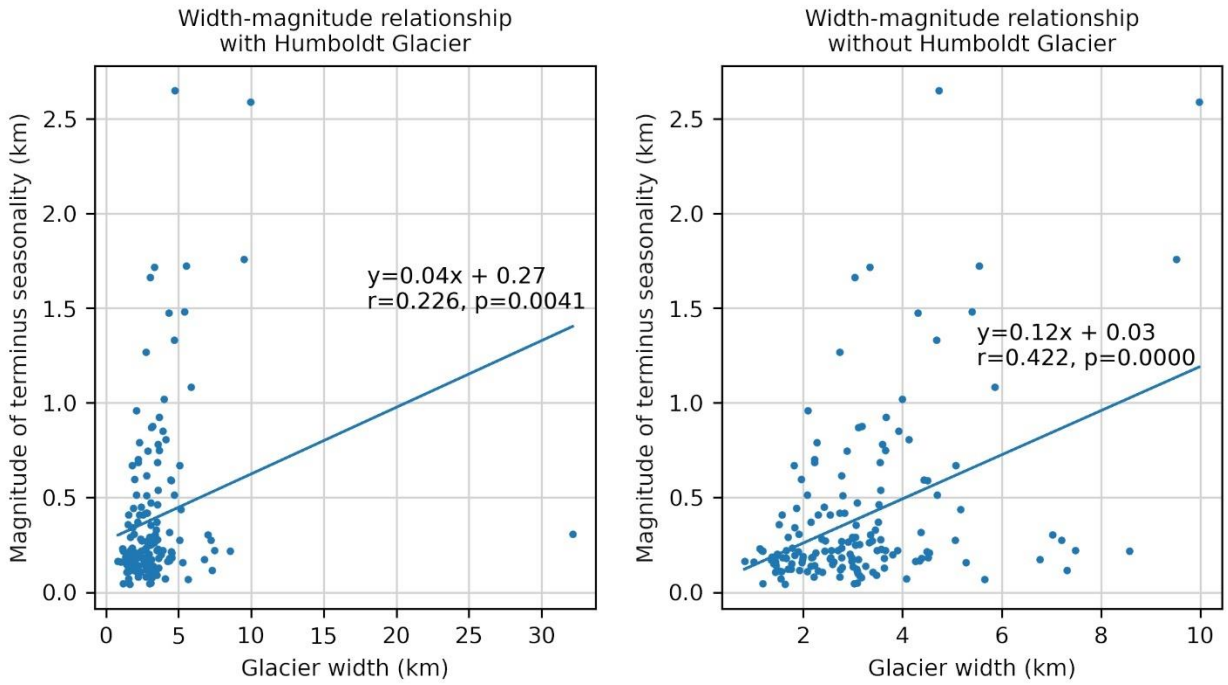

Figure C. 6: Relationship between glacier width and magnitude of terminus seasonality. Relationship between glacier width and the magnitude of terminus position seasonality, with (left) and without (right) Humboldt Glacier, a major width outlier.

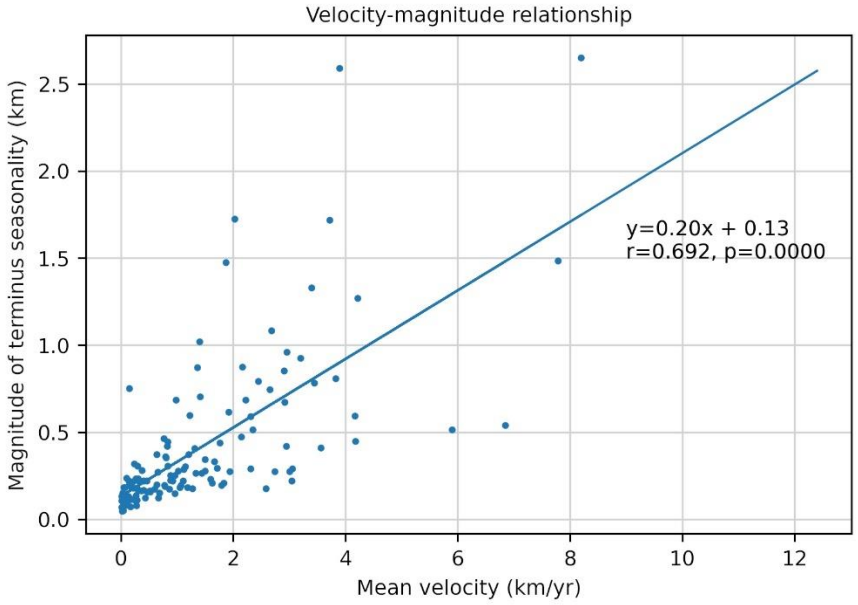

Figure C. 7: Relationship between glacier velocity and magnitude of terminus seasonality. Relationship between glacier velocity and the magnitude of terminus position seasonality.